MONTE CARLO CALCULATIONS OF SHOT NOISE

IN MESOSCOPIC STRUCTURES

Tomás González

Departamento de Física Aplicada, Universidad de Salamanca

Plaza de la Merced s/n, 37008 Salamanca, Spain

E-mail: tomasg@usal.es

TABLE OF CONTENTS

1. Introduction
   1.1. Shot-noise suppression and enhancement
   1.2. Monte Carlo simulations of noise in mesoscopic structures
2. Physical model
   2.1. Simulated structure
   2.2. Monte Carlo method
   2.3. Contact modeling
      2.3.1. Nondegenerate contacts
      2.3.2. Degenerate contacts
   2.4. Scattering mechanisms
   2.5. Trapping-detrapping processes
   2.6. Noise calculation
3. Results
   3.1. Ballistic regime
      3.1.1. Nondegenerate contacts
         a. Static characteristics
         b. Shot-noise suppression
         c. Frequency dependence of noise
      3.1.2. Degenerate contacts
   3.2. Crossover ballistic-diffusive regime
   3.3. Diffusive regime
      3.3.1. Energy-independent scattering time
      3.3.2. Energy-dependent scattering time
   3.4. Influence of trapping-detrapping processes in quasiballistic regime
4. Summary
5. Acknowledgements
   References

1. INTRODUCTION

Macroscopic conductors and devices, where inelastic scattering is dominant, exhibit levels of noise close to the thermal value. In contrast, mesoscopic structures, with active lengths L much shorter than the characteristic length of inelastic scattering ℓ_{inel} ($L << \ell_{inel}$), are known to display shot noise.

Shot noise is caused by the randomness in the flux of carriers crossing the active region of a given device, and it is associated with the discreteness of the electric charge that carries the current [1-5]. At low frequency (small compared to the inverse of the transit time through the active region, $f << 1/\tau_T$, but sufficiently high to avoid $1/f$ contributions), the power spectral density of shot noise is given by $S_I = \gamma 2qI$, where I is the dc current, q the elementary quantum of charge determining I and $\gamma \geq 0$ a numerical factor called Fano factor.

In the absence of correlation between current pulses $\gamma = 1$, carriers exhibit Poissonian statistics, and this case corresponds to full shot noise. Full shot noise was originally described by Schottky [4] for vacuum diodes under current saturation conditions, when all electrons emitted by the cathode reach the anode and there is no charge accumulated in front of the cathode.

1.1. Shot-noise suppression and enhancement

Deviations from the previous ideal case constitute a signature of existing correlations between different current pulses. Negative correlations between carriers reduce the shot-noise level leading to suppressed shot noise with $\gamma < 1$ (sub-Poissonian carrier statistics), while positive correlations increase the noise and give rise to enhanced shot noise with $\gamma > 1$ (super-Poissonian carrier statistics).

In this way, the Fano factor can provide very valuable information about the carrier kinetics and existing correlations inside the devices [5]. For this reason, and with the advent

of mesoscopic conductors in recent years, the analysis of shot noise is attracting increasing attention from both theoretical and experimental points of view [6,7]. In particular, being a signature of correlations among particles, the phenomena of suppression and enhancement have emerged as a subject of relevant interest.

The suppression has been predicted theoretically as a consequence of Pauli exclusion principle under strongly degenerate conditions in very different situations by using both phase coherent [8,9] and semiclassical models [3]. In the ballistic regime, shot noise is completely suppressed [10,11] due to the non-fluctuating occupation number of incoming states. In a point contact, a peak in the noise is predicted in between the conductance plateaus [11]. In symmetric double-barrier junctions, a 1/2 Fano factor has been theoretically explained by different authors [12-15]. In the case of elastic diffusive conductors, a 1/3 reduction of the noise has been calculated for noninteracting electrons [16-24], while in the case of strong electron-electron scattering the value of the Fano factor is $\sqrt{3}/4$ [25,26]. Finally, when devices become macroscopic and inelastic processes are present, like scattering with phonons, the noise is expected to reduce to the thermal value [27,28].

Shot-noise enhancement, though less explored, have also been predicted. So far, apart from Andreev reflections [29-32], the only mechanism found to be responsible for shot-noise enhancement is the positive feedback between Coulomb interaction and tunneling probability, as evidenced in structures controlled by tunneling, like double-barrier resonant tunneling diodes [33,34] and single-barrier structures [35-37].

Remarkably, many of these predictions have been experimentally confirmed [38-53], thus opening new and interesting perspectives. Within this scenario, the understanding of the physical mechanisms originating shot noise and its suppression/enhancement in mesoscopic conductors, and more generally in small-dimensional devices, is a field of key importance.

Most of the theoretical works carried out so far consider degenerate conductors, where the Pauli exclusion principle plays a major role, and neglect long-range Coulomb interaction among carriers. The influence of this interaction is known to be relevant to the noise reduction since the times of vacuum tubes [54,55], and its possible role in the case of mesoscopic samples [56] was repeatedly claimed by Landauer [57-60]. Only recently some works include explicitly long-range Coulomb interaction. In the case of degenerate conductors [61,62], its influence on the high-frequency spectrum of shot noise has been widely analyzed [63-67]. In the case of nondegenerate conductors, and mainly motivated by previous results of Monte Carlo (MC) simulations, some theoretical works including Coulomb correlation as an essential mechanism for shot-noise suppression/enhancement have also recently appeared [68-77]. However, the inclusion of self-consistency (long-range Coulomb interaction) in the theoretical approaches is usually a cumbersome and complex problem, only solvable in very specific cases.

It is here where MC calculations can be extremely useful. By coupling a simulator of carrier transport with a Poisson solver (PS), the MC technique is especially suitable to investigate the influence of Coulomb correlations on shot noise in mesoscopic structures. The scattering mechanisms and interactions, as well as the fluctuations of the self-consistent potential, are intrinsically accounted for by this approach. It can analyze different voltage-bias conditions, ranging from thermal equilibrium to high electric fields necessary for shot noise to appear, without the difficulties that other methods meet. In addition, it has the advantage that it provides a full temporal (and frequency) description of noise by means of the direct calculation of correlation functions (and spectral densities by Fourier transformation) of current fluctuations [78].

1.2. Monte Carlo simulations of noise in mesoscopic structures

In the field of mesoscopic shot noise, the MC technique has been successfully applied in recent years for the investigation of shot-noise suppression and enhancement due to the joint action of Coulomb interaction and other mechanisms controlling transport in the structures under analysis. Typically, semiclassical models are considered, like those used to analyze heterostructure tunnel-barrier diodes [35,79-82], and (ballistic and diffusive) degenerate [83-85] and nondegenerate homogenous structures [86-96]. Just very recently, a first attempt to analyze shot noise with a MC technique using a phase coherent model has been developed and applied to the case of single tunnel-barrier diodes [97]. Let us briefly indicate the main achievements accomplished by using semiclassical models.

Liu *et al.* [83], by using a simple model, analyze the case of completely degenerate elastic diffusive conductors. They reproduce the 1/3 Fano factor predicted theoretically, which appears as a result of the redistribution of electrons in energy by random scattering subject to the Pauli exclusion principle. However, this work ignores Coulomb interaction.

By using self-consistent simulations, Reklaitis and Reggiani have analyzed suppression and enhancement of shot noise in GaAs/AlGaAs heterostructure tunnel-barrier diodes [35,79-82]. In this case transport is controlled by tunneling, which, jointly with Coulomb interaction between carriers, is responsible for the different effects observed in the shot-noise behavior. As an example of the type of results that this analysis provides, Fig. 1 shows the Fano factor for the case of one- to four-barrier nonresonant heterostructure diodes with two different contact dopings [82]. A significant shot-noise suppression is found (more pronounced in the case of the low-doped contact), with the Fano factor found to reduce systematically by increasing the number of barriers, besides exhibiting a significant voltage dependence. The presence of inelastic scattering through optical-phonon emission combined with tunneling is the key element to explain the suppression mechanism. Shot-noise

enhancement can also be found in these type of heterostructure diodes. Reklaitis and Reggiani propose a mechanism of enhancement for the case a single-barrier heterostructure, like that shown in Fig. 2, based on the positive feedback between (strong-enough) space charge and the energy dependence of single electron tunneling probability, which leads to a super-Poissonian pulse distribution [35]. This is illustrated in Fig. 3, where the Fano factor is found to increase with the applied voltage, reaching values as high as 7 for appropriate biasing conditions, for then decreasing at the highest voltages when the barrier becomes transparent. Remarkably, when Coulomb interaction is frozen (space-charge effects are neglected) no enhancement is observed and full shot noise is always found.

In this review chapter we will focus on the calculations performed by our group in the University of Salamanca (Spain) for the case of homogeneous structures in the presence of space charge under different transport regimes [84-96]. Thus, the case of ballistic transport, both for nondegenerate and degenerate injection, will be initially analyzed [84-86,88,90,92]. We will after include the presence of scattering (both elastic and inelastic) to study the crossover from ballistic to diffusive regime [87,89,91]. The diffusive regime with several energy dependences of the scattering time will be subsequently investigated [89,91,93,94]. In all the previous regimes, mainly shot-noise suppression of different intensity is found. To finish, we will address a regime where an increase of the noise is predicted, even reaching enhanced shot noise: quasiballistic transport in the presence of electron traps [96].

We must remark here that the results on shot noise obtained by MC simulations have motivated the development of several analytical theories trying to explain them [68-70,72,74,76,77]. In some sense, MC calculations have played the role of numerical experiments needing a physical analytical interpretation, thus leading to the advance of basic theory in the field of mesoscopic shot noise.

2. PHYSICAL MODEL

In this section we describe the type of structures where shot noise is analyzed, the physical model used in the simulations to include all the different mechanisms controlling transport, and the procedures for the noise calculation.

2.1. Simulated structure

As prototype for our analysis we consider the simple structure shown in Fig. 4, formed of a lightly-doped semiconductor active region of length L sandwiched between two heavily-doped contacts (of the same semiconductor) which act as thermal reservoirs by injecting carriers, with appropriate statistics, into the active region. The structure is assumed to be sufficiently thick in transversal directions to allow a one-dimensional electrostatic treatment. The doping of the contacts n_c is always taken to be much higher than that of the active region N_D. Hence, when a voltage U is applied to the structure, all the potential drop is assumed to take place inside the active region between positions $x = 0$ and $x = L$. The contacts are considered to remain always at thermal equilibrium. Scattering mechanisms and trapping-detrapping processes will be considered in the active region following the models described in next subsections.

2.2. Monte Carlo method

The transport analysis is carried out by simulating the carrier dynamics only in the active region of the structure. The influence of the contacts is included in the simulation by means of a stochastic injection rate taking place at positions $x = 0$ and $x = L$, whose statistics depends on the degenerate or nondegenerate character of contacts. Under the action of a dc applied voltage U, the carrier dynamics is simulated by an ensemble MC technique self-consistently coupled with a PS [98]. The simulation is one-dimensional in real space (the

Poisson equation is solved only in the direction of the applied voltage) and three-dimensional in momentum space (unless otherwise indicated).

The carriers move inside the active region according to the classical equations of motion with a constant effective mass. Under the condition of a constant applied voltage between the contacts, the instantaneous current in a one-dimensional structure is given by [78]:

$$I(t) = \frac{q}{L}\sum_{i=1}^{N(t)} v_i(t) \quad (1)$$

where $N(t)$ is the number of particles inside the structure and $v_i(t)$ the velocity component of the *i-th* particle along the field direction. It must be stressed that, although not explicitly appearing in Eq. (1), the displacement current is implicitly taken into account by constant voltage conditions [78].

To better analyze the importance of Coulomb correlations we provide the results for two different simulation schemes. The first one involves a *dynamic* PS, which means that any fluctuation of space charge due to the random injection from the contacts causes a redistribution of the potential, which is self-consistently updated by solving the Poisson equation at each time step during the simulation to account for the fluctuations associated with the long-range Coulomb interaction. The second scheme uses a *static* PS that calculates only the stationary potential profile; i.e., once the steady state is reached, the PS is switched off, so that carriers move in a *frozen* non-fluctuating electric field profile. Both schemes are checked to give exactly the same steady-state spatial distributions and total current, but the noise characteristics and the statistical distributions of transmitted carriers are different. Of course, the PS scheme that is physically correct is the dynamic one. The static case is just used to evaluate quantitatively the influence of the self-consistent potential fluctuations on the total noise.

For the calculations we have typically considered a structure where L=200 nm, $T = 300$ K, $m = 0.25m_0$ and $\varepsilon = 11.7$ (relative dielectric constant). Several values of contact doping n_c (and therefore several injection rates Γ), from 10^{13} to 4×10^{17} cm^{-3} in the nondegenerate case and higher in the degenerate case (1.37×10^{20} cm^{-3}), will be analyzed, thus leading to different levels of space-charge effects inside the active region. These effects will be characterized by the dimensionless parameter $\lambda = L/L_{Dc}$, with L_{Dc} the Debye length associated with the carrier concentration at the contacts [88]. Accordingly, λ will vary from very low values (0.15 for $n_c = 10^{13}$ cm^{-3}), for which space-charge effects are negligible, to high values (30.9 for $n_c = 4\times10^{17}$ cm^{-3}, and 90.95 for $n_c = 1.37\times10^{20}$ cm^{-3} and L=100 nm), which imply a significant action of electrostatic screening.

Typically, 100 to 200 cells in real space are used to solve the Poisson equation. The time step is always lower than 2 fs, its value depending on the time scale of the mechanism with shortest characteristic time among those involved in the transport properties of the structures (scattering time, transit time, dielectric relaxation time, etc.). The average number of simulated particles in the active region depends on the working conditions and statistical resolution required in the calculations; it may range between 100 and 20000 particles. As test of numerical reliability, we systematically check that by reducing the time step, or by increasing the number of meshes and carriers, the results remain the same.

2.3. Contact modeling

The modeling of contacts is crucial in the analysis of shot noise in mesoscopic devices, especially in the case when the carrier motion in the active region of the structures is ballistic, and the noise originates from carrier injection. To provide a complete model for the contact injection taking place in our structures at positions $x = 0$ and $x = L$ (see Fig. 4), and define the associated sources of randomness in the carrier flux, we have to specify the

velocity (or momentum) distribution of the injected carriers $f_{inj}(\mathbf{v})$, the injection rate Γ and its statistical properties. These features of the contacts are different depending on their nondegenerate or degenerate character.

2.3.1. *Nondegenerate contacts*

Let us consider the process of electron injection from contact 1 into the active region at $x = 0$ (see Fig. 4). According to the equilibrium and nondegenerate conditions at the contacts, the injected carriers follow a Maxwellian distribution weighted by the velocity component v_x normal to the surface of the contact

$$f_{inj}(\mathbf{v}) = v_x f_{MB}(\mathbf{v}), \tag{2}$$

where $f_{MB}(\mathbf{v})$ is the Maxwell-Boltzmann distribution at the lattice temperature. The injection rate Γ, i.e., the number of carriers that are entering the sample per unit time, is given by

$$\Gamma = n_c \bar{v}_+ S , \tag{3}$$

where S is the cross-sectional area of the device, and

$$\bar{v}_+ = \int_0^\infty \int_{-\infty}^\infty \int_{-\infty}^\infty f_{inj}(\mathbf{v}) dv_x dv_y dv_z = \sqrt{\frac{k_B T}{2\pi m}} . \tag{4}$$

This injection rate is considered to be independent of the applied voltage. Due to the very high value of n_c as compared with the sample doping, any possible influence of the applied voltage (especially for high values) on the contact and, consequently, on the injection rate, is neglected. Therefore, the maximum current that a contact can provide I_S (saturation current) will then be given by $I_S = q\Gamma$.

In accordance with the nondegenerate character of contacts, the injection rate follows a Poissonian statistics. Thus, the time between two consecutive electron injections t_{inj} is generated with a probability per unit time given by

$$P(t_{inj}) = \Gamma e^{-\Gamma t_{inj}} . \tag{5}$$

We note that the carrier number in the sample $N(t)$ is a stochastic quantity. Electrons are injected at $x=0$ and $x=L$ into the active region of the structure following the above fluctuating rate. When a carrier exits through any of the contacts it is canceled from the simulation statistics, which accounts only for the carriers that are inside the active region at the given time *t*. Thus $N(t)$ fluctuates in time due to the random injection from the contacts (and also to possible trapping-detrapping processes) and we can evaluate both the time-averaged value $\langle N \rangle$ and its fluctuations $\delta N(t) = N(t) - \langle N \rangle$.

Unless otherwise indicated, calculations in the case of nondegenerate contacts will make use of the Poissonian-Maxwellian injection model previously described, which is physically plausible under nondegenerate conditions. However, to analyze the influence of the contact injecting statistics on the noise behavior, alternative models will also be used. In particular, for the injected carriers we consider: (i) fixed velocity instead of Maxwellian distribution and, (ii) uniform-in-time instead of Poissonian injection. In case (i) we take the same injection rate Γ as in the basic model, but all carriers are injected with identical *x*-velocity $v_x = \sqrt{\pi k_B T / 2m}$, which corresponds to the average velocity of the injected electrons when they follow a Maxwellian distribution. In case (ii) carriers are injected into the active region equally spaced in time at intervals of $1/\Gamma$.

2.3.2. *Degenerate contacts*

In this case, electron injection must be consistent with Fermi statistics, and thus it is necessary to consider the specific population of the different energy levels at the contacts [92]. Due to the Pauli principle, the instantaneous occupancy of an incoming electron state $\mathbf{k} = (k_x, k_y, k_z)$ with energy $\varepsilon_{\mathbf{k}} = \hbar^2 \mathbf{k}^2 / 2m$ impinging on the boundary between an ideal thermal reservoir and the active region fluctuates in time obeying a binomial distribution [99,100] with a probability of success given by $f(\varepsilon_{\mathbf{k}}) = \{1 + \exp[(\varepsilon_{\mathbf{k}} - \varepsilon_F)/k_B T]\}^{-1}$ (with ε_F

the Fermi level at the contacts), which corresponds to the average occupancy of such state according to the Fermi-Dirac distribution. This statistics is implemented in the MC simulation of the contact injection by means of a discretization of **k**-space and the use of the rejection technique [92].

Momentum space is divided into a grid of meshes with volume $\Delta k_x \Delta k_y \Delta k_z$ around discrete values of **k**, with energy $\varepsilon_{\mathbf{k}}$. For each of these meshes, the number of incoming electron states per unit time with wave vector **k** is given by

$$\xi_{\mathbf{k}} = g_{\mathbf{k}} v_{x\mathbf{k}} \Delta k_x \Delta k_y \Delta k_z = 1/(4\pi^3)(\hbar k_x / m) \Delta k_x \Delta k_y \Delta k_z , \qquad (6)$$

where $g_{\mathbf{k}}$ is the density of states in momentum space and $v_{x\mathbf{k}}$ the velocity component normal to the boundary contact/active region. These incoming states have a probability of occupancy $f(\varepsilon_{\mathbf{k}})$. In the simulation, at each time interval of duration $1/\xi_{\mathbf{k}}$ an attempt to introduce an electron with wave vector **k** takes place. At this point a random number r uniformly distributed between 0 and 1 is generated, and the attempt is considered successful only if $r < f(\varepsilon_{\mathbf{k}})$. This rejection-technique scheme properly accounts for the injection statistics at each mesh in **k**-space [92]. As limiting cases, when $\varepsilon_{\mathbf{k}} - \varepsilon_F << -k_B T$, $f(\varepsilon_{\mathbf{k}}) \cong 1$ and the injection statistics of the corresponding **k**-state is uniform in time. On the contrary, when $\varepsilon_{\mathbf{k}} - \varepsilon_F >> k_B T$, $f(\varepsilon_{\mathbf{k}}) << 1$ and the injection statistics is Poissonian.

For a completely degenerate reservoir, in every mesh of energy up to ε_F an electron is injected every time interval $1/\xi_{\mathbf{k}}$, and there is no need of the rejection technique. This is the case of the simple contact modeling used in [83]. For a nondegenerate reservoir, since $f(\varepsilon_{\mathbf{k}}) << 1$ for all **k**-states, it is possible (and more convenient from a computational point of view) to use a global Poissonian statistics as that described previously, even if this general injection model is also valid and generates exactly the same statistics.

To show the validity of this injection scheme to describe the injection statistics from nondegenerate to degenerate conditions, Fig. 5 shows the low-frequency value of the current spectral density S_I (see section 2.6 for the details about its calculation) at equilibrium, normalized to $2qI_S$, as a function of the degeneracy factor $\varepsilon_F / k_B T$ (with ε_F measured with respect to the bottom of the conduction band), in the case of a conductor one-dimensional in momentum space and in the absence of Coulomb interaction. $I_S = q\int_0^\infty g_k v_k f(\varepsilon_k)\mathrm{d}k$ is the saturation current, i.e., the maximum current the contact can provide. In the classical limit, corresponding to large negative values of the degeneracy factor, $S_I = 4qI_S$. Here all carriers contribute to the current noise and S_I is just the sum of the full shot noise related to the two opposing currents I_S injected by the contacts [101]. Under degenerate conditions, corresponding to positive values of the degeneracy factor, S_I decreases with respect to $4qI_S$ in accordance with the suppression factor $k_B T / \varepsilon_F$ related to Fermi correlations at the reservoirs [9,101]. Here, as known, only carriers around the Fermi level contribute to the noise. As shown by the figure, the agreement between the results of the MC simulations and the analytical expectations in the nondegenerate and degenerate limits is excellent, thus indicating that the carrier injecting statistics achieved with the proposed model is valid in both regimes. Moreover, this scheme is able to describe correctly degenerate conditions at $T \neq 0$ and the crossover between classical and degenerate statistics.

Finally, we want to remark that in the models previously described we are assuming that the doping of the contacts is so high as compared with that of active region that all the built-in effects associated with the diffusion of carriers around the contacts take place exclusively in the active region. As a consequence, the models are not fully consistent, since the effects related to the possible fluctuations of the concentration at the contacts are not taken into account. In any case we are mostly interested in the low-frequency region of the

noise spectrum, and these effects are expected to appear at very high frequencies, beyond the cutoff of shot noise.

2.4. Scattering mechanisms

Elastic and inelastic isotropic scattering mechanisms are introduced (separately) in the simulation by means of a characteristic scattering time τ. In the case of inelastic collisions, the carrier is thermalized after each scattering event. Initially τ will be considered as energy independent, and its value will be appropriately varied (from 10^{-11} to 10^{-15} s) to cover both the ballistic and diffusive transport regimes. The transition between both regimes will be characterized by the ratio between the carrier mean free path ℓ (estimated as $v_{th}\tau$, with $v_{th} = \sqrt{2k_B T / \pi m}$ the carrier thermal velocity) and the sample length *L*, so that $\ell / L >> 1$ and $\ell / L << 1$ correspond to the ballistic and diffusive limits, respectively.

In a second step we will include the energy dependence of the scattering time in the case of elastic collisions. To this end we take a power-law dependence of the type $\tau(\varepsilon) = \tau_0 \varepsilon^{\alpha}$ and perform calculations for values of α ranging between –2 and 3/2. Appropriate values of τ_0 must be chosen to ensure diffusive transport in the wide range of electron energies found in the simulations and to make computer times affordable. Formally, one can analyze any value of α [102], however, only some of the values considered here correspond to real cases of elastic scattering mechanisms, like short-range impurity scattering or scattering with acoustic phonons by deformation potential ($\alpha = -1/2$), neutral impurities ($\alpha = 0$), and acoustic piezoelectric phonons ($\alpha = 1/2$) [69,70,72,77].

2.5. Trapping-detrapping processes

In section 3.4 we will include the presence of electrons traps in the active region of a structure that otherwise would be ballistic. We will consider that a single type of electron traps, initially neutral and empty, at energy E_n below the bottom of the conduction band is

present in the active region. We use the following simplified model [103,104] for the trapping-detrapping processes in order to detect plainly their influence on the noise. It is assumed that the traps only interact with electrons in the conduction band. Two time constants are involved in these processes: the recombination time τ_r (average *free time* of an electron), and the generation time τ_g (average *captured time* of an electron). These times are respectively given by the expressions [105]: $1/\tau_r = v_{th}s(N_t - n_t)$, where s is the capture cross section of the traps, N_t the density of electron traps, and n_t the density of trapped electrons; and $1/\tau_g = \upsilon_0 \exp(-qE_n / k_B T)$, where υ_0 is a vibration frequency. As long as $n_t << N_t$, and N_t is uniform in the active region (as it is assumed in our model), τ_r can be considered to be independent of the electron position. To evidence more clearly the associated effects on the noise, as first approximation τ_r is also considered as energy independent [103]. Once a carrier is captured, it remains trapped (with null velocity) until it is released, with its velocity components randomly determined according to a Maxwellian distribution at the lattice temperature. Traps become negatively charged when electrons are captured. The values of τ_r and τ_g considered in our calculations are τ_r =20 ps and τ_g ranging between 1 and 7.5 ps. These times, being short enough to bring about affordable computation times [104], are still within the range of real values [105].

2.6. Noise calculation

In our analysis of shot noise we are mostly interested in calculating the Fano factor. To this end, from the simulation we firstly evaluate the autocorrelation function of current fluctuations, $\delta I(t) = I(t) - \langle I \rangle$, which under stationary conditions is given by

$$C_I(t) = \langle \delta I(t')\delta I(t'+t) \rangle . \qquad (7)$$

Fourier transformation of $C_I(t)$, provides the spectral density

$$S_I(f) = 2\int_{-\infty}^{\infty} C_I(t)\mathrm{e}^{i2\pi ft}\, dt \; . \tag{8}$$

The Fano factor is then obtained as

$$\gamma = \frac{S_I}{2qI} \; . \tag{9}$$

Once a sufficiently long sequence of current values $I(t)$ is obtained from the simulation, the time average of the current $\langle I \rangle$ is determined and the current autocorrelation function is easily calculated following Eq. (7). To clarify the role of different contributions to the current noise we decompose the current autocorrelation function and the spectral density into three main contributions as

$$C_I(t) = C_V(t) + C_N(t) + C_{VN}(t) \, , \quad S_I(f) = S_V(f) + S_N(f) + S_{VN}(f) \, , \tag{10}$$

respectively given by

$$C_V(t) = (q/L)^2 \langle N \rangle^2 \langle \delta v(t')\delta v(t'+t) \rangle \, , \tag{11a}$$

$$C_N(t) = (q/L)^2 \langle v \rangle^2 \langle \delta N(t')\delta N(t'+t) \rangle \, , \tag{11b}$$

$$C_{VN}(t) = (q/L)^2 \langle v \rangle \langle N \rangle \langle \delta v(t')\delta N(t'+t) + \delta N(t')\delta v(t'+t) \rangle \; . \tag{11c}$$

In the above equations $C_V(t)$ is associated with fluctuations in the mean carrier velocity, $C_N(t)$ with fluctuations in the carrier number, and $C_{VN}(t)$ with their cross correlation [78,98].

To distinguish between the results obtained by using static and dynamic PS schemes, we will denote the corresponding current spectral densities as S_I^s and S_I^d, respectively.

3. RESULTS

In this section we present the results corresponding to the shot-noise analysis under different transport regimes.

3.1. Ballistic regime

Initially we will consider the case when carriers move in the active region without undergoing any scattering mechanism. In this regime, shot-noise suppression will be found.

3.1.1. *Nondegenerate contacts*

In this case the injection statistics is Poissonian, as described in section 2.3.1. Several values of n_c (and therefore several injection rates Γ) are considered. As n_c increases, space-charge effects become more and more relevant, the dimensionless parameter λ being the indicator of their importance. In particular, we have considered the following values of n_c (in cm^{-3}, with the corresponding λ): 10^{13}, $\lambda = 0.15$; 2×10^{15}, $\lambda = 2.18$; 10^{16}, $\lambda = 4.88$; 2.5×10^{16}, $\lambda = 7.72$; 10^{17}, $\lambda = 15.45$; 4×10^{17}, $\lambda = 30.90$.

a. *Static characteristics*

Figure 6 shows the electron concentration and potential profiles inside the active region for several values of λ under thermodynamic equilibrium conditions. As λ increases, the higher injection rate at the contacts leads to a larger carrier concentration inside the sample and to a stronger nonuniformity of its spatial distribution, showing maximum values at the contacts due to the electron injection and decaying toward the middle of the sample. Accordingly, the potential profile exhibits a minimum in the middle of the active region of amplitude U_m that increases with λ, thus evidencing the stronger influence of space charge. For the highest value of λ, U_m reaches $4\,k_BT/q$. When a positive voltage U is applied to the anode (contact 2 in Fig. 4), the minimum is displaced toward the cathode (contact 1) while its

amplitude decreases, as shown in Fig. 7(a) for the case of $\lambda = 30.9$. Physically, this minimum provides a potential barrier for the electrons moving between the contacts. The injected electrons not having sufficient energy to pass over the barrier are reflected back to the contacts. The mechanism of shot-noise suppression is based on the fact that the barrier height and, as a consequence, the transmission through it, fluctuate with the passage of electrons and modify the Poissonian statistics of the incoming carriers. Of course, the fluctuations of the barrier are more important when strong space-charge effects are present (high λ).

The dependence of the current *I* on the applied voltage *U* for different values of λ is shown in Fig. 7(b). The current flowing through the diode reflects the evolution of U_m with *U* shown in Fig. 7(a). It consists of two opposite contributions $I = I^+ - I^-$, I^+ flowing from the cathode to the anode and I^- in the opposite direction. Since the injected carriers follow a Maxwellian distribution and move ballistically, the value of both currents depends exponentially on the amplitude of the potential barrier that the electrons injected at each contact find when moving towards the opposite one. For I^+ the amplitude is just U_m and for I^- is $U_m + U$. Therefore

$$I^+ = I_S \exp\left[-qU_m / k_B T\right], \tag{12a}$$

$$I^+ = I_S \exp\left[-q(U_m + U) / k_B T\right]. \tag{12b}$$

As a result, while the presence of the minimum U_m persists, the current increases practically linearly with *U*, up to a certain value of the external bias U_{sat} for which the barrier vanishes, so that all the electrons injected at the cathode can reach the anode, the current saturates and becomes independent of the bias. As λ is increased, the barrier induced by the space charge is more important, the current is lower and the saturation takes place for higher applied voltages. In the case of $\lambda = 0.15$, when space-charge effects are negligible, the *I-U* curve

corresponds exactly to that obtained in [106] within an approach where Coulomb correlations are disregarded.

Figure 8 shows the profiles of the electron concentration *n*, carrier average energy ε and velocity *v* along the active region of the structure with $\lambda = 30.9$ for several values of *U*. When a voltage is applied to the right contact, the symmetry of the carrier concentration profile at equilibrium is clearly destroyed in order to ensure current conservation through the sample. Accordingly, near the anode, where *v* reaches the highest values, *n* takes the lowest ones. The extension of the region near the anode contact where the carrier concentration is high and both the velocity and energy are low decreases at increasing applied voltages. In this region, most of the carriers are thermal electrons proceeding from the right contact that are reflected back to the anode by the opposite electric field. The greater the applied voltage, the higher the opposite field and the shorter the distance they penetrate before being reflected. When *U* is high and the potential barrier is near to disappear or just vanished [see Fig. 7(a), $U = 40$, 80 $k_B T / q$] the energy increases systematically along the sample up to a maximum value close to qU near the anode contact, as expected from the ballistic transport inside the sample.

We remark that all the results presented in this section are independent of the PS scheme used for the calculations.

b. *Shot-noise suppression*

Once the static characteristics are analyzed, the shot-noise suppression effects can be more easily understood. The difference between the results of the static and dynamic PS schemes will evidence the influence of the dynamic fluctuations of the potential on the noise characteristics of the structures. Firstly we will analyze which are the statistical properties of the transmitted carriers to check if they are temporally correlated. To address this question we register at the receiving contact the times of passage of electrons that were injected at the

cathode. These are the only electrons contributing to the low-frequency current noise once $qU >> k_B T$. With this procedure we are able to study how the carrier statistics imposed at $x = 0$ (in our case Poissonian) has been modified when reaching the anode. From the different times of arrival registered, we calculate the distribution function $P_n(t)$, which is the probability of detecting *n* electrons during the observation time interval *t*. For a Poissonian process all time occurrences are statistically independent, which leads to the simple formula

$$P_n(t) = \frac{(\Gamma_e t)^n}{n!} \mathrm{e}^{-\Gamma_e t}, \quad n = 0, 1, 2, \ldots, \tag{13}$$

where Γ_e is the rate density of events. Distribution (13) is characteristic of uncorrelated transport and is tested to correctly describe the carrier statistics at the injecting contact (at $x = 0$). The distribution of carriers at the receiving contact depends crucially on the PS scheme (see Fig. 9, corresponding to $U = 40 k_B T / q$ and $\lambda = 30.9$). For the static PS $P_n(t)$ is perfectly fitted by the same Poissonian formula (13) as for the injected carriers, but with a smaller value of the rate density $\Gamma_e = \kappa\Gamma$, with $\kappa \approx 0.65$. This reduction is caused by the part of injected carriers that is reflected by the potential barrier back to the contact (in fact, the current for the present applied voltage is $I = \kappa I_S$). In contrast, for the dynamic PS the distribution function no longer obeys the formula (13), and becomes sub-Poissonian. The following differences between the dynamic and static PS are observed: (i) for each $n > 1$ the maximum of the distribution is shifted to longer *t*; (ii) the probability distribution is narrowed; (iii) the higher the index *n*, the more the dynamic case deviates from the static one, the distribution profiles becoming more symmetrical and closer to a Gaussian shape. We remark that the difference at point (ii) can be interpreted as a *motional squeezing of electron number* and corresponds to a higher regularization of the carrier passage due to correlations among electrons.

Let us investigate how this modification of the carrier passage statistics due to Coulomb correlations affects the behavior of shot noise in the structures. Fig. 10 shows the low-frequency value of the spectral density of current fluctuations S_I normalized to $2qI_S$. This normalization is performed in order to compare the results for different values of Γ (different n_C and λ). We provide the results for both the static and dynamic PS schemes. In the static case, by increasing the applied voltage U we always obtain an excellent coincidence with the well-known formula used to describe the crossover from thermal to shot noise when carrier correlations play no role (represented in the figure by dashed lines) [2]:

$$S_I^s = 2q\left(I^+ + I^-\right) = 2qI \coth\left(qU / 2k_B T\right) \tag{14}$$

where $I = I^+ - I^-$ is the total current flowing through the diode, as previously explained. This agreement supports the validity of the simulation scheme used for the calculations. For $qU << k_B T$, $I^+ \sim I^-$, thermal noise is dominant and $S_I^s \approx 4qI_S \exp\left[-qU_m / k_B T\right]$. Therefore, for the lowest value of λ (when space charge is negligible and $U_m \to 0$) $S_I^s \to 4qI_S$, while as λ increases U_m becomes significant and S_I^s decreases. When $qU > k_B T$, $I^+ >> I^-$, the transition from thermal to shot noise takes place and $S_I^s \approx 2qI^+$. And finally, for the highest values of $U > U_{sat}$, saturation occurs, U_m vanishes and $S_I^s \approx 2qI_S$.

For the lowest values of λ no difference between the dynamic and static cases is obviously detected. However, for higher λ, when space-charge effects become significant, the picture is drastically different for the dynamic case. Starting from $qU \sim k_B T$, S_I^d, instead of increasing, decreases until the proximity of saturation, where it exhibits a minimum before jumping to the saturation value. Under saturation, the results for both schemes coincide (no barrier modulating the current) and full shot noise $S_I^d = S_I^s = 2qI_S$ is recovered. When compared with the static case the noise suppression is stronger for higher λ (more important space-charge effects).

This behavior of S_I^d is illustrated in Fig. 11, where the Fano factor γ is shown as a function of U for different λ. The sequence thermal noise ($qU < k_BT$), suppressed shot noise ($k_BT < qU < qU_{sat}$), full shot noise ($U > U_{sat}$) behavior is clearly evidenced. The curves corresponding to the different structures only differ in the suppressed shot noise range. For the lowest values of λ, when no suppression takes place, $\gamma = \coth(qU/2k_BT)$. Shot-noise reduction becomes more pronounced and covers a wider range of voltages as λ increases (e.g., for $\lambda = 30.9$ it is $\gamma = 0.045$). Thus, the present self-consistent approach predicts values of the Fano factor much lower than those of previous analytical models [107] where the dependence of the potential minimum and its position on the applied voltage was not taken into account. In principle, the value of γ has no lower limit. By enlarging λ, γ can reach values as low as desired. However, by increasing the device length (or the lattice temperature) the carrier transport actually goes from ballistic to diffusive regime and the action of Coulomb interaction on shot noise changes a lot, as we will see in section 3.2. Moreover, when the carrier concentration at the contacts is increased, so that the electron gas becomes degenerate, Fermi correlations between carriers act as an additive contribution to shot-noise suppression, as we will show in the case of degenerate contacts.

To better understand the physical reason of shot-noise suppression in the present ballistic structures, Fig. 12 reports the decomposition of S_I into the three additive contributions S_V, S_N and S_{VN} [Eqs. (11)] for λ=7.72 and different values of U. Both S_N and S_{VN} vanish at equilibrium ($U \to 0$), since they are proportional to $\langle v \rangle^2$ and $\langle v \rangle$ respectively, and $\langle v \rangle \to 0$. Thus, for small biases ($qU << k_BT$) $S_I \sim S_V$, which means that the current noise is thermal noise associated with velocity fluctuations and it is governed by the Nyquist theorem $S_I \approx 4k_BTG$, with $G = (dI/dV)_{V=0}$ the static conductance. In this case the results for the static [Fig. 12(a)] and dynamic [Fig. 12(b)] schemes evidently coincide. However,

starting from $qU \sim k_B T$ the difference between the two schemes becomes relevant. For the dynamic case, S_{VN} is negative, while for the static case it is positive. Furthermore, for the current fluctuations calculated using the self-consistent potential, S_N^d and S_{VN}^d are of opposite sign and compensate each other, so that S_I^d approximately follows S_V^d as long as the current is space-charge controlled. As a consequence, the current noise, which now corresponds to shot noise, is considerably suppressed below the value $2qI$ given by the static case. This result reflects the fact that as the carriers move through the active region, the dynamic fluctuations of the electric field modulate the transmission through the potential minimum and smooth out the current fluctuations imposed by the random injection at the contacts. Therefore, the coupling between number and velocity fluctuations induced by the self-consistent potential fluctuations is the main responsible, through S_{VN}^d, for the shot-noise suppression. This velocity-number coupling becomes especially pronounced just before current saturation ($U \approx 7\, k_B T / q$), when the potential minimum is close to vanish completely ($U_m \to 0$) and the fluctuations of the potential barrier modulate the transmission of the most populated states of injected carriers (the low-velocity states). Under saturation conditions space-charge effects do not modulate the random injection (no potential minimum is present) and again both dynamic and static cases provide the same additive contributions and total noise ($2qI_S$).

The MC results shown in this section have motivated the development of analytical theories able to explain them. Many of the low-frequency results reported here have been reproduced and extended by general self-consistent theories in the works by Bulashenko *et al.* [68,74], also for the case of non-Poissonian injection statistics [75].

c. *Frequency dependence of noise*

One of the advantages of the MC technique is the possibility to investigate the time and frequency (beyond low-frequency) dependence of current fluctuations, that we analyze here in the case of ballistic transport in the presence of space charge. Figure 13 reports the autocorrelation function of current fluctuations $C_I(t)$ and the corresponding spectral density $S_I(f)$ under thermal-equilibrium conditions at increasing values of λ, thus evidencing the influence of space-charge effects. These results are independent of the PS scheme used. For low values of λ, when U_m is negligible, $C_I(t)$ recovers the typical dependence obtained analytically for the ballistic case when Coulomb interaction is neglected [108,109]. At increasing values of λ, the shape of $C_I(t)$ changes and tends to exhibit a behavior determined by two processes with different (short and long) characteristic times. The short time is related to the injected carriers that are not able to pass the potential barrier and return back to the contacts (*returning carriers*). Here, the greater the value of λ, the higher the amplitude of U_m, and the shorter the characteristic *returning time*, as it is shown in Fig. 13(a). The long characteristic time in $C_I(t)$ is associated with the *passing carriers*, whose longitudinal velocity component is significantly reduced while crossing the barrier region. The difference between these two times (and the fraction of reflected/transmitted carriers) becomes more pronounced at high values of U_m. Accordingly, the slopes of $C_I(t)$ related to each time are more easily identified at increasing values of λ. The corresponding spectral densities [Fig. 13(b)] reflect the behavior of $C_I(t)$ previously described, by exhibiting higher cutoff frequencies as λ increases and characteristic structures in the cutoff region related to the transit time through the sample.

To illustrate how the noise changes under far-from-equilibrium conditions, Fig. 14 shows $C_I(t)$ and $S_I(f)$ calculated with the dynamic PS for the case of $\lambda = 7.72$ at several voltages. Starting from the standard shape of equilibrium conditions, $C_I(t)$ tends to exhibit a

triangular shape, more pronounced as the applied voltage increases. This triangular shape is typical of a constant velocity emitter with all the electrons reaching the opposite contact [101]. In our case, electrons are injected at the cathode with a velocity which is Maxwellian distributed, but, due to the acceleration provided by the high electric field in the active region, the transit time of all the carriers becomes practically the same, decreasing with the increase of the applied voltage. The carriers injected at the anode immediately come back to the contact and thus play only an insignificant role at the shortest times. In the spectral density it can be observed that once saturation is reached ($qU > 8k_BT$, see Fig. 10) S_I takes the same value $2qI_S$ at low frequency for the different applied voltages, but the spectra after the cutoff are distinguished by showing smoothed *geometrical resonances* at different characteristic frequencies related to the corresponding transit times.

3.1.2. *Degenerate contacts*

In the case when contacts are degenerate, the injection is no longer Poissonian and the occupation of the different energy levels at the contacts must be taken into account (see section 2.3.2). Thus, a further noise reduction related to Fermi statistics is present [110]. To illustrate this fact we will consider as first example a structure with L=100 nm and $n_C = 1.37 \times 10^{20}$ cm^{-3} ($\varepsilon_F = 15k_BT$). These values lead to λ=90.35, which implies a significant action of space-charge effects in the structure.

The current-voltage ($I - U$) characteristic normalized to the saturation value I_S is reported in Fig. 15. At the lowest voltages a linear behavior is found, while for high voltages near saturation a superlinear behavior close to a $U^{3/2}$-dependence is observed (space-charge limited conditions). The inset of Fig. 15 shows the potential profile along the structure for different applied voltages, which exhibits the characteristic minimum decreasing in amplitude and shifting towards the cathode as U increases. The amplitude of this minimum U_m is

reported in the main figure as a function of the applied voltage. For the values used here $U_m = 19.44\, k_B T/q$ at equilibrium ($U = 0$) and $U_m = 0$ for $U \geq 2500\, k_B T/q$.

When using the static PS, no correlation among carriers takes place in the active region, and the only source of suppression is the Fermi statistics electrons obey at the contacts. Once the value of U_m is known from the simulation, the Fermi suppression factor can be calculated analytically as $\gamma_F = S_I^s / 2qI$, with the low-frequency *static* current spectral density S_I^s and the current *I* given by

$$S_I^s = \int_{qV_m}^{\infty} S_{I_C}(\varepsilon_x)\, d\varepsilon_x + \int_{q(V_m+U)}^{\infty} S_{I_C}(\varepsilon_x)\, d\varepsilon_x, \tag{15}$$

$$I = \int_{qV_m}^{\infty} I_C(\varepsilon_x)\, d\varepsilon_x - \int_{q(V_m+U)}^{\infty} I_C(\varepsilon_x)\, d\varepsilon_x, \tag{16}$$

where ε_x is the longitudinal energy, and $I_C(\varepsilon_x)d\varepsilon_x$ and $S_{I_C}(\varepsilon_x)d\varepsilon_x$ are, respectively, the current associated with electrons injected between ε_x and $\varepsilon_x + d\varepsilon_x$ and the low-frequency spectral density of its fluctuations, which are given by [76,84,110]

$$I_C(\varepsilon_x) = \frac{qmA}{2\pi^2\hbar^3} \int_0^{\infty} f(\varepsilon_x + \varepsilon_t) d\varepsilon_t\,, \tag{17}$$

$$S_{I_C}(\varepsilon_x) = 2q\frac{qmA}{2\pi^2\hbar^3} \int_0^{\infty} f(\varepsilon_x + \varepsilon_t)\left[1 - f(\varepsilon_x + \varepsilon_t)\right] d\varepsilon_t = 2qI_C(\varepsilon_x)\left[1 - \frac{\int_0^{\infty} f^2(\varepsilon_x + \varepsilon_t) d\varepsilon_t}{\int_0^{\infty} f(\varepsilon_x + \varepsilon_t) d\varepsilon_t}\right], \tag{18}$$

where ε_t is the transversal electron energy and $f(\varepsilon) = \{1 + \exp[(\varepsilon - \varepsilon_F)/k_B T]\}^{-1}$ the Fermi-Dirac distribution. The suppression effect associated with Fermi correlations, which takes place through the injecting statistics, is clearly observed in Fig. 16, which shows $I_C(\varepsilon_x)$ and $S_{I_C}(\varepsilon_x)$ as a function of ε_x. Carriers injected with $\varepsilon_x >> \varepsilon_F$ obey Poissonian statistics and exhibit full shot noise $S_{I_C}(\varepsilon_x) = 2qI_C(\varepsilon_x)$. By contrast, carriers injected with $\varepsilon_x << \varepsilon_F$ exhibit a significantly suppressed shot noise $S_{I_C}(\varepsilon_x) < 2qI_C(\varepsilon_x)$. Fig. 17 shows an excellent agreement between theoretical and simulated values of γ_F. At low *U*, when $qU < k_B T$,

thermal noise is dominant and $\gamma_F > 1$. For intermediate values of *U*, when $k_B T < qU$ and $qU_m > \varepsilon_F$, *I* is carried by Poissonian carriers with $\varepsilon_x > \varepsilon_F$ at the tail of Fermi distribution (low-occupation states) and thus $\gamma_F = 1$. At higher *U*, when $qU_m < \varepsilon_F$, the contribution to *I* of carriers injected with sub-Poissonian statistics ($\varepsilon_x < \varepsilon_F$, high-occupation states) becomes more and more important and, accordingly, γ_F decreases, until saturating for $U > U_{sat}$ ($qU_m = 0$) at a value $\gamma_F = 2k_B T / \varepsilon_F$ [76].

When using the dynamic PS, as carriers move through the active region the temporal fluctuations of the electric field modulate the transmission over the potential minimum and thus, in addition to Fermi suppression, a further noise reduction due to Coulomb correlations takes place. Since the two suppression mechanisms are independent, the low-frequency *dynamic* spectral density S_I^d can be expressed as $S_I^d = \gamma 2qI = \gamma_F \gamma_C 2qI$, where $\gamma = \gamma_F \gamma_C$ is the total shot-noise suppression factor (or Fano factor) and γ_C the Coulomb suppression factor. This factorization is reported in Fig. 17, both as a function of the applied voltage *U* and the amplitude of the potential minimum U_m. At the lowest values of *U*, thermal noise is dominant, and thus $S_I^d = S_I^s$ and $\gamma_C \approx 1$ (absence of Coulomb suppression). Then, at increasing *U*, three different regimes of suppression are identified. The first regime ($k_B T < qU$, $qU_m > \varepsilon_F$) is related only to Coulomb correlations ($\gamma_F = 1, \gamma_C < 1$); here *I* is due to Poissonian carriers (with $\varepsilon_x > \varepsilon_F$) which originate fluctuations of U_m modulating the passage of further electrons, thus leading to increasing Coulomb suppression. The second regime ($qU_m < \varepsilon_F$) is related to both Coulomb and Fermi correlations ($\gamma_F < 1, \gamma_C < 1$). Here, interestingly, γ_C tends to saturate while γ_F keeps decreasing with *U*. This is due to the fact that, as *U* increases, the additional carriers contributing to the current come from the energy region below ε_F ($\varepsilon_x < \varepsilon_F$, characterized by sub-Poissonian statistics) and do not lead to further significant fluctuations of U_m. Finally, in the third regime (under current saturation)

the suppression is constant and only due to Fermi correlations ($\gamma_F = 2k_BT/\varepsilon_F, \gamma_C = 1$). We note the remarkable agreement between the results of the simulation and the analytical expectations for the dependence of γ on U for the intermediate ($1.93k_BT/qU$) and highest (k_BT/qU) values of U [76].

Within our model carriers at the contacts injected at different ε_x-levels are uncorrelated. However electrons in the volume of the conductor are expected to be strongly correlated by Coulomb interaction. To investigate this correlation, responsible for shot-noise suppression, Fig. 18 reports the low-frequency value of the cross-correlation between current fluctuations due to carriers injected with different ε_x at the left contact $S_{I_L}(\varepsilon_x, \varepsilon'_x)$ for $U = 1000\, k_BT/q$. At this high value of the applied voltage ($qU >> \varepsilon_F$) the average current $\bar{I}$ and the low-frequency current spectral density S_I^d are given only by the contributions coming from carriers injected at the left contact with $\varepsilon_x > qU_m$. Thus, the fluctuating current can be written as

$$I(t) = \int_0^\infty I_L(\varepsilon_x, t) d\varepsilon_x , \tag{19}$$

where $I_L(\varepsilon_x, t)d\varepsilon_x$ is the instantaneous current due to carriers injected with ε_x at the left contact. The fluctuations of the current are then given by

$$\delta I(t) = \int_0^\infty \delta I_L(\varepsilon_x, t) d\varepsilon_x = \int_0^\infty \left[I_L(\varepsilon_x, t) - \bar{I}_L(\varepsilon_x) \right] d\varepsilon_x , \tag{20}$$

with $\bar{I}_L(\varepsilon_x)d\varepsilon_x$ the time-average value of $I_L(\varepsilon_x, t)d\varepsilon_x$. The autocorrelation function of current fluctuations can be calculated as

$$C_I(t) = \overline{\delta I(t')\delta I(t'+t)} = \int_0^\infty \int_0^\infty \overline{\delta I_L(\varepsilon_x, t')\delta I_L(\varepsilon'_x, t'+t)}\, d\varepsilon_x d\varepsilon'_x = \int_0^\infty \int_0^\infty C_{I_L}(\varepsilon_x, \varepsilon'_x, t)\, d\varepsilon_x d\varepsilon'_x , \tag{21}$$

with $C_{I_L}(\varepsilon_x, \varepsilon'_x, t)$ the cross-correlation function between current fluctuations due to carriers injected with energies ε_x and ε'_x at the left contact (quantity that can be readily calculated

from the MC simulations), so that the low-frequency current spectral density can be expressed as

$$S_I^d = 2\int_{-\infty}^{\infty} C_I(t)\,dt = \int_0^{\infty}\int_0^{\infty} S_{I_L}(\varepsilon_x,\varepsilon'_x)\,d\varepsilon_x d\varepsilon'_x\,, \tag{22}$$

with

$$S_{I_L}(\varepsilon_x,\varepsilon'_x) = 2\int_{-\infty}^{\infty} C_{I_L}(\varepsilon_x,\varepsilon'_x,t)\,dt\,. \tag{23}$$

Therefore, $S_{I_L}(\varepsilon_x,\varepsilon'_x)$ is the key quantity to evaluate Coulomb correlations between carriers injected at different energies.

In the case of using the static PS carriers in the active region are uncorrelated and thus $S_{I_L}^s(\varepsilon_x,\varepsilon'_x) = S_{I_C}(\varepsilon'_x)\delta(\varepsilon'_x-\varepsilon_x)$, with $S_{I_C}(\varepsilon_x)$ given by Eq. (18). However, with the dynamic PS one obtains the correlations shown in Fig. 18. Carriers injected with $\varepsilon_x > qU_m$, apart from the autocorrelation associated with their injecting statistics $S_{I_C}(\varepsilon'_x)\delta(\varepsilon'_x-\varepsilon_x)$, are only (negatively) correlated with those electrons injected with $\varepsilon'_x \approx qU_m$. This anticorrelation is at the origin of the noise suppression (since it reduces the value of S_I^d), and it is due to the modulation of carrier transmission at $\varepsilon_x \approx qU_m$ caused by the barrier fluctuations induced by electrons passing over the barrier. Remarkably, carriers with $\varepsilon_x \approx qU_m$ are confirmed to be strongly autocorrelated [74,111].

We must point out that the regimes of suppression reported in the previous case are not always found. The behavior of γ_F and γ_C depends on the relative values of L/L_{Dc} and ε_F/k_BT [112]. Fig. 19 shows the different suppression factors as a function of U for a second structure with $L = 50$ nm, $m = 0.066\,m_0$, $n_c = 5\times10^{17}$ cm^{-3} ($\varepsilon_F = 5.08\,k_BT/q$), $\varepsilon = 12.55\,\varepsilon_0$ and $T = 77$ K. For this set of parameters, one obtains that at equilibrium $qU_m \approx \varepsilon_F$ (in contrast with the previous structure where $qU_m > \varepsilon_F$). As a consequence, Fermi suppression is significant in the whole range of applied voltages (once $qU > k_BT$), and there is no regime

like that of the previous case where $\gamma_F = 1$. Here Coulomb suppression is less pronounced, since the range of applied voltages for which the barrier persists is much shorter than in the first example.

The noise properties of ballistic structures with degenerate contacts like those investigated here have been analytically studied in [76] under the limit of “virtual cathode approximation” ($U_m << U < U_{sat}$), obtaining results similar to those of the MC simulations. Only very recently a full theory, able to reproduce both the static and noise MC results in the full range of applied voltages and level of degeneracy, has been developed [112].

3.2. Crossover ballistic-diffusive regime

In this section, elastic and inelastic (thermalizing) isotropic scattering mechanisms are introduced (separately) in the simulations by means of an energy independent relaxation time τ, whose value is appropriately varied (from 10^{-11} to 10^{-15} s) to cover the transition from ballistic to diffusive transport regimes. In this section all the results correspond to the case of nondegenerate contacts and λ=30.9 ($n_C = 4\times10^{17}$ cm^{-3}).

Fig. 20 shows the low-frequency spectral density of current fluctuations S_I normalized to $2qI_S$ as a function of ℓ / L for an applied voltage $U = 40\, k_B T / q$, calculated using static and dynamic PS schemes. The evolution of the current in terms of $2qI$ is also shown. This evolution exhibits two limiting behaviors: a first one ($\ell / L > 10^{-1}$) of saturation typical of ballistic or quasiballistic regime, and a second one ($\ell / L < 10^{-2}$) of linear decrease at decreasing ℓ / L typical of diffusive regime. Both in the elastic and inelastic cases S_I^s, calculated with the static PS, coincides exactly with $2qI$, thus revealing full shot-noise conditions when the dynamic fluctuations of the potential are ignored. On the contrary, with the dynamic PS, S_I^d is systematically lower than $2qI$, thus evidencing a suppression effect. Here, in the ballistic limit elastic and inelastic cases present the same value, the suppression

corresponding to that induced by the barrier fluctuations already reported in Figs. 10 and 11. As the diffusive regime is approached, the suppression remains active, more pronounced in the inelastic case, being related to the joint action of the Coulomb repulsion and the presence of scattering.

In Fig. 21 the Fano factor γ calculated with the dynamic potential is shown as a function of ℓ/L for several values of the applied voltage. The reason for the different behavior found between the different curves in the ballistic limit is the presence or absence of the potential barrier related to the space charge. As compared with 40 k_BT/q, when the barrier is still present and the suppression is important ($\gamma \cong 0.045$), for the highest voltages (80 and 100 k_BT/q) the barrier has already disappeared, the current is saturated and the Fano factor takes on the full shot-noise level. In the elastic case, when the diffusive regime is achieved γ remains constant with ℓ/L and takes the same value of about 1/3 for all the applied voltages. On the contrary, in the inelastic case the higher the applied voltage, the lower the value of γ reached in the diffusive regime. Remarkably, when the ballistic regime is abandoned the value of ℓ/L at which γ starts decreasing is the same in the elastic and inelastic cases for a given applied voltage ($\ell/L \approx$ 0.3 and 0.1, for 80 and 100 k_BT/q, respectively). However, when the diffusive regime is approached, for γ to become constant a lower value of ℓ/L must be reached in the inelastic case with respect to the elastic one. This behavior can be explained in terms of the different elastic and inelastic scattering intensity required by the electron system to achieve a significant energy equipartition into the three directions of momentum space [91].

To check the influence of the contact injection on the evolution of the Fano factor with ℓ/L, Fig. 22 shows γ as a function of ℓ/L for an applied voltage of 40 k_BT/q and the four different contact models resulting from combining Poissonian/uniform injection

statistics and Maxwellian/fixed-velocity distribution of the injected carriers, as explained in section 2.3.1. The Poissonian-Maxwellian injection scheme is that typically used, and the only one physically plausible for nondegenerate contacts. As expected, in the ballistic case, when carrier transport in the structure is deterministic, the Fano factor crucially depends on the contact-injection model. For example, in the case of the uniform-fixed velocity contact, when the injection introduces no noise in the current flux, the Fano factor decreases drastically with the increase of ℓ / L, since the noise tends to vanish in the absence of scattering mechanisms. The noise does not vanish completely since, unless $\ell / L \to \infty$, there is always some probability of undergoing a scattering event. In this limit, when the noise is produced just by a few scattering events, it is clearly observed that elastic interactions lead to more important current fluctuations than inelastic mechanisms. By approaching the perfect diffusive regime the Fano factor is found to be independent of the model used. In diffusive regime, the results obtained with the four contact models are the same. This leads to the important conclusion that the noise in the diffusive regime (and particularly the 1/3 Fano factor obtained in the elastic-diffusive case) is independent of the carrier injecting statistics, and it is only determined by the effect of scattering mechanisms (jointly with Coulomb interaction).

3.3. Diffusive regime

In this section we consider scattering times short enough to ensure a diffusive transport regime ($\ell / L \leq 3\times10^{-3}$). Contacts are nondegenerate and λ=30.9 (unless indicated).

3.3.1. *Energy-independent scattering time*

Initially we consider that the scattering time does not depend on energy, as in the previous section. Fig. 23 shows the dependence of the Fano factor γ on the applied voltage U in both the elastic and inelastic cases calculated with the dynamic PS. In the inelastic case,

due to the strong thermalizing action of scattering, the noise is just thermal Nyquist noise at any bias and, as a consequence, γ decreases systematically as the current increases (higher *U*). In the elastic case, at the lowest voltages the thermal behavior is recovered; however, at the highest voltages, when the velocity distribution exhibits a strong deviation from equilibrium [91], the level of noise increases, its ratio with the current remaining constant and providing a value of 1/3 for the Fano factor γ. We remark that this result is only obtained with the dynamic PS. In the absence of Coulomb correlations (static PS), full shot noise is obtained for $qU > k_B T$, which in the inelastic case confirms that inelastic scattering alone (without the action of Coulomb interaction) is not enough to suppress shot noise [56].

The 1/3 suppression factor found in the elastic case for $qU >> k_B T$ coincides with the value obtained in degenerate elastic conductors by very different theoretical approaches, going from the quantum-phase-coherent model of Beenakker and Büttiker [16] to the semiclassical degenerate models of Nagaev [17] and de Jong and Beenakker [20]. In all these cases degenerate conditions are assumed, and the noise reduction comes from the regulation of electron motion by the Pauli exclusion principle. However, in our calculations neither phase-coherence nor Fermi statistics are necessary for its appearance. Some controversy has emerged about the possibility that there could exist a common origin for the 1/3 factor found under these so different conditions [5,60,113,114].

In our case, by fully suppressing carrier-number fluctuations, long-range Coulomb interaction is found to be determinant in providing the 1/3 value in the low-frequency limit. To illustrate the physical origin of this effect, Fig. 24(a) reports a typical spectrum of the Fano factor under elastic diffusive conditions. Calculations are performed for static and dynamic PS schemes. Here the current spectrum is decomposed into velocity, number and cross-correlation contributions $S_I(f) = S_V(f) + S_N(f) + S_{VN}(f)$ [see Eqs. (11)]. In the static PS scheme the spectrum clearly shows that the three terms contribute to $S_I^s(f)$, and two

different time scales can be identified. The longest one is associated with the transit time of carriers through the active region $\tau_T \approx 5$ ps, and it is evidenced in the terms $S_N^s(f)$ and $S_{VN}^s(f)$. The shortest one is related to the relaxation time of elastic scattering $\tau = 5$ fs, and it is manifested in $S_V^s(f)$. Remarkably, the velocity contribution yields 1/3 of the full shot-noise value, while the other two terms provide the remaining 2/3. Thus, in the static PS scheme full shot noise is recovered as sum of the three contributions. On the contrary, in the dynamic PS scheme $S_N^d(f)$ and $S_{VN}^d(f)$ are found to compensate each other and, as a result, $S_I^d(f)$ coincides with $S_V^d(f)$ in all the frequency range. Moreover, $S_N^d(f)$ takes values much smaller than $S_N^s(f)$. The characteristic time scale of $S_N^d(f)$ and $S_{VN}^d(f)$ differs from that found within the static PS scheme, which was related to the transit time τ_T. Now, in the dynamic case, it is the dielectric relaxation time corresponding to the carrier concentration at the contacts $\tau_d = 0.46$ ps which determines the cutoff of the contributions related to number fluctuations. In the frequency range between the transit and collision frequency values it is interesting to notice that both static and dynamic PS schemes yield $\gamma = 1/3$, thus relating the suppression factor to velocity fluctuations only. However, at low frequencies only the dynamic scheme takes this value by virtue of Coulomb correlations, which are responsible for the reduction of $S_N^d(f)$ and the mutual compensation of $S_N^d(f)$ and $S_{VN}^d(f)$ contributions. It is remarkable that $S_V^s(f) = S_V^d(f)$ in all the frequency range, which implies that velocity fluctuations are not affected by long-range Coulomb interactions, but just by scattering mechanisms. Coulomb repulsion affects only the contributions where carrier-number fluctuations are involved. Figure 24(b) reports the spectrum for inelastic scattering. Here, the same features of the elastic case are observed, with the important difference that $S_V^d(f)$ is much lower than when there is no energy dissipation.

So far we have analyzed structures where Coulomb repulsion plays an important role (i.e., $\lambda >> 1$). To check to which extent this interaction is determinant for noise suppression, Fig. 25 reports the Fano factor γ and the three contributions into which it has been decomposed as a function of λ. Here, we present the elastic case calculated under far-from-equilibrium conditions ($U = 100 k_B T / q$) within the dynamic PS scheme. For the lowest values of λ, when space-charge effects and in turn Coulomb interaction are negligible, full shot noise is observed. As λ increases, γ starts decreasing from unity until reaching a constant value for $\lambda \geq 30$. It is remarkable that the contribution of velocity fluctuations to γ does not vary significantly with λ. On the contrary, the contributions associated with number and velocity-number fluctuations are strongly affected by the increase of λ. Indeed, their absolute value decreases systematically and, being opposite in sign, they compensate each other at the highest values of λ, so that $S_I \approx S_V$.

The results reported so far refer to a three-dimensional momentum space. In contrast to degenerate diffusive systems where, provided quasi-one dimensional conditions in real space are attained, noise suppression is independent of the number *d* of momentum space dimensions, an interesting feature of nondegenerate diffusive systems is that noise suppression can depend on *d*. For the model of inelastic scattering considered here, no dependence of γ on *d* has been found, since there is no influence of the velocity components transversal to the electric field direction on the transport and noise properties of the structures. On the contrary, in the elastic case the Fano factor is found to depend significantly on *d*, since the transversal velocity components constitute a channel for energy redistribution which affects the transport properties of the structure. Therefore, below we focus our analysis on the elastic case. Accordingly, when $d = 2$ the carrier velocity is randomized in the simulation into two components after each scattering event, and when $d = 1$ the isotropic

character of scattering is accomplished by inverting the carrier velocity with an average (back-scattering) probability $P_b = 0.5$.

Figure 26(a) reports the Fano factor γ as a function of ℓ / L for the cases $d = 1$, 2, 3 at high voltages (40 $k_B T / q$) calculated within the dynamic PS scheme. We note that, when calculated within the static PS scheme, the results do not exhibit any shot-noise suppression. For the highest values of ℓ / L, in all three cases γ approaches the asymptotic value corresponding to the ballistic limit ($\gamma = 0.045$), where the behavior is independent of *d*. At a given value of ℓ / L, a higher deviation from the asymptotic ballistic value is observed for lower *d*. This is due to the fact that, in average, elastic interactions introduce higher fluctuations of the carrier *x*-velocity the lower is the number of available momentum states after the scattering mechanism (in particular, just 2 in the case $d = 1$). For this same reason, the increasing presence of scattering as ℓ / L is reduced leads to higher values of the Fano factor the lower is the dimensionality. Remarkably, within numerical uncertainty the limit value reached by γ in the perfect diffusive regime is found to be about, respectively, of 1/3, 1/2, and 0.7 for $d = 3, 2, 1$. Figure 26(b), by reporting γ in the diffusive regime as a function of the applied voltage, provides evidence that these limit values are independent of the bias once $qU >> k_B T$. The origin of the suppression is the same in all three cases: the joint action of Coulomb correlations and elastic scattering, which leads to the result $S_I = S_V$ [as shown in Fig. 25 in the case $d = 3$], where $S_V / 2qI$ under perfect diffusive regime is a function of the dimensionality of momentum space.

Motivated by the MC results shown in this section, several authors, like Beenakker [69], Schomerus *et al.* [70] and Gurevich and Muradov [77], have developed analytical theories to explain the suppression found in the elastic diffusive regime under space-charge

limited conditions, being able to reproduce the MC results and their dependence on dimensionality.

3.3.2. *Energy-dependent scattering time*

In the previous section we have found that within our model the 1/3 value of the Fano factor obtained in the elastic diffusive regime for $d = 3$ exhibits several *universal* properties, namely, it is independent of: (i) the scattering strength (once $\ell / L << 1$); (ii) the applied voltage (once $qU >> k_B T$), (iii) the screening length (once $\lambda >> 1$), and (iv) the carrier injecting statistics. However, several authors have pointed out that the possible universality of this value is broken by the fact that the Fano factor in this regime changes with the energy dependence of the scattering time τ. This is, the 1/3 value appears only for energy independent τ. By considering a scattering time of the type $\tau(\varepsilon) = \tau_0 \varepsilon^{\alpha}$, the Fano factor is predicted to depend on α, the power of energy in this expression. Thus, by using an analytical drift model, Schomerus *et al.* obtain the following dependence of the Fano factor on α for $d = 3$ [70,72]

$$\gamma = \frac{6(\alpha - 1)(\alpha + 2)(16\alpha^2 + 36\alpha - 157)}{5(2\alpha - 5)(8\alpha - 17)(13\alpha + 8\alpha)} . \tag{24}$$

Also Nagaev indicates that for $\alpha = -3/2$ and $d = 3$ the Fano factor should be 1, this is, Coulomb interaction should play no role on the noise behavior [102]. Gurevich and Muradov calculate γ for several values of α (0.4257 and 0.1974 for $\alpha = -1/2$ and $1/2$, respectively) [77]. And finally Gomila and Reggiani [71], by using the concept of differential conductivity in energy space $\sigma'(\varepsilon)$, indicate that $\sigma'(\varepsilon) > 0$ leads to noise suppression, $\sigma'(\varepsilon) = 0$ to a Fano factor equal to 1, and, what is the most interesting prediction, that $\sigma'(\varepsilon) < 0$ can originate shot-noise enhancement. The differential conductivity depends on α and momentum space dimensionality d in this way $\sigma'(\varepsilon) \propto (\alpha + d/2)\varepsilon^{\alpha + d/2 - 1}$.

To check these predictions, we have performed MC calculations considering the above dependence of the scattering time on energy. We must note that in this case theoretical predictions are preceding MC simulations. We have performed calculations for the following values of α (and associated τ_0): -2 (8.35×10^{-16} s eV^2), -3/2 (6.76×10^{-16} s eV$^{3/2}$), -1 (3.88×10^{-16} s eV), -1/2 (4.41×10^{-16} s eV$^{1/2}$), 0 (2.00×10^{-15} s, energy-independent case), 1/2 (3.11×10^{-15} s eV$^{-1/2}$), 1 (1.55×10^{-14} s eV^{-1}) and 3/2 (2.40×10^{-14} s eV$^{-3/2}$). The values of τ_0 are chosen in such a way to ensure diffusive transport in the wide range of electron energies found in the simulations and to make computer times affordable.

Fig. 27 reports the Fano factor γ as a function of the energy exponent α for an applied voltage of 40 $k_B T/q$ (within the limit $qU >> k_B T$) in the cases of $d = 3$ and $d = 2$. The current in the high-voltage range (see inset) exhibits different behavior for each value of α, going from a superlinear (and similar) dependence on U for values of $\alpha \geq 0$ to a sublinear behavior for $\alpha < 0$, more pronounced the lower is α (and for $d = 2$). Squares in Fig. 27 refer to MC simulations with $d = 3$ and the continuous curve to the analytical expression reported in Eq. (24). MC data compare well with analytical results in the limited range $-3/2 < \alpha < 1/2$. Outside this range, the analytical theory predicts completely suppressed shot noise (at $\alpha = 1$), while the MC results take values close to 1/3 (or slightly lower) for the range $\alpha \geq 0$. These discrepancies are probably due to the simplifying assumptions inherent to the drift model [70]. Within uncertainty, MC data confirm the predictions that $\gamma = 1$ (no role of Coulomb interaction) for $\alpha = -d/2$ (when $\sigma'(\varepsilon) = 0$), and what is more important, that enhanced shot noise ($\gamma > 1$) should be found for $\alpha < -d/2$ (when $\sigma'(\varepsilon) < 0$), which is especially evident for $d = 2$. Thus, we corroborate that the Fano factor associated with Coulomb correlations is in general a sensitive probe of the energy dependence of the scattering time.

To further investigate the mechanism responsible for shot-noise suppression and enhancement we report in Fig. 28 the profiles of the relevant average quantities for an applied voltage of 80 $k_B T/q$ and $d = 3$. For $\alpha \geq 0$, the behavior of the different profiles is systematic: the velocity increases more and more near the anode while the carrier concentration decreases as α is enlarged. However for $\alpha < 0$ this behavior is broken, and the signature of a key qualitative change in the profiles emerges for $\alpha \leq -1$ [116]. Here, the transition from a quasiballistic region near the cathode contact [71] to a diffusive region inside the structure leads to the appearance of a maximum (minimum) in the velocity (concentration), more pronounced the lower is α. Simultaneously, simulations evidence the onset of a region of dynamic negative differential mobility which covers most of the active region of the structure. These qualitative changes are accompanied by a systematic increase of the Fano factor, as can be seen in Fig. 27, what indicates the onset of a mechanism inducing positive correlation among the fluctuations. We conclude that for $\alpha \leq -3/2$ the structure exhibits the simultaneous presence of two distinct transport regimes, a ballistic one near to the contacts and a diffusive one around the center of the active region. The presence of these regimes leads to a region of dynamical negative differential mobility, which in turns moves the structure towards a state of electrical instability, as well known for the analogous case of Gunn diodes [115]. The tendency of the the *I-U* characteristics to exhibit negative differential resistance, more pronounced in the case of $d = 2$ (see insets of Fig. 27), further supports the present interpretation. The increase of the Fano factor stems as a precursor of the fact that the system is evolving towards such an electrical instability. The condition under which enhanced shot noise is observed coincides with the analytical condition that the differential conductivity in energy space becomes negative [116].

3.4. Influence of trapping-detrapping processes in quasiballistic regime

In this section we will show that the presence of generation-recombination (GR) phenomena in quasiballistic conductors can lead to an enhancement of shot noise, via Coulomb correlations, similar to that found in other systems like resonant tunneling diodes [34,50]. To this end, the presence of electron traps in the active region of an otherwise ballistic structure is considered. The trapping-detrapping processes are characterized in a simple way, described in section 2.5, by means of the times τ_r (recombination time) and τ_g (generation time), initially assumed as independent of the position and energy of electrons. We consider also that the scattering mean free path ℓ is much longer than the sample length L; consequently, electrons move ballistically inside the active region, only interrupted by trapping processes. Again, λ=30.9 and nondegenerate contacts will be used in the calculations. We will analyze a case with τ_r =20 ps. Taking into account that the average transit time of electrons through the active region of the structure τ_T is about 1.05 ps under equilibrium conditions, which fulfils $\tau_T < \tau_r$, electrons will cross the sample in a quasiballistic way, with very low probability of suffering a trapping process. Anyway, due to the continuous flux of carriers, a significant density of negative fixed charge $n_t(x)$ is present in the active region. According to the model used for GR processes, $n_t(x) = n(x)\tau_g/(\tau_r + \tau_g)$ with $n(x)$ the local free carrier concentration [104,105]. This density of fixed charge will affect the carrier transport. As concerns fluctuations, since $\tau_T < \tau_r$, number fluctuations associated to the trapping-detrapping processes are not expected to be significant. However, the fluctuations of the negative fixed charge may have a very important influence on the noise via Coulomb interaction.

Figure 29(a) shows the mean velocity of free electrons in the active region of the structure, for an applied voltage of 40 k_BT/q, when GR processes are characterized by

τ_r =20 ps and several values of τ_g are considered. The purely ballistic case is also plotted for comparison. The velocity increases continuously along the structure until approaching the end of the active region, where it decreases due to the thermal carriers injected by the anode, as already observed in Fig. 8. No significant differences are detected between the diverse curves. The probability of suffering a recombination mechanism by an electron crossing the active region is so low that the transport regime is not substantially altered by the presence of the traps and, thus, it remains quasiballistic. For this applied voltage the potential profile presents a minimum close to the cathode acting as a potential barrier for the electrons moving between the contacts, as already explained in section 3.1.1.a. This potential minimum is reported in the inset of Fig. 29(a) for the previous cases. For a fixed value of τ_r, as τ_g increases electrons remain longer trapped, and thus a higher concentration of fixed charge $n_t(x)$ is present. This increment of n_t leads to a higher potential barrier and, as consequence, to lower values of the current for a given applied voltage, as observed in the current-voltage characteristics shown in Fig. 29(b). We remark that the current decreases because there are less free electrons injected with sufficient energy to pass over the barrier, and not because of a reduction of the mean velocity associated with the GR processes. The saturation of the current (due to the disappearance of the barrier) in the presence of GR processes takes place for higher applied voltages (increasing with τ_g) than in the ballistic case, in accordance with the larger potential barrier originated by the fixed charge concentration. Two processes with different characteristic times can lead to fluctuations in the amplitude of this barrier controlling the current: the flow of carriers through the structure, characterized by the transit time τ_T; and the trapping-detrapping processes, characterized by the electron lifetime $\tau_l = \tau_r\tau_g/(\tau_r + \tau_g)$ [105]. The former process is responsible for the shot-noise suppression found in the ballistic case by introducing negative correlations between transmitted carriers,

while the latter, as we will show in the following, leads to positive correlations which increase the level of noise with respect to that found in the purely ballistic case.

Figure 30 shows the Fano factor at low frequency as a function of the applied voltage for the same cases of the previous figure. Calculations performed with a static PS, thus in the absence of long-range Coulomb interaction, coincide for all cases, and are represented by the thick solid line. Without this interaction, full shot noise associated with the Poissonian carrier injection at the contacts is always found (for $qU > k_B T$), what indicates that all the differences observed between the reported results are related to Coulomb repulsion. With the dynamic PS, the presence of GR processes increases the level of shot noise with respect to the ballistic case in the range of applied voltages for which suppression was found under ballistic conditions. As τ_g becomes longer, so that the influence of capture processes is more important (a higher density of fixed charge is present), increasing values of the Fano factor are found, even reaching enhanced shot noise ($\gamma > 1$) for τ_g =5 and 7.5 ps. Remarkably, the maximum enhancement of noise in the presence of GR processes occurs at the applied voltages for which the most significant suppression takes place in the ballistic case (40 $k_B T / q$, see Fig. 11), this is, when Coulomb interaction exerts the strongest influence on the noise. For applied voltages for which this interaction is not expected to modify the noise, the values of the Fano factor for the different τ_g and in the ballistic case are practically the same. This happens for low applied voltages, when the noise is basically thermal, and under saturation conditions, when there is no longer a barrier modulating the current. The fact that the noise level under saturation does not increase with respect to the ballistic case confirms that, as expected since $\tau_T < \tau_r$, number fluctuations related to GR processes provide a negligible direct contribution to the current noise; their influence takes place only by means of Coulomb interaction.

In the following we illustrate the origin of the outstanding result reported in Fig. 30. To this end we will focus on the significant case of τ_r =20 ps and τ_g =5 ps, for which enhanced shot noise appears. Figure 31 shows the autocorrelation function of current fluctuations $C_I(t)$ for applied voltages of 10 and 40 $k_B T/q$, at which the potential barrier modulates the current and enhances the noise. Firstly, a short-time decay related to the transit time through the active region (about 0.2-0.4 ps for these values of *U*) is observed (inset), also found when transport is completely ballistic (see Fig. 14). Then, the autocorrelation functions present a further exponential decay with a characteristic time of about 4 ps (as indicated by the exponential fittings shown in the figure), which corresponds exactly to the lifetime τ_l of the trapping-detrapping processes. Thus, this exponential contribution, responsible for the noise enhancement, is clearly associated with the GR phenomena; its influence being more significant the higher is the applied voltage (and therefore the current). Remarkably, the long-time decay is not observed when a static PS is used, or under conditions when long-range Coulomb interaction is not expected to affect the noise, like saturation (in the absence of a potential barrier). This confirms again that the exponential contribution is not caused directly by number fluctuations related to GR phenomena. Actually, the shot-noise enhancement found in our results is due to the influence of the trapped-charge fluctuations on the current taking place by means of the associated potential barrier modulation induced by long-range Coulomb interaction.

To identify more clearly the origin of the enhanced shot noise related to the exponential decay found in $C_I(t)$, Fig. 32 shows the velocity-number component $C_{VN}(t)$ of the autocorrelation function for an applied voltage of 40 $k_B T/q$. It can be observed that the previous positive long-time contribution is also present in the cross correlation between fluctuations of mean velocity and free-carrier number *N*. Initially, at the shortest times, $C_{VN}(t)$ is negative, like under ballistic conditions, due to the transit of carriers through the

active region. However, $C_{VN}(t)$ becomes positive at longer times, thus revealing a positive correlation between carriers related to the trapping-detrapping processes. When an electron is captured, it becomes a negative fixed charge that increases the potential barrier (leading to a decrease of *N*). As a consequence, fewer electrons have sufficient energy to pass over this barrier; the electron mean velocity and the current decrease. On the other hand, when a trapped electron is released, the potential barrier decreases (allowing an increase of *N*) and more electrons are able to surpass the barrier; the mean velocity and the current increase. Thus, a positive correlation is established between carriers contributing to the current with energies around the potential barrier, leading to a super-Poissonian distribution of transmitted carriers and hence to shot-noise enhancement. Of course, the characteristic time of these correlations is the lifetime associated with the GR processes, since this is the time that governs the time evolution of captured electrons. We have checked that the described effect is more pronounced the closer is the captured electron to the potential barrier [117].

The spectral density of current fluctuations $S_I(f)$ for an applied voltage of 40 k_BT/q is shown in Fig. 33, calculated as the Fourier transform of the corresponding $C_I(t)$ reported in Fig. 31. $S_I(f)$ in the ballistic case is also plotted for comparison. According to the short- and long-time behaviors found in $C_I(t)$, two plateaus are observed in $S_I(f)$. At low frequency, a first plateau relative to the enhanced shot noise due to GR processes is observed, associated with the long-range decay in the autocorrelation function. At high frequency, beyond the cutoff of GR phenomena ($f >> 1/2\pi\tau_l$), a second plateau is detected, associated with the short-time decay. The value of $S_I(f)$ in the second plateau practically coincides with the low-frequency value of $S_I(f)$ in the ballistic case, related to shot-noise suppression. Therefore, our system displays enhanced or suppressed shot noise depending on the frequency range of observation.

The effect of the trapping-detrapping processes on the noise takes place because of the determining control that the potential barrier exerts on the current flow. If such a control is diminished, or even washed out, the observed enhanced shot noise is predicted to disappear. To check this fact, we will consider now, apart from GR processes, the additional presence of elastic and inelastic (thermalizing) scattering mechanisms in the active region of the structure, characterized by an energy independent relaxation time τ and assumed to be isotropic as described in previous sections. Figure 34 presents the Fano factor at low frequency as a function of ℓ / L, for an applied voltage of 40 $k_B T / q$, when τ is decreased from 10^{-11} to 10^{-15} s, in the presence of GR processes characterized by τ_r =20 ps and τ_g =5 ps. Both elastic and inelastic mechanisms are considered (separately). For the highest values of ℓ / L, when transport is quasiballistic, the Fano factor exhibits values corresponding to enhanced shot noise related to GR processes. For lower values of ℓ / L in the transition from quasiballistic to diffusive regime, γ decreases and enters a range of values corresponding to shot-noise suppression ($\gamma < 1$). Finally, under fully diffusive regime ($\ell / L < 3 \times 10^{-3}$), γ becomes independent of the scattering rate. Remarkably, in this regime the Fano factor exhibits the same values as those found in the absence of GR processes: about 1/3 in the case of elastic diffusive transport, and about 0.09 in the inelastic case (see Fig. 21). As explained, these levels of shot-noise suppression are due to the joint action of Coulomb repulsion and scattering mechanisms under space-charge limited conduction. When a scattering process occurs, the velocity is randomized; in particular, the electron energy in the direction of the potential barrier is modified. As a consequence, in the diffusive regime the potential barrier no longer controls the current flowing through the device, and GR processes lose their influence on the noise. Therefore, the presence of GR processes (under the condition $\tau_T < \tau_r$) is determining in the noise behavior under quasiballistic regime, but it has no influence under diffusive conditions.

Finally, we point out that if more realistic models including energy and space (through the local density and occupancy of the traps) dependence of τ_r are considered, the predicted effect is reduced, but it is still clearly noticeable [117].

4. SUMMARY

In this chapter, shot-noise suppression and enhancement due to the action of long-range Coulomb interaction (jointly with other mechanisms) in a homogenous active region connected to ideal reservoirs has been analyzed under different transport regimes. A semiclassical model consisting in an ensemble MC simulation self-consistently coupled with a one-dimensional PS is used for the calculations. Carrier dynamics is simulated in the active region, and contact injection is appropriately modeled by using different statistics according to the nondegenerate or degenerate character of contacts. The influence of Coulomb interaction on the noise has been identified by using static and dynamic schemes to solve the Poisson equation. Predicted effects take place when long-range Coulomb interaction plays a major role, i.e., in the presence of significant space charge in the active region.

In the case of ballistic structures with nondegenerate contacts, the dynamic fluctuations of the self-consistent potential (in the presence of a barrier related to the space charge), modify the carrier statistics imposed at the contacts, and are found to be responsible for a remarkable noise suppression, which becomes stronger as space-charge effects are more important. The main contribution to the suppression is found to originate from the velocity-number correlations induced by the self-consistent field. The time and frequency dependences of the fluctuations have also been analyzed. The noise spectra show different features related to transit time, returning carriers and geometrical resonances, and are also

modified by Coulomb correlations among carriers. When contacts are degenerate, a further suppression related to Fermi statistics is found, while the behavior of Coulomb suppression, still very important, changes slightly. We have identified and evaluated the negative correlations among carriers induced by Coulomb interaction, which take place between the carriers injected with sufficient energy to pass over the barrier and those injected around the barrier energy.

The presence of scattering significantly modifies the behavior of shot noise. In the crossover from ballistic to diffusive regime, for high voltages ($qU >> k_B T$) a value of the Fano factor independent of the scattering strength (ℓ / L) is not achieved until a significant energy redistribution among momentum space directions takes place. For energy independent scattering time, in the elastic case an asymptotic value of 1/3 is found for the Fano factor, while in the inelastic case the higher is the applied voltage the stronger is the suppression. The action of Coulomb repulsion in suppressing shot noise occurs through the reduction of the contributions associated with carrier-number fluctuations to the total noise spectral density. The 1/3 value found in the elastic diffusive nondegenerate regime shows several universal properties, broken by the fact that it changes with momentum space dimensionality (the Fano factor being higher the lower is the dimensionality) and with the energy dependence of the scattering time. Interestingly, by considering a power-law dependence of the scattering time on energy, for specific energy exponents enhanced shot noise is found, associated to the presence of negative differential conductivity in energy space.

In the case when trapping-detrapping processes with a recombination time longer than the electron transit time are included in the active region of an otherwise ballistic structure (quasiballistic regime), an increase of the noise level at low frequency with respect to the values found in the ballistic case is observed. The potential barrier fluctuations induced by the fluctuating fixed charge via long-range Coulomb interaction are at the origin of this

effect by introducing positive correlations among transmitted carriers. At high frequency, beyond the cutoff of GR phenomena, the suppressed shot noise of the ballistic case is recovered. When carrier transport becomes diffusive, the potential barrier does not control the current, and thus no influence of GR processes is observed.

In view of all the above results, we finally emphasize that the knowledge of the noise properties of mesoscopic structures (like the value of the Fano factor) provides very valuable information about the carrier kinetics inside them, not available from dc or conductance measurements. We remark also that, in some sense, the results presented in this chapter have played the role of *numerical experiments*, leading to the development of several analytical theories with the aim of providing a detailed physical explanation for them.

5. **AKNOWLEDGMENTS**

The author gratefully acknowledges the contribution of several colleagues to this work: O. M. Bulashenko, L. Reggiani, G. Gomila, J. Mateos, B. García, C. González and D. Pardo. This work has been partially supported by the Dirección General de Enseñanza Superior e Investigación Científica through the project PB97-1331, the Ministerio de Ciencia y Tecnología through the project TIC2001-1754 and the Consejería de Educación y Cultura de la Junta de Castilla y León through the project SA44/99.

REFERENCES

1. A.van der Ziel, *Noise, Source, Characterization, Measurement*, New Jersey, Prentice-Hall (1970).
2. A. van der Ziel, *Noise in Solid State Devices and Circuits*, Wiley, New York (1986).
3. Sh. Kogan, *Electronic Noise and Fluctuations in Solids*, Cambridge University Press, Cambridge (1996).
4. W. Schottky, Ann. Phys. (Leipzig) **57**, 541 (1918).
5. R. Landauer, Nature **392**, 659 (1998).
6. M. J. M. de Jong and C. W. J. Beenakker, in *Mesoscopic Electron Transport*, L. L. Sohn, L. P. Kowenhoven and G. Schön, Eds., NATO ASI Series E, Kluwer, Dordrecht (1996), Vol. 345, p. 225.
7. Y. M. Blanter and M. Büttiker, Phys. Rep. **336**, 1 (2000), and references therein.
8. M. Büttiker, Phys. Rev. Lett. **65**, 2901 (1990).
9. M. Büttiker, Phys. Rev. B **46**, 12485 (1992).
10. I. O. Kulik and A. N. Omel'yanchuk, Fiz. Nizk. Temp. **10**, 305 (1984) [Sov. J. Low Temp. Phys. **10**, 158 (1984)].
11. G. B. Lesovik, JETP Lett. **49**, 594 (1989).
12. L. Chen and C. Ting, Phys. Rev. B **43**, 4534 (1991).
13. J. H. Davies, P. Hyldgaard, S. Hershfield and J. W. Wilkins, Phys. Rev. B **46**, 9620 (1992).
14. M. J. M. de Jong and C. W. J. Beenakker, Phys. Rev. B **51**, 16867 (1995).
15. M. M. G. Iannaccone, M. Macucci and B. Pellegrini, Phys. Rev. B **55**, 4539 (1997).
16. C. W. J. Beenakker and M. Büttiker, Phys. Rev. B **46**, 1889 (1992).
17. K. E. Nagaev, Phys. Lett. A **169**, 103 (1992).
18. B. L. Altshuler, L. S. Levitov and A. Yakovets, JETP Lett. **59**, 857 (1994).

19. Yu V. Nazarov, Phys. Rev. Lett. **73**, 134 (1994).

20. M. J. M. de Jong and C. W. J. Beenakker, Phys. Rev. B **51**, 16867 (1995).

21. Ya M. Blanter and M. Büttiker, Phys. Rev. B **56**, 2127 (1997).

22. E. V. Sukhorukov and D. Loss, Phys. Rev. Lett. **80**, 4959 (1998).

23. E. V. Sukhorukov and D. Loss, Phys. Rev. B **59**, 13054 (1999).

24. M. Macucci, G. Iannacone and B. Pellegrini, in *Proc. of 15th Int. Conf. on Noise in Physical Systems and 1/f Fluctuations*, C. Surya, Ed., Bentham Press, London (1999), p. 325.

25. K. E. Nagaev, Phys. Rev. B. **52**, 4740 (1995).

26. V. I. Kozub and A. M. Rudin, Phys. Rev. B **52**, 7853 (1995).

27. A. Shimizu and M. Ueda, Phys. Rev. Lett. **69**, 1403 (1992).

28. R. C. Liu and Y. Yamamoto, Phys. Rev. B **50**, 17411 (1994).

29. P. Dieleman, H. G. Bukkems, T. M. Klapwijk, M. Schicke and K. H. Gundlach, Phys. Rev. Lett. **79**, 3486 (1997).

30. X. Jehl, P. Payet-Burin, C. Baraduc, R. Calemczuk and M. Sanquer, Phys. Rev. Lett. **83**, 1660 (1999).

31. E. V. Bezuglyi, E. N. Bratus', V. S. Shumeiko and G. Wendin, Phys. Rev. Lett. **83**, 2050 (1999).

32. T. Hoss, C. Strunk, T. Nussbaumer, R. Huber, U. Staufer and C. Schönenberger, Phys. Rev. B **62**, 4079 (2000).

33. E. R. Brown, IEEE Trans. Electron Devices **39**, 2686 (1992).

34. Y. M. Blanter and M. Büttiker, Phys. Rev. B **59**, 10217 (1999).

35. A. Reklaitis and L. Reggiani, Phys. Rev. B **62**, 16773 (2000).

36. V. Y. Aleshkin, L. Reggiani and A. Reklaitis, Semicond. Sci. Technol. **15**, 1045 (2000).

37. V. Y. Aleshkin, L. Reggiani and A. Reklaitis, Phys. Rev. B **63**, 085302 (2001).

38. Y. P. Li, D. C. Tsui, J. J. Heremans, J. A. Simmons and G. W. Weimann, Appl. Phys. Lett. **57**, 774 (1990).

39. Y. P. Li, A. Zaslavsky, D. C. Tsui, M. Santos and M. Shayegan, Phys. Rev. B **41**, 8388 (1990).

40. F. Liefrink, J. I. Dijkhuis, M. J. M. de Jong, L. W. Molenkamp and H. van Houten, Phys. Rev. B **49**, 14066 (1994).

41. H. C. Liu, J. Li, G. C. Aers, C. R. Leavens, M. Buchanan and Z. R. Wasilewski, Phys. Rev. B **51**, 5116 (1995).

42. H. Birk, M. J. M. de Jong and C. Schönenberger, Phys. Rev. Lett. **75**, 1610 (1995).

43. M. Reznikov, M. Heiblum, H. Shtrikman and D. Mahalu, Phys. Rev. Lett. **75**, 3340 (1995).

44. A. Kumar, L. Saminadayar, D. C. Glattli, Y. Jin and B. Etienne, Phys. Rev. Lett. **76**, 2778 (1996).

45. M. Henny, H. Birk, R. Huber, C. Strunk, A. Bachtold, M. Krüger and C. Schönenberger, Appl. Phys. Lett. **71**, 773 (1997).

46. A. H. Steinbach, J. M. Martinis and M. H. Devoret, Phys. Rev. Lett. **76**, 3806 (1996).

47. R. J. Schoelkopf, P. J. Burke, A. A. Kozhevnikov, D. E. Prober and M. J. Rooks, Phys. Rev. Lett. **78**, 3370 (1997).

48. R. de-Picciotto, M. Reznikov, M. Heiblum, V. Umansky, G. Bunin and D. Mahalu, *Nature* **389**, 162 (1997).

49. H. Pothier, S. Guéron, N. O. Birge, D. Esteve and M. H. Devoret, Phys. Rev. Lett. **79**, 3490 (1997).

50. G. Iannacone, G. Lombardi, M. Macucci and B. Pellegrini, Phys. Rev. Lett. **80**, 1054 (1998).

51. V. V. Kuznetsov, E. E. Méndez, J. D. Bruno and J. T. Pham, Phys. Rev. B **58**, R10159 (1998).

52. R. J. Schoelkopf, A. A. Kozhevnikov, D. E. Prober and M. J. Rooks, Phys. Rev. Lett. **80**, 2437 (1998).

53. M. Henny, S. Oberholzer, C. Strunk and C. Schönenberger, Phys. Rev. B **59**, 2871 (1999).

54. B. J. Thompson, D. O. North and W. A. Harris, RCA Rev. **4**, 269 (1940)

55. B. J. Thompson, D. O. North and W. A. Harris, RCA Rev. **4**, 441 (1940).

56. M. Büttiker, in *Proc. of 13th Int. Conf. on Noise in Physical Systems and 1/f Fluctuations*, V. Bareikis and R. Katilius, Eds., World Scientific, Singapore (1995), p. 35.

57. Landauer and Th. Martin, Physica B **175**, 167 (1991).

58. Th. Martin and R. Landauer, Phys. Rev. B **45**, 1742 (1992).

59. R. Landauer, Phys. Rev. B **47**, 16427 (1993).

60. R. Landauer, Physica B **227**, 156 (1996).

61. F. Green and M. P. Das, J. Phys.: Cond. Matter **12**, 5233 (2000).

62. F. Green and M. P. Das, J. Phys.: Cond. Matter **12**, 5251 (2000).

63. Y. Naveh, D. V. Averin and K. K. Likharev, Phys. Rev. Lett. **79**, 3482 (1997).

64. K. E. Nagaev, Phys. Rev. B **57**, 4628 (1998).

65. Y. Naveh, D. V. Averin and K. K. Likharev, Phys. Rev. B **58**, 15371 (1998).

66. K. E. Nagaev, Phys. Rev. B **58**, R7512 (1998).

67. Y. Naveh, D. V. Averin and K. K. Likharev, Phys. Rev. B **59**, 2848 (1999).

68. O. M. Bulashenko, J. M. Rubí and V. A. Kochelap, Appl. Phys. Lett. **75**, 2614 (1999).

69. C. W. J. Beenakker, Phys. Rev. Lett. **82**, 2761 (1999).

70. H. Schomerus, E. G. Mishchenko and C. W. Beenakker, Phys. Rev. B **60**, 5839 (1999).

71. G. Gomila and L. Reggiani, Semicond. Sci. Technol. **15**, 829 (2000).

72. H. Schomerus, E. G. Mishchenko and C. W. Beenakker, in *Statistical and Dynamical Aspects of Mesoscopic Systems*, D. Reguera, G. Platero, L. L. Bonilla and J. M. Rubí, Eds., Springer, Berlin (2000), p. 96.

73. G. Gomila and L. Reggiani, Phys. Rev. B **62**, 8068 (2000).

74. O. M. Bulashenko, J. M. Rubí and V. A. Kochelap, Phys. Rev. B **61**, 5511 (2000).

75. O. M. Bulashenko, J. M. Rubí and V. A. Kochelap, Phys. Rev. B **62**, 8184 (2000).

76. O. M. Bulashenko and J. M. Rubí, Phys. Rev. B **64**, 045307 (2001).

77. V. L. Gurevich and M. I. Muradov, cond-mat/0107293.

78. L. Varani, L. Reggiani, T. Kuhn, T. González and D. Pardo, IEEE Trans. Electron Devices **ED-41**, 1916 (1994).

79. A. Reklaitis and L. Reggiani, J. Appl. Phys. **82**, 3161 (1997).

80. A. Reklaitis and L. Reggiani, Semicond. Sci. Technol. **14**, L5 (1999).

81. A. Reklaitis and L. Reggiani, Physica B **272**, 279 (1999).

82. A. Reklaitis and L. Reggiani, Phys. Rev. B **60**, 11683 (1999).

83. R. C. Liu, P. Eastman and Y. Yamamoto, Solid State Commun. **102**, 785 (1997).

84. T. González, J. Mateos, D. Pardo and L. Reggiani, Physica B **272**, 285 (1999).

85. T. González, J. Mateos, D. Pardo and L. Regginai, in *Proc. of the 25th Int. Conf. on the Physics of Semiconductors*, N. Miura and T. Ando, Eds., Springer Proc. in Physics, Berlin (2001), Vol.87, p. 1343.

86. T. González, O. M. Bulashenko, J. Mateos, D. Pardo and L. Reggiani, Phys. Rev. B **56**, 6424 (1997).

87. T. González, O. M. Bulashenko, J. Mateos, D. Pardo, L. Reggiani and J. M. Rubí, Semicond. Sci. Technol. **12**, 1053 (1997).

88. T. González, J. Mateos, D. Pardo, O. M. Bulashenko and L. Reggiani, Semicond. Sci. Technol. **13**, 714 (1998).
89. T. González, C. González, J. Mateos, D. Pardo, L. Reggiani, O. M. Bulashenko and J. M. Rubí, Phys. Rev. Lett. **80**, 2901 (1998).
90. O. M. Bulashenko, J. Mateos, D. Pardo, T. González, L. Reggiani and J. M. Rubí, Phys. Rev. B **57**, 1366 (1998).
91. T. González, J. Mateos, D. Pardo, O. M. Bulashenko and L. Reggiani, Phys. Rev. B **60**, 2670 (1999).
92. T. González, J. Mateos, D. Pardo, L. Varani and L. Reggiani, Semicond. Sci. Technol. **14**, L37 (1999).
93. T. González, J. Mateos, D. Pardo, L. Reggiani and O. M. Bulashenko, Physica B **272**, 282 (1999).
94. T. González, C. González, J. Mateos, D. Pardo, L. Reggiani, O. M. Bulashenko and J. M. Rubí, Phys. Rev. Lett. **83**, 1268 (1999).
95. T. González, in *Proc. of 16th Int. Conf. on Noise in Physical Systems and 1/f Fluctuations*, G. Bosman, Ed., World Scientific, Singapore (2001), p. 431.
96. B. G. Vasallo, J. Mateos, D. Pardo and T. González, Semicond. Sci. Technol. (submitted).
97. X. Oriols, F. Martín and J. Suñé, Appl. Phys. Lett. **79**, 1703 (2001).
98. T. González and D. Pardo, J. Appl. Phys. **73**, 7453 (1993).
99. L. S. Levitov and G. B. Lesovik, JETP Lett. **58**, 230 (1993).
100. L. S. Levitov, H. Lee and G. B. Lesovik, J. Math. Phys. **37**, 4845 (1996).
101. T. Kuhn, L. Reggiani and L. Varani, Superlatt. Microstruct. **11**, 205 (1992).
102. K. E. Nagaev, Phys. Rev. Lett. **83**, 1267 (1999).
103. M. Macucci, B. Pellegrini, P. Terreni and L. Reggiani, J. Appl. Phys. **63**, 5369 (1988).

104. S. Pérez, T. González, S. L. Delage and J. Obregon, J. Appl. Phys. **88**, 800 (2000).

105. A. van der Ziel, *Solid-State Physical Electronics*, Prentice-Hall, New Jersey (1976).

106. L. Reggiani, L. Varani, T. González, D. Pardo and T. Kuhn, *in Proc. of the 22nd Int. Conf. on the Physics of Semiconductors*, D. J. Lockwood, Ed., World Scientific, Singapore (1995), p. 1963.

107. A. van der Ziel and G. Bosman, Phys. Stat. Sol. A **73**, K93 (1982).

108. J. C. Stanton and J. W. Wilkins, Physica B **134**, 255 (1985).

109. L. Varani, L. Reggiani, P. Houlet, J. C. Vaissere, J. P. Nougier, T. Kuhn, T. González and D. Pardo, Semicond. Sci. Technol. **9**, 584 (1994).

110. Y. Naveh, A. N. Korotkov and K. K. Likharev, Phys. Rev. B **60**, R2169 (1999).

111. O. M. Bulashenko, J. M. Rubí and V. A. Kochelap, cond-mat/9906179.

112. G. Gomila, T. González and L. Regginai (unpublished).

113. R. Landauer, Microel. Eng. **47**, 7 (1999).

114. T. González, J. Mateos, D. Pardo, O. M. Bulashenko and L. Reggiani, D. Abbot and L. B. Kish, Eds., AIP Conf. Proc., New York (2000), Vol. 511, p. 71.

115. M. P. Shaw, V. V. Mitin, E. Schöll and H.L. Grubin, *The Physics of Instabilities in Solid State Electron Devices*, Plenum Press, New York (1992).

116. G. Gomila, T. González and L. Reggiani, Physica B (in press).

117. B. G. Vasallo and T. González (unpublished).

FIGURE CAPTIONS

Figure 1. Fano factor vs bias voltage for one-, two-, three-, and four-barrier GaAs/AlGaAs nonresonant heterostructure diodes (with transport controlled by tunneling) obtained from direct MC calculations for contact concentrations of: (a) 10^{14} cm^{-3}, and (b) 10^{17} cm^{-3}. Dashed line in (a) corresponds to the case of the four-barrier structure with a contact concentration of 10^{17} cm^{-3}. From [82], A. Reklaitis and L. Reggiani, Phys. Rev. B **60**, 11683 (1999). Copyright 1999 by the American Physical Society.

Figure 2. Potential profile (solid line) and distribution of electron kinetic energy (points) for a voltage of 1.5 V applied to a GaAs/AlGaAs tunneling heterostructure diode at T=300 K, formed of three layers: a 50 nm GaAs emitter, a 50 nm AlGaAs barrier and a 10 nm GaAs collector. From [35], A. Reklaitis and L. Reggiani, Phys. Rev. B **62**, 16773 (2000). Copyright 2000 by the American Physical Society.

Figure 3. Fano factor vs bias voltage for the diode of Fig. 2. Continuous and dashed curves refer respectively to dynamic and static PS schemes. From [35], A. Reklaitis and L. Reggiani, Phys. Rev. B **62**, 16773 (2000). Copyright 2000 by the American Physical Society.

Figure 4. Schematic drawing of the system under investigation, which includes the active region of the structure and the ideal contacts. Several regimes of carrier transport will be considered in the active region.

Figure 5. Low-frequency current spectral density at equilibrium normalized to $2qI_S$ as a function of the degeneracy factor $\varepsilon_F / k_B T$, at T=300 K, in a one-dimensional, two-terminal ballistic conductor. Symbols correspond to MC calculations and full line and dotted curve to predictions for nondegenerate and degenerate conditions, respectively.

From [92], T. González *et al.*, Semicond. Sci. Technol. **14**, L37 (1999), with permission from the Institute of Physics Publishing @ 1999.

Figure 6. Spatial profiles along the active region of (a) electron concentration and (b) normalized potential $q\phi(x)/k_BT$ at equilibrium for different values of λ. From [88], T. González *et al.*, Semicond. Sci. Technol. **13**, 714 (1998), with permission from the Institute of Physics Publishing @ 1998.

Figure 7. (a) Spatial profiles of the normalized potential $q\phi(x)/k_BT$ for different applied voltages U for the case of $\lambda = 30.9$. (b) Current flowing through the sample normalized to the saturation value as a function of the applied voltage U for different values of λ. From [88], T. González *et al.*, Semicond. Sci. Technol. **13**, 714 (1998), with permission from the Institute of Physics Publishing @ 1998.

Figure 8. Spatial profiles along the active region of (a) electron concentration, (b) average energy and (c) average velocity for the case of $\lambda = 30.9$ and several applied voltages. From [88], T. González *et al.*, Semicond. Sci. Technol. **13**, 714 (1998), with permission from the Institute of Physics Publishing @ 1998.

Figure 9. Distribution function $P_n(t)$ of electron counting statistics at the receiving contact as a function of time (in units of $1/\Gamma$) for the static PS (dotted line, Poissonian statistics) and for the dynamic PS (solid line, sub-Poissonian statistics), in a structure with $U = 40\, k_BT/q$ and $\lambda = 30.9$. Adapted from [90], O. M. Bulashenko *et al.,* Phys. Rev. B **57**, 1366 (1998). Copyright 1998 by the American Physical Society.

Figure 10. Current noise spectral density vs applied voltage calculated by using static (open symbols) and dynamic (closed symbols, solid line) PS schemes for several contact concentrations n_c (in cm^{-3} with the corresponding λ): (⎡) 10^{13}, 0.15; (⎨) 2×10^{15}, 2.18; (⌡)

10^{16}, 4.88; (⌠) 2.5×10^{16}, 7.72; (〈) 10^{17}, 15.45; (□) 4×10^{17}, 30.9. The static case is shown to be nicely described by Eq. (14). The dotted lines represent $2qI$ (marked for each injection rate density by the corresponding symbol). Adapted from [86], T. González *et al.*, Phys. Rev. B **56**, 6424 (1997). Copyright 1997 by the American Physical Society.

Figure 11. Fano factor vs applied voltage for several values of λ. From [88], T. González *et al.*, Semicond. Sci. Technol. **13**, 714 (1998), with permission from the Institute of Physics Publishing @ 1998.

Figure 12. Decomposition of the spectral density of current fluctuations S_I into velocity, number, and velocity-number contributions vs applied voltage for the case $\lambda = 7.72$ calculated using (a) the static and (b) the dynamic PS schemes. From [88], T. González *et al.*, Semicond. Sci. Technol. **13**, 714 (1998), with permission from the Institute of Physics Publishing @ 1998.

Figure 13. (a) Autocorrelation function and (b) spectral density of current fluctuations at equilibrium for several values of λ. Static and dynamic PS schemes provide the same results. From [88], T. González *et al.*, Semicond. Sci. Technol. **13**, 714 (1998), with permission from the Institute of Physics Publishing @ 1998.

Figure 14. (a) Autocorrelation function and (b) spectral density of current fluctuations calculated using the dynamic PS for the case of $\lambda = 7.72$ at several applied voltages. From [88], T. González *et al.*, Semicond. Sci. Technol. **13**, 714 (1998), with permission from the Institute of Physics Publishing @ 1998.

Figure 15. Current (normalized to the saturation value $I_S = \int_0^\infty I_C(\varepsilon_x)d\varepsilon_x$) and amplitude of the potential minimum vs applied voltage. The inset shows the spatial profile of the potential $q\phi(x)/k_BT$ for different applied voltages.

Figure 16. Current $I_C(\varepsilon_x)$ (normalized to the saturation value I_S) and noise $S_{I_C}(\varepsilon_x)$ (normalized to $2qI_S$) contributions of the injected electrons as a function of the longitudinal energy ε_x, and ratio between both quantities. From [85], T. González *et al.*, in *Proc. of the 25th Int. Conf. on the Physics of Semiconductors*, N. Miura and T. Ando, Eds., Springer Proc. in Physics, Berlin (2001), Vol.87, p. 1343, with permission from Springer-Verlag @ 2001.

Figure 17. Total suppression (Fano) factor γ (calculated under static and dynamic PS schemes), Coulomb γ_C and Fermi γ_F suppression factors as a function of: (a) applied voltage, and (b) amplitude of the potential minimum U_m. The two limiting behaviors of γ for low and high applied voltages are also shown. From [85], T. González *et al.*, in *Proc. of the 25th Int. Conf. on the Physics of Semiconductors*, N. Miura and T. Ando, Eds., Springer Proc. in Physics, Berlin (2001), Vol.87, p. 1343, with permission from Springer-Verlag @ 2001.

Figure 18. Cross-correlation between current fluctuations due to carriers injected with energies ε_x and ε'_x at the left contact as a function of ε_x for several values of ε'_x and $qU/k_BT = 1000$. Vertical lines indicate the position of qU_m. From [85], T. González *et al.*, in *Proc. of the 25th Int. Conf. on the Physics of Semiconductors*, N. Miura and T. Ando, Eds., Springer Proc. in Physics, Berlin (2001), Vol.87, p. 1343, with permission from Springer-Verlag @ 2001.

Figure 19. Total (squares), Fermi (circles) and Coulomb (diamond) suppression factors as a function of the applied voltage in a structure with $L = 50$ nm, $m = 0.066\,m_0$, $n_c = 5\times10^{17}$ cm^{-3} $(\varepsilon_F = 5.08\,k_BT/q)$, $\varepsilon = 12.55\,\varepsilon_0$ and $T = 77$ K.

Figure 20. Low-frequency spectral density of current fluctuations normalized to $2qI_S$ vs the ballistic parameter ℓ / L for an applied voltage $U = 40\, k_B T / q$. Calculations are performed by using static and dynamic PS schemes, and considering elastic and inelastic scattering mechanisms. $2qI$ is also plotted for comparison. From [91], T. González *et al.*, Phys. Rev. B **60**, 2670 (1999). Copyright 1999 by the American Physical Society.

Figure 21. Fano factor vs the ballistic parameter ℓ / L for the cases of elastic and inelastic scattering at different applied voltages. Calculations are performed by using the dynamic PS scheme. From [91], T. González *et al.*, Phys. Rev. B **60**, 2670 (1999). Copyright 1999 by the American Physical Society.

Figure 22. Fano factor vs the ballistic parameter ℓ / L for an applied bias $U = 40\, k_B T / q$ calculated with different contact models. Calculations refer to the dynamic PS considering elastic and inelastic scattering. From [91], T. González *et al.*, Phys. Rev. B **60**, 2670 (1999). Copyright 1999 by the American Physical Society.

Figure 23. Fano factor vs applied voltage calculated with the dynamic potential under diffusive regime for the cases of elastic and inelastic scattering mechanisms. Adapted from [89] T. González *et al.*, Phys. Rev. Lett. **80**, 2901 (1998). Copyright 1998 by the American Physical Society.

Figure 24. Spectrum of the Fano factor under diffusive regime calculated within static and dynamic PS schemes for (a) elastic and (b) inelastic scattering, and an applied voltage $U = 100\, k_B T / q$. The different contributions to the total spectrum are reported in the figure. From [91], T. González *et al.*, Phys. Rev. B **60**, 2670 (1999). Copyright 1999 by the American Physical Society.

Figure 25. Fano factor as a function of the characteristic parameter of space charge λ under diffusive regime calculated within dynamic PS scheme for $U = 100\, k_B T / q$. The different contributions to the Fano factor are also shown in the figure. Adapted from [91], T. González *et al.*, Phys. Rev. B **60**, 2670 (1999). Copyright 1999 by the American Physical Society.

Figure 26. Fano factor for the cases of 1, 2 and 3 dimensions of momentum space calculated within the dynamic PS scheme for elastic scattering as a function of (a) ballistic parameter ℓ / L with an applied voltage $U = 40\, k_B T / q$ and (b) applied bias U under diffusive regime ($\ell / L = 1.07 \times 10^{-3}$). Adapted from [91], T. González *et al.*, Phys. Rev. B **60**, 2670 (1999). Copyright 1999 by the American Physical Society.

Figure 27. Fano factor γ for $U = 40\, k_B T / q$ as a function of the energy exponent of the relaxation time α. Symbols correspond to MC calculations performed for the cases of 2 and 3 dimensions of momentum space and solid line to analytical calculations within a drift approximation for the case $d = 3$ [70]. The insets show the $I - U$ curves for the different values of α.

Figure 28. Spatial profiles of average quantities along the active region of the structure for an applied voltage $U = 80\, k_B T / q$ and several values of the energy exponent of the relaxation time α. (a) Concentration, (b) electric field, (c) velocity, and (d) scattering time.

Figure 29. (a) Spatial profiles along the active region of average velocity and (inset) normalized potential barrier $q\phi(x) / k_B T$ at an applied voltage $U = 40\, k_B T / q$, and (b) current flowing through the sample normalized to the saturation value I_S as a function of the applied voltage, for $\tau_r = 20$ ps and different values of τ_g. The ballistic case is also

plotted for comparison. From [96], B. G. Vasallo *et al.*, Semicond. Sci. Technol., with permission from the Institute of Physics Publishing @ 2002.

Figure 30. Fano factor vs bias voltage for $\tau_r = 20$ ps and different values of τ_g, and in the ballistic case. The thick solid line corresponds to the case when long-range Coulomb interaction is not considered (for any of the previous conditions). From [96], B. G. Vasallo *et al.*, Semicond. Sci. Technol., with permission from the Institute of Physics Publishing @ 2002.

Figure 31. Autocorrelation function of current fluctuations $C_I(t)$ normalized to the zero-time value $C_I(0)$ corresponding to two applied voltages for which enhanced shot noise is found. The short-time decay is reported in the inset. The GR characteristic times are $\tau_r = 20$ ps and $\tau_g = 5$ ps. From [96], B. G. Vasallo *et al.*, Semicond. Sci. Technol., with permission from the Institute of Physics Publishing @ 2002.

Figure 32. Velocity-number contribution $C_{VN}(t)$ to the autocorrelation function $C_I(t)$ for an applied voltage $U = 40\, k_B T / q$ and GR characteristic times $\tau_r = 20$ ps and $\tau_g = 5$ ps. The inset details the short-time behavior. From [96], B. G. Vasallo *et al.*, Semicond. Sci. Technol., with permission from the Institute of Physics Publishing @ 2002.

Figure 33. Spectral density of current fluctuations $S_I(f)$ as a function of frequency for an applied voltage $U = 40\, k_B T / q$ and GR characteristic times $\tau_r = 20$ ps and $\tau_g = 5$ ps. $S_I(f)$ in the ballistic case is also plotted. From [96], B. G. Vasallo *et al.*, Semicond. Sci. Technol., with permission from the Institute of Physics Publishing @ 2002.

Figure 34. Fano factor vs ℓ / L in the transition from quasiballistic to diffusive regime considering elastic and inelastic scattering mechanisms (separately) and GR processes

characterized by $\tau_r = 20$ ps and $\tau_g = 5$ ps. From [96], B. G. Vasallo *et al.*, Semicond. Sci. Technol., with permission from the Institute of Physics Publishing @ 2002.

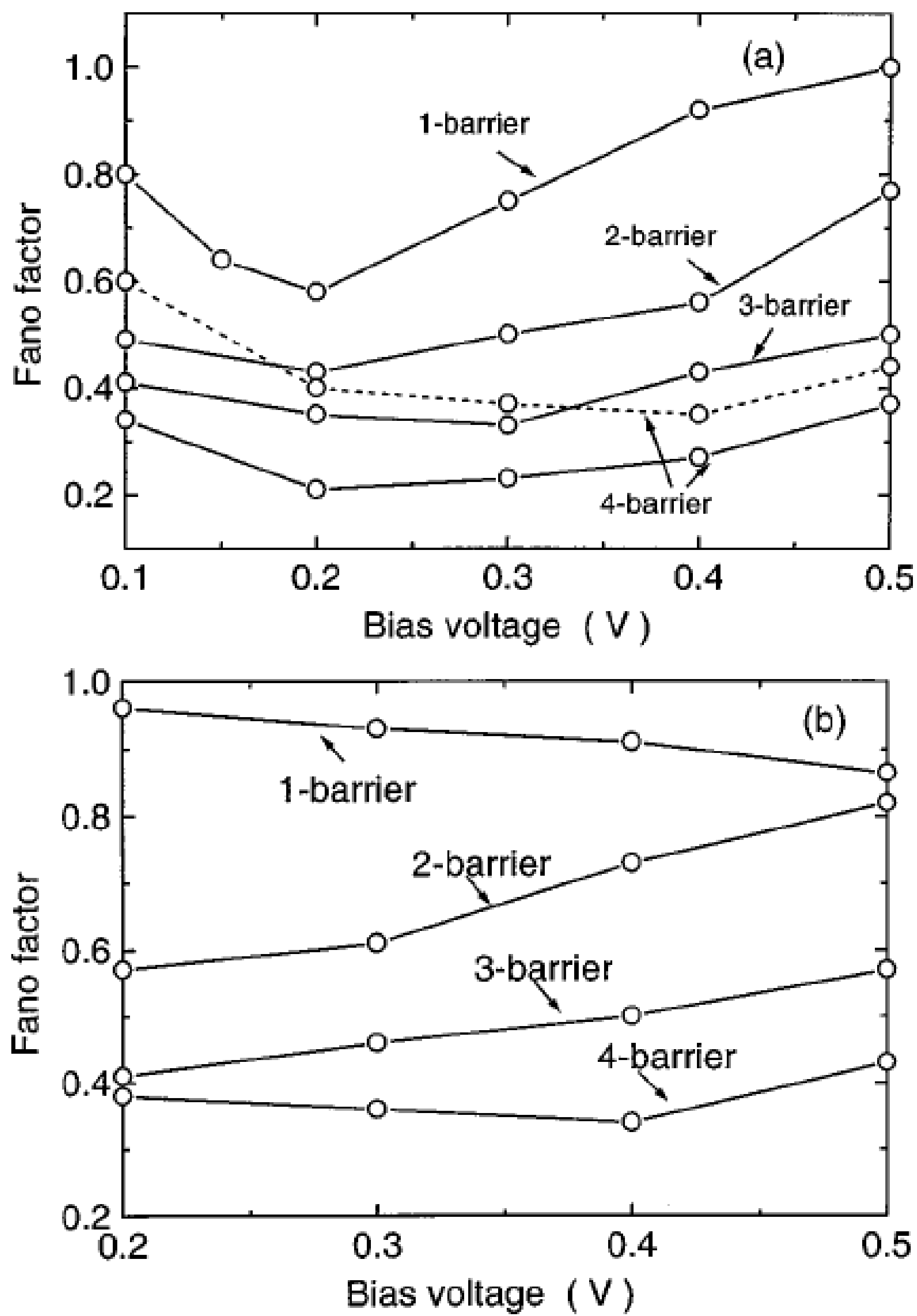

Figure 1

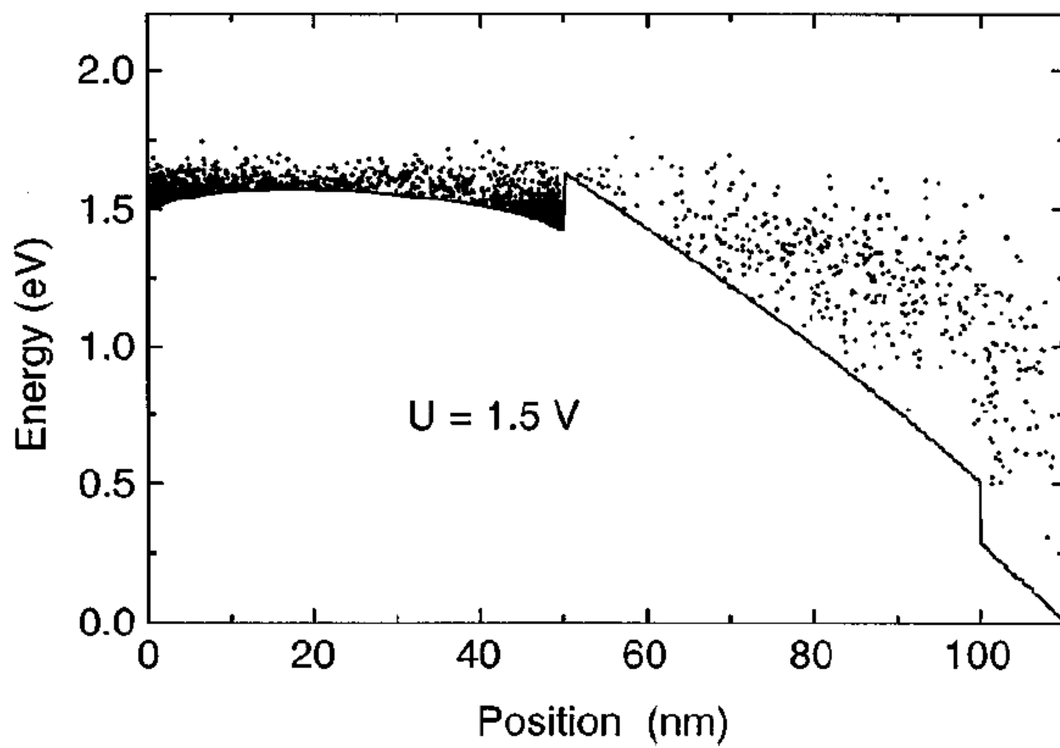

Figure 2

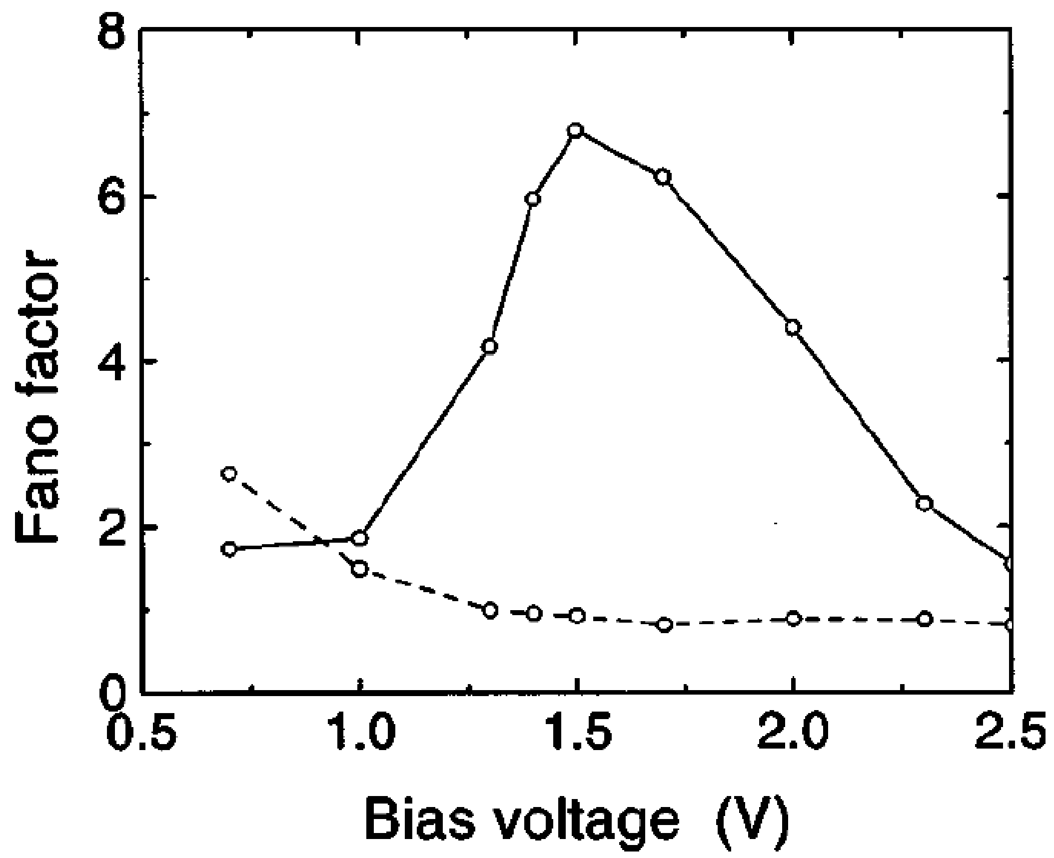

Figure 3

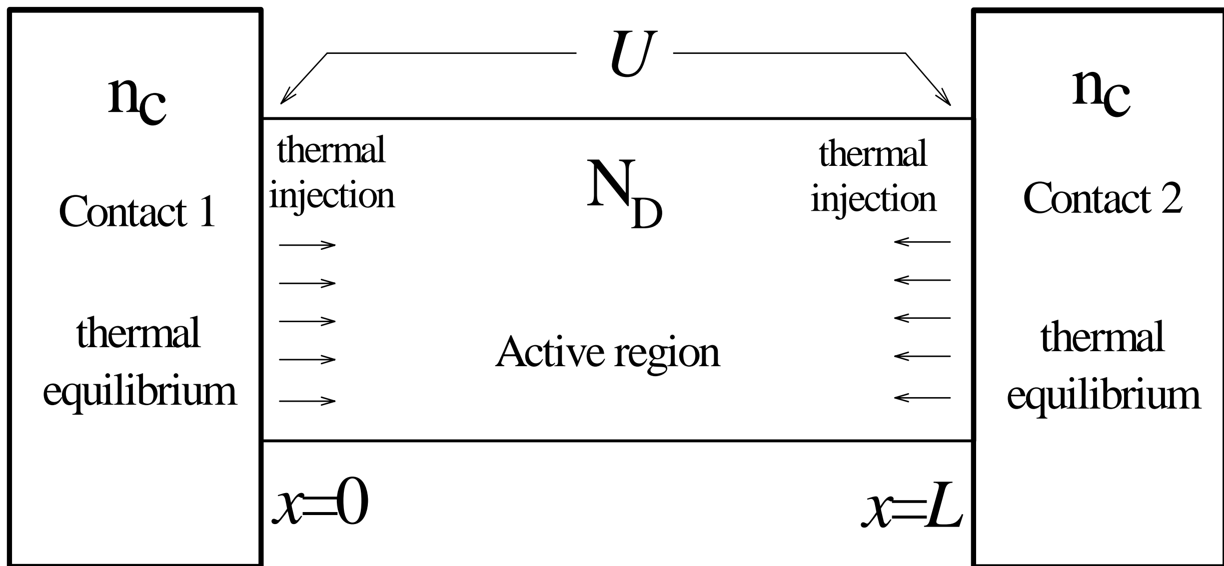

Figure 4

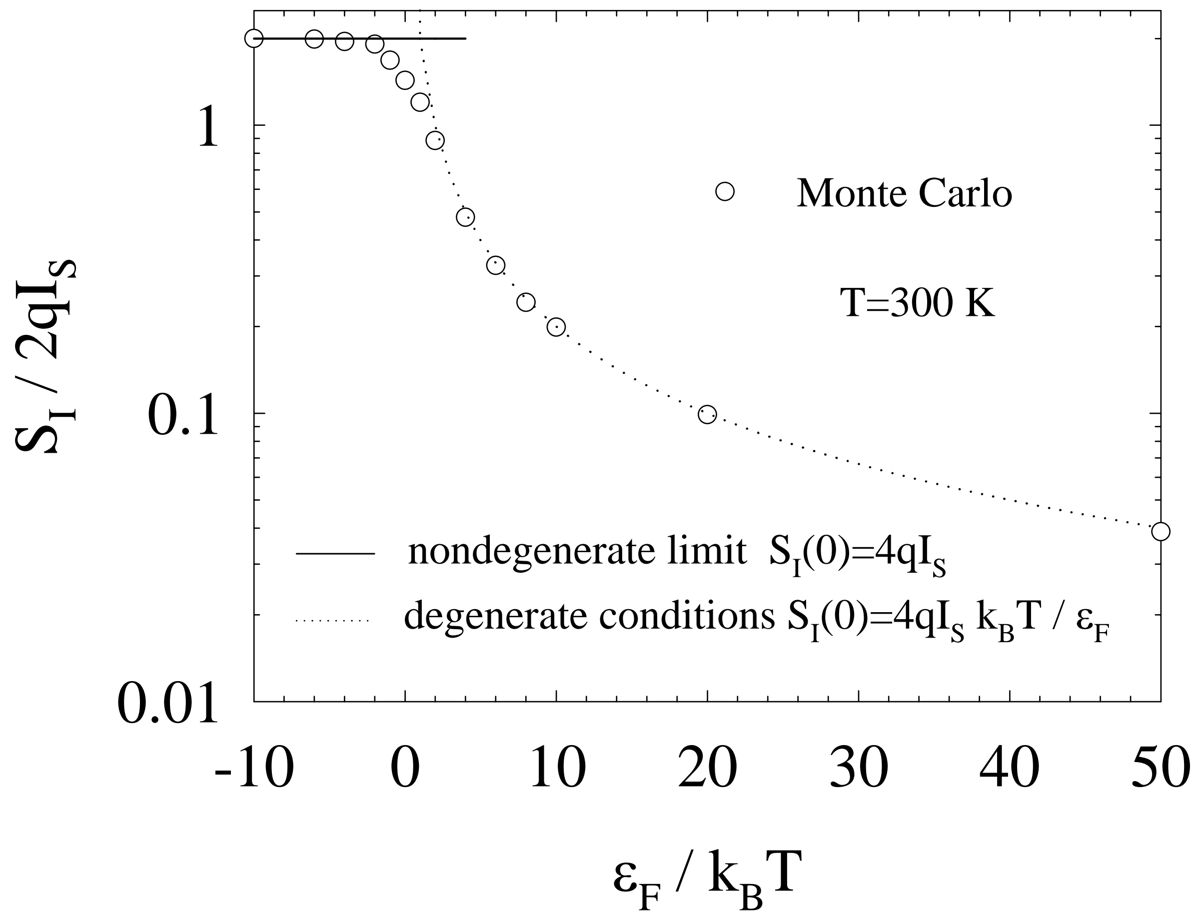

Figure 5

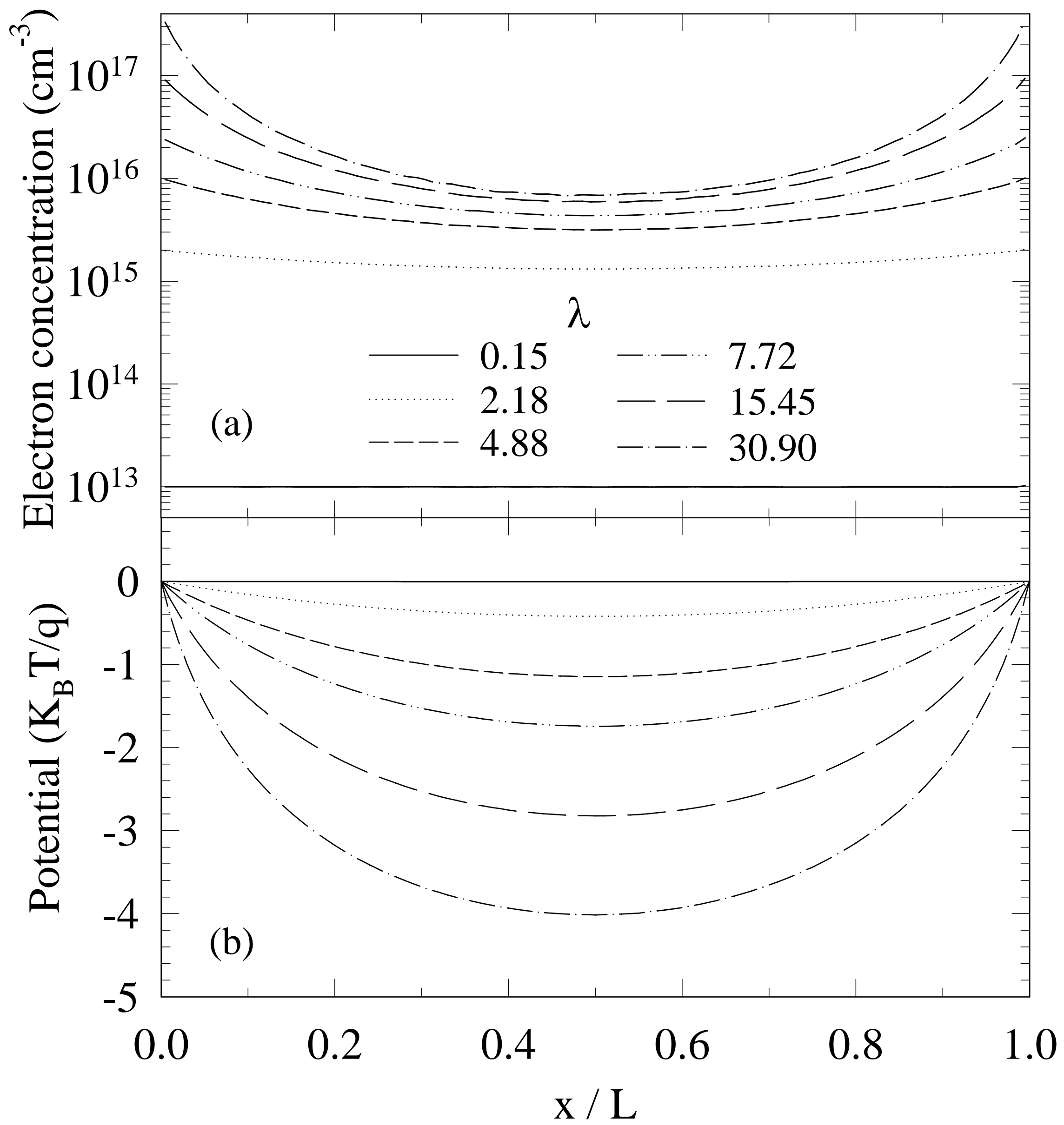

Figure 6

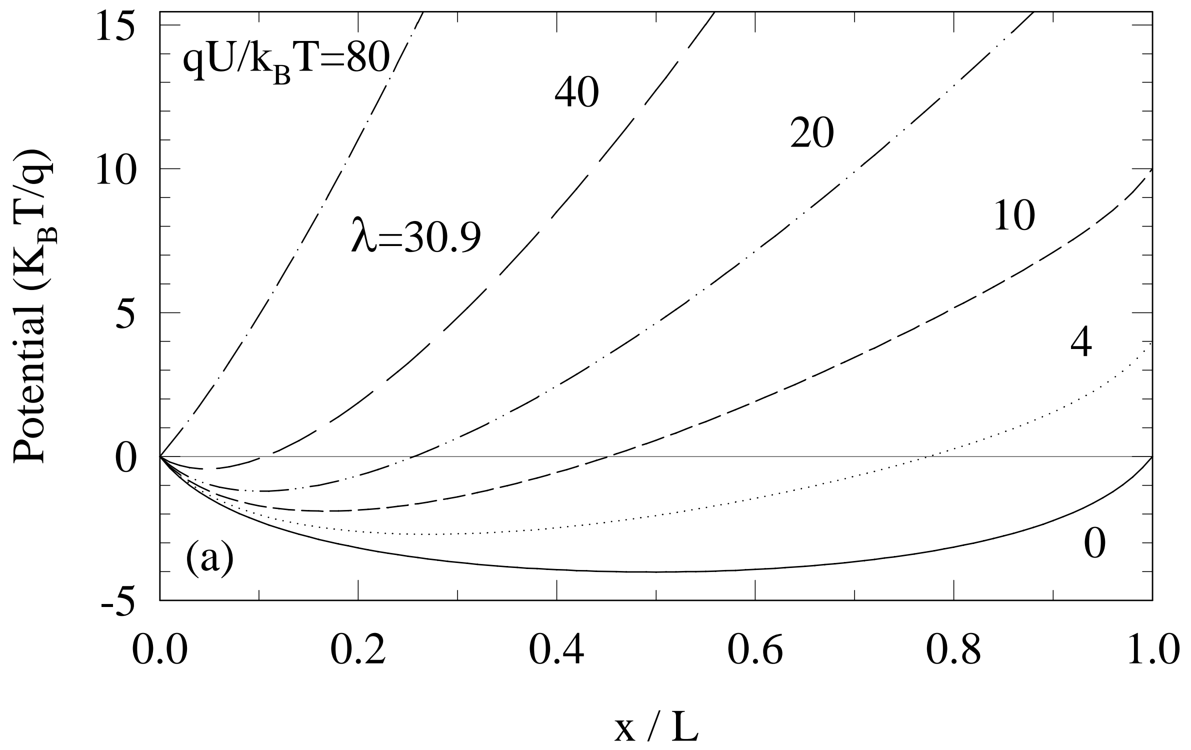

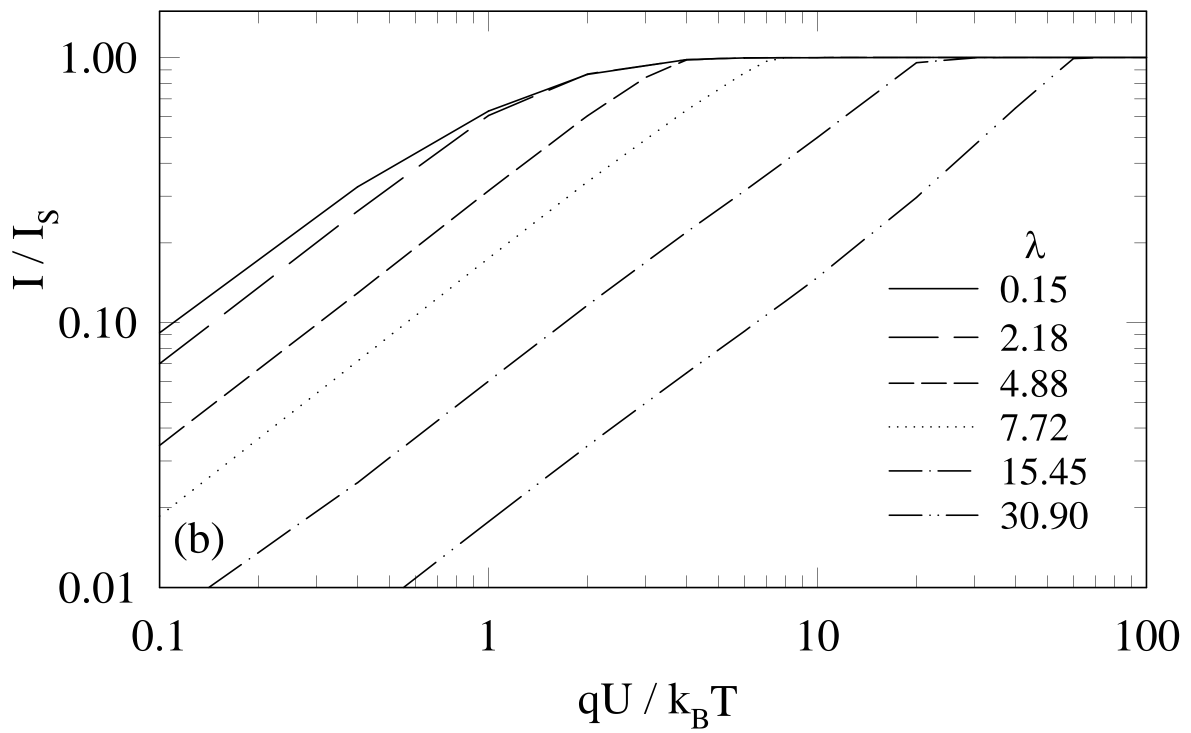

Figure 7

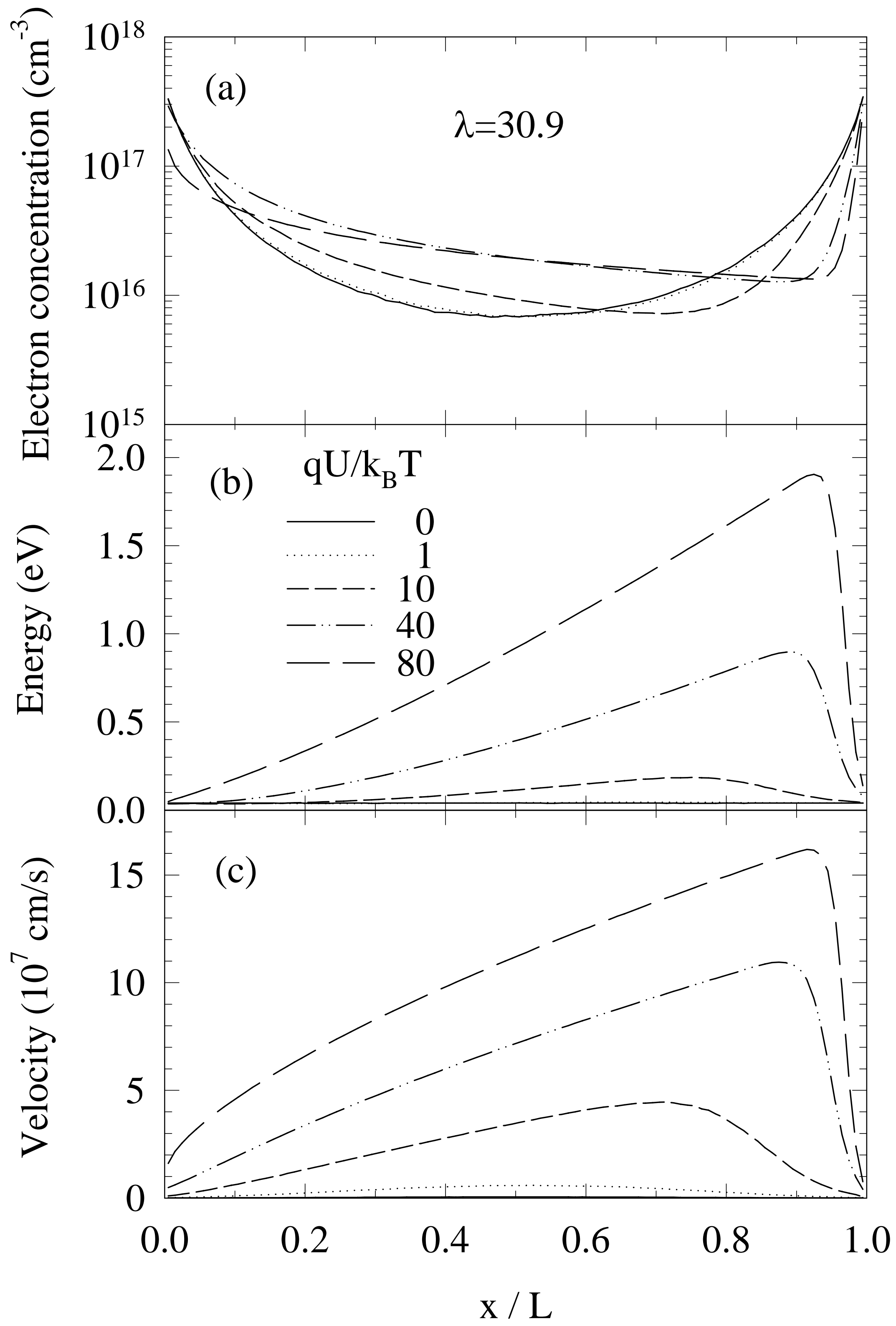

Figure 8

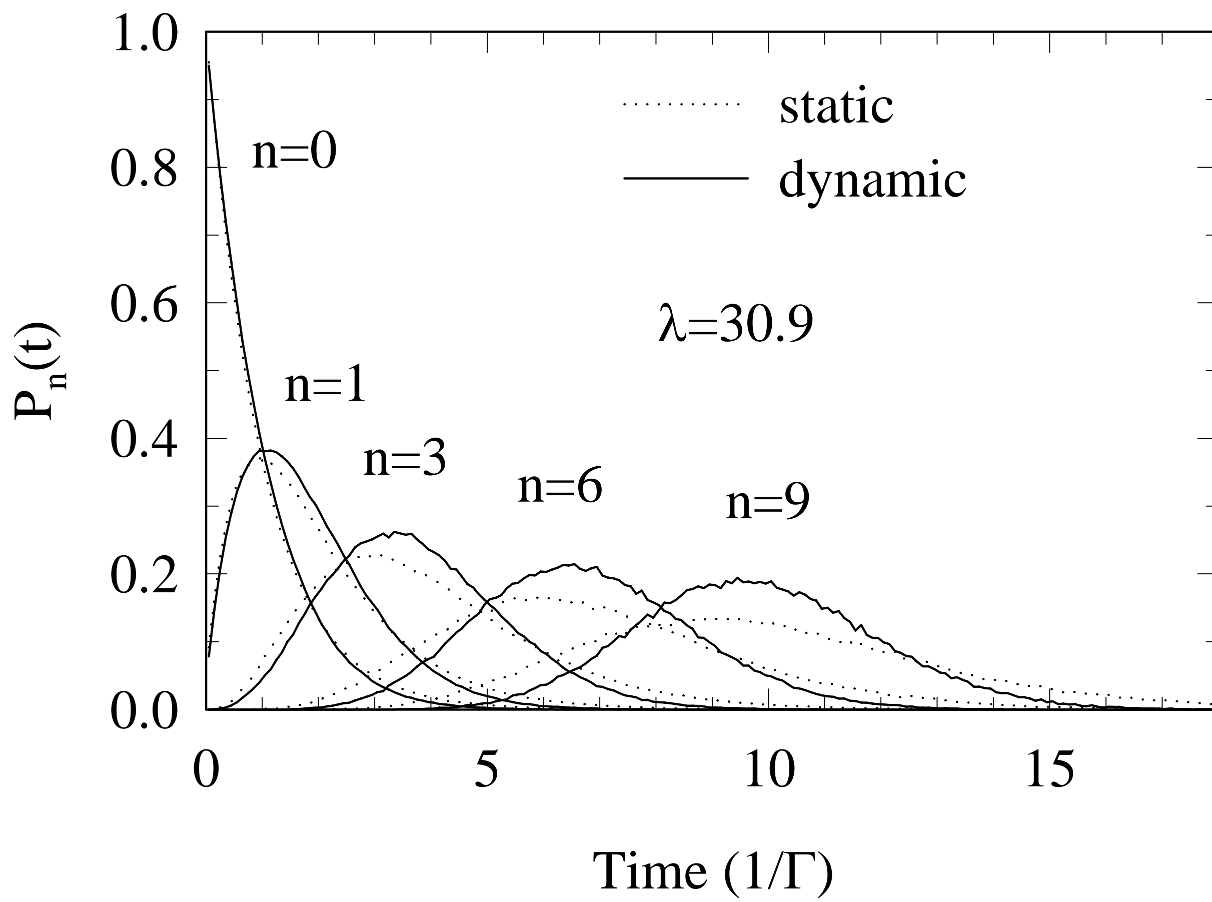

Figure 9

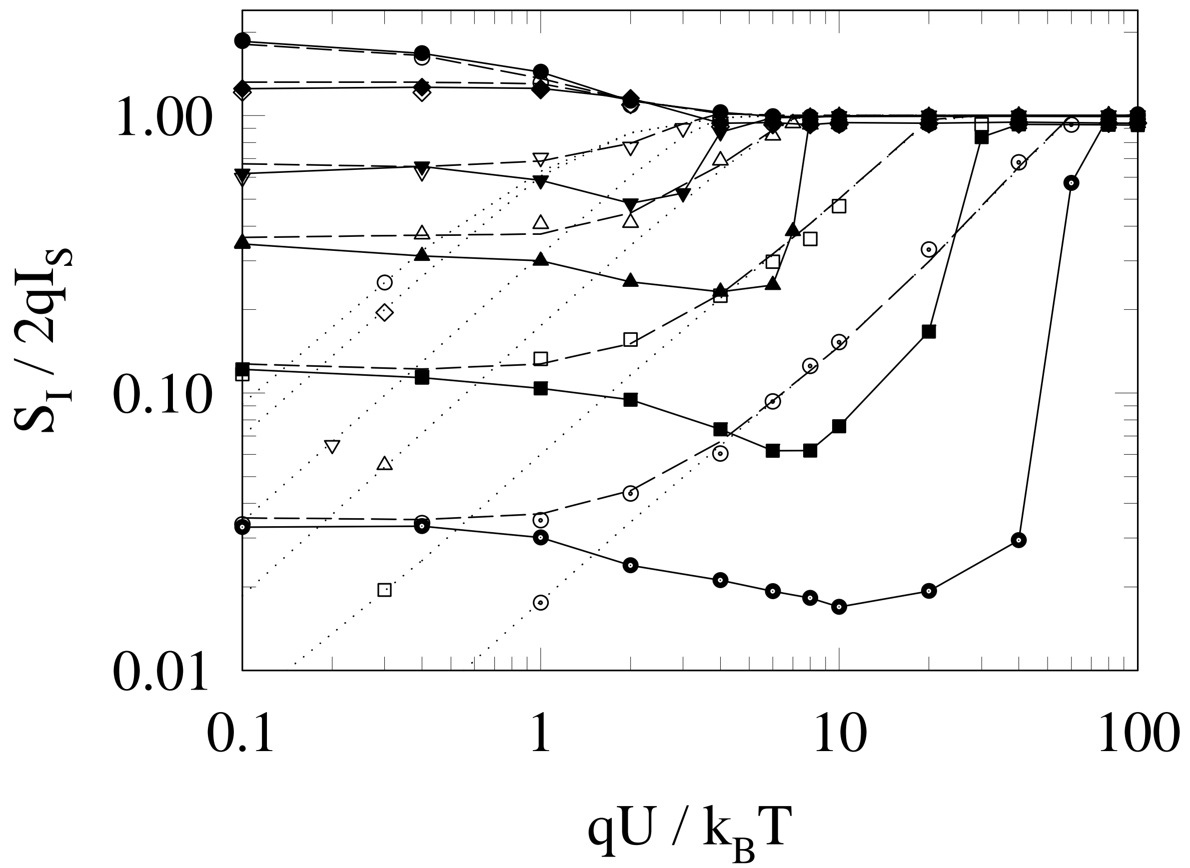

Figure 10

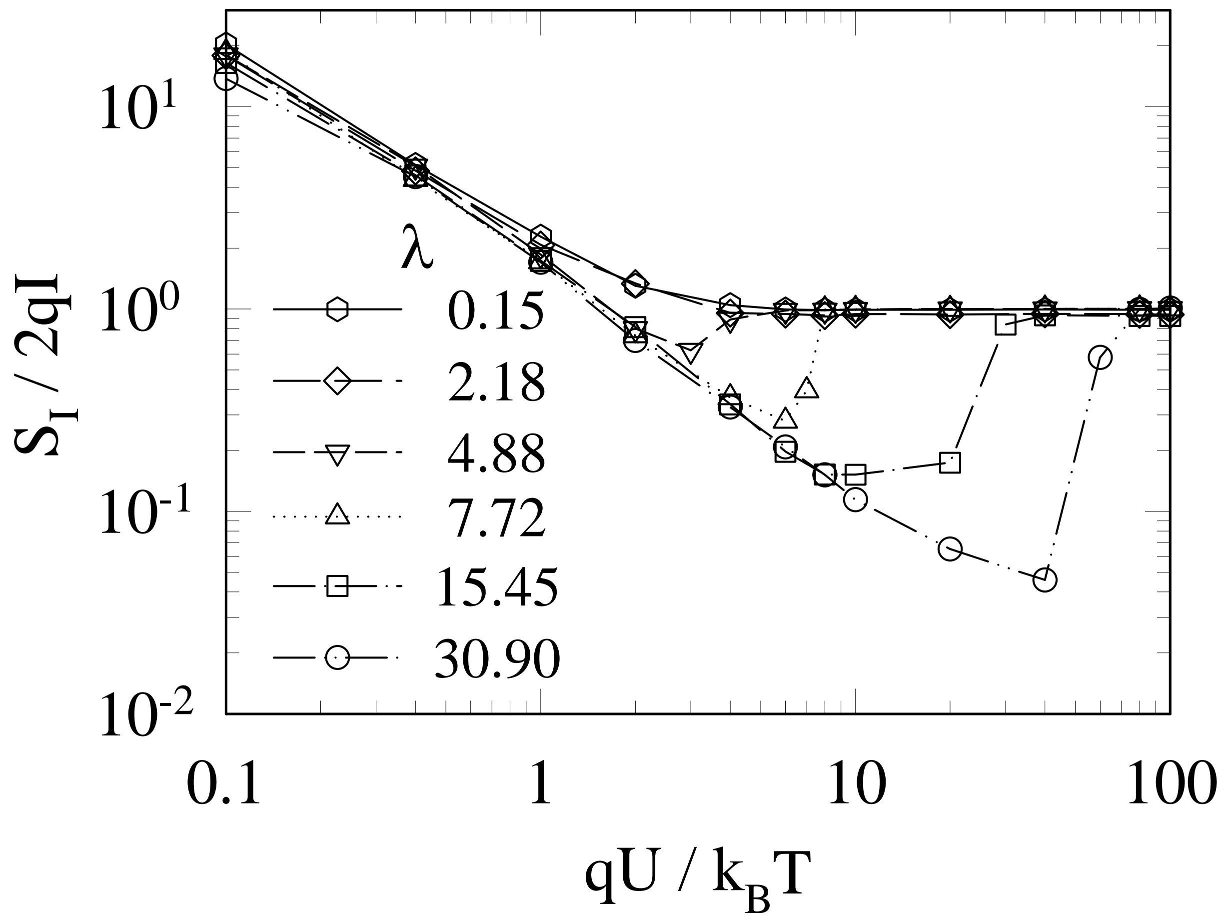

Figure 11

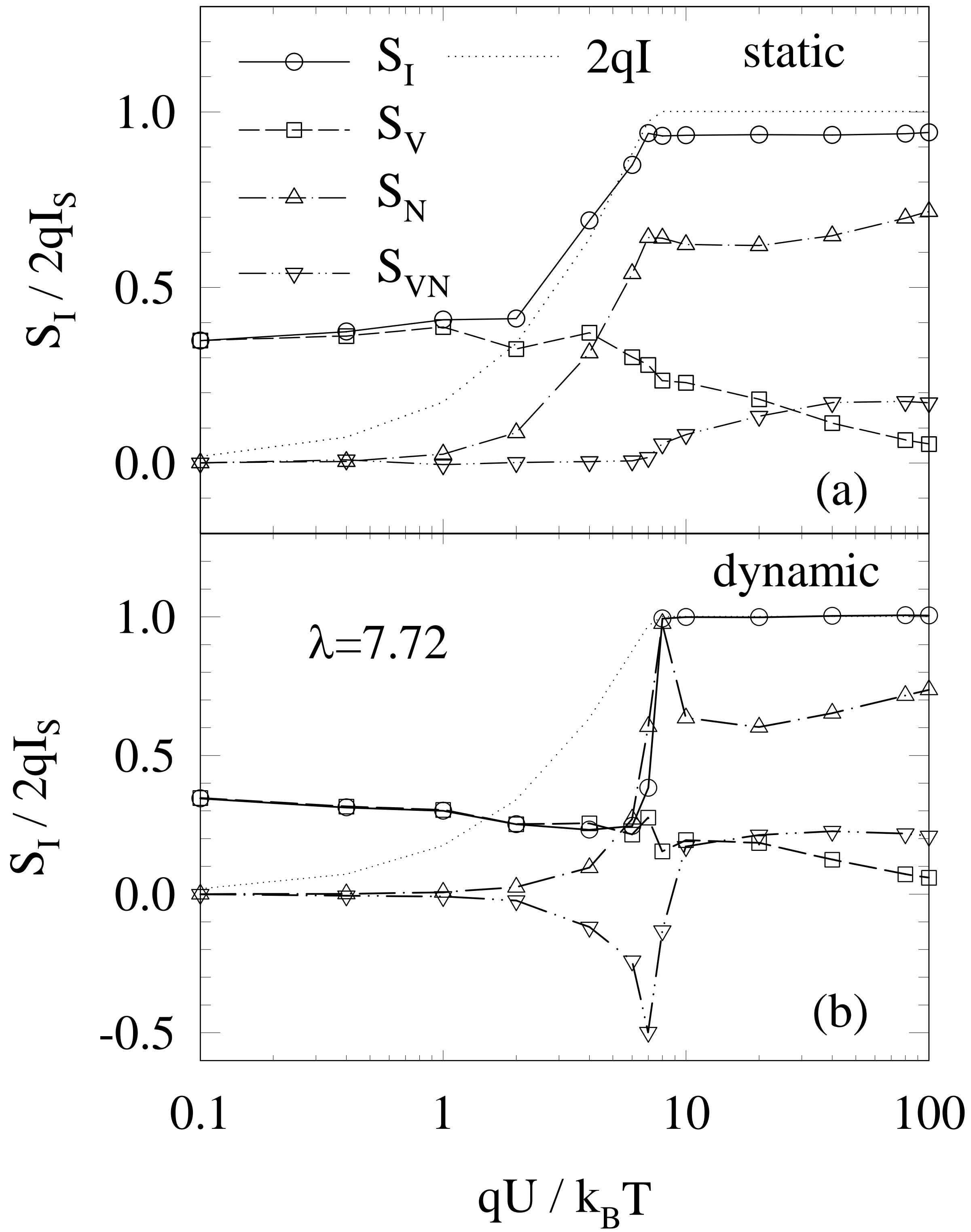

Figure 12

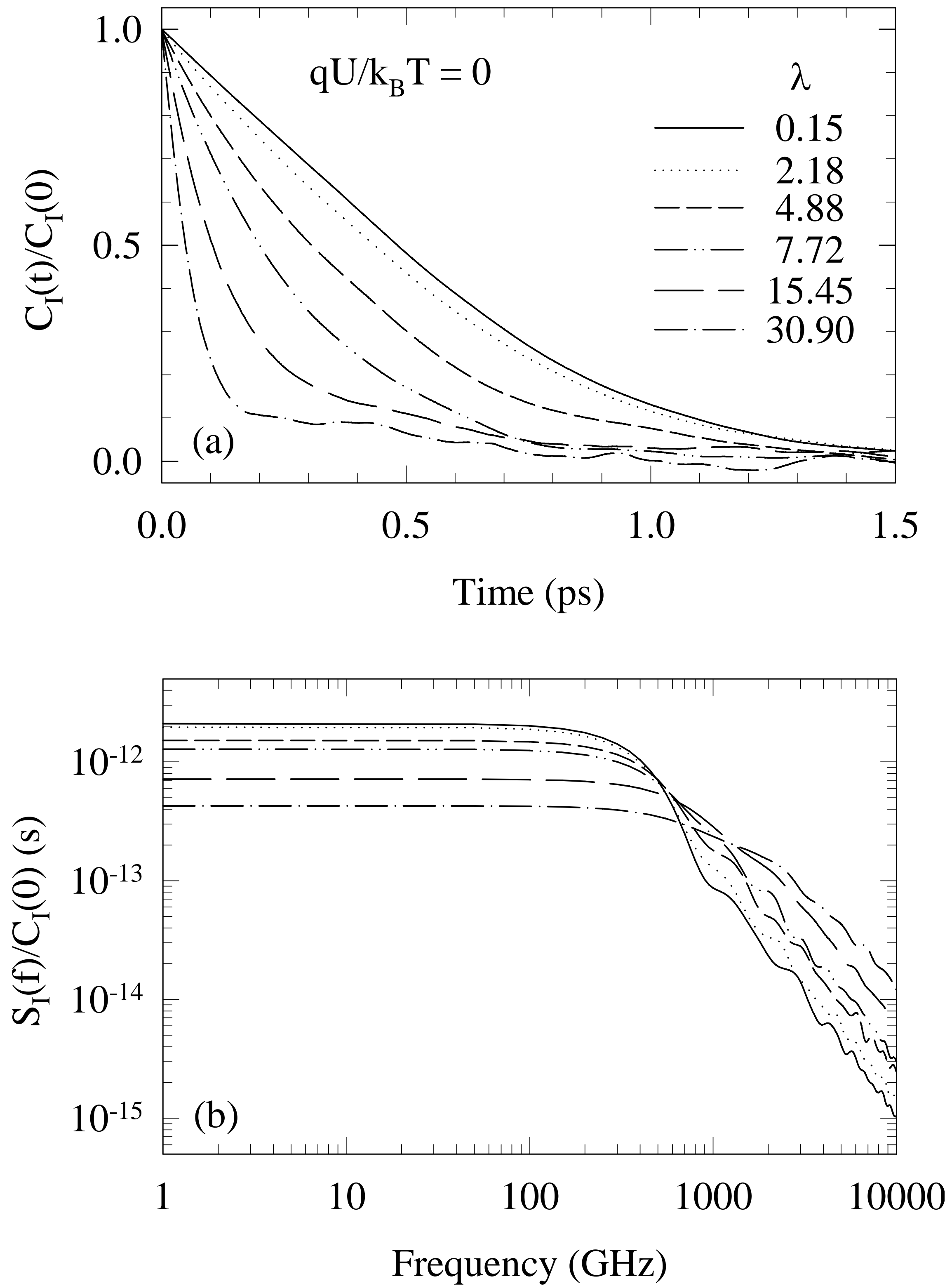

Figure 13

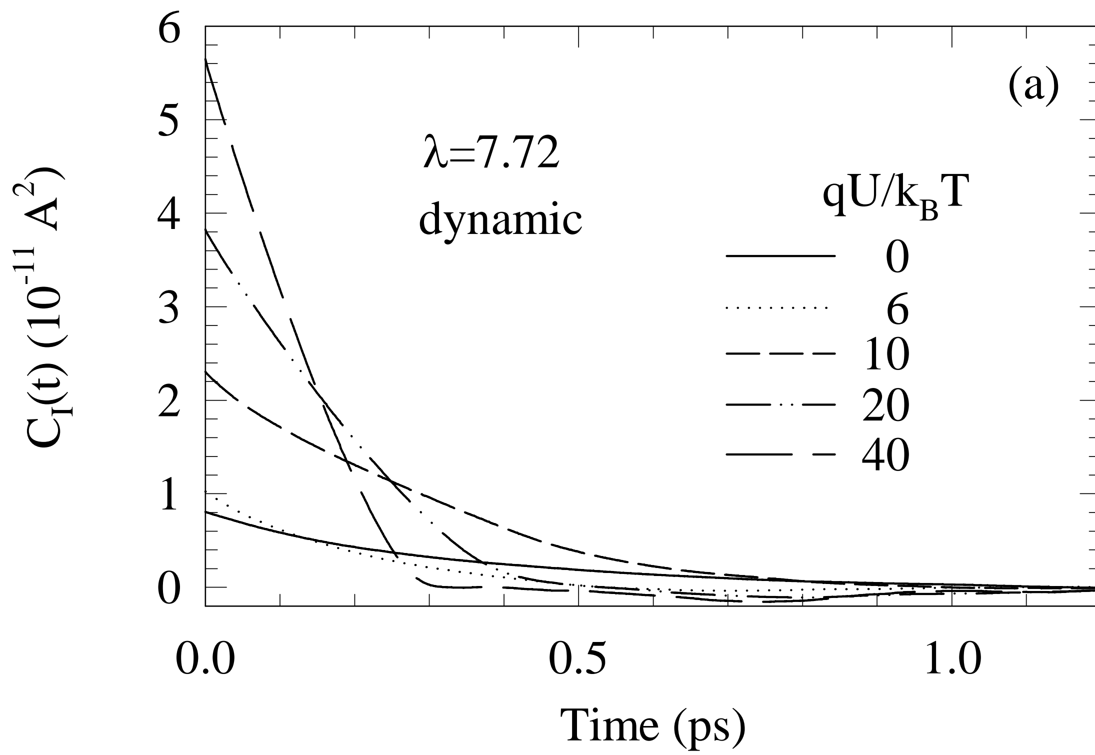

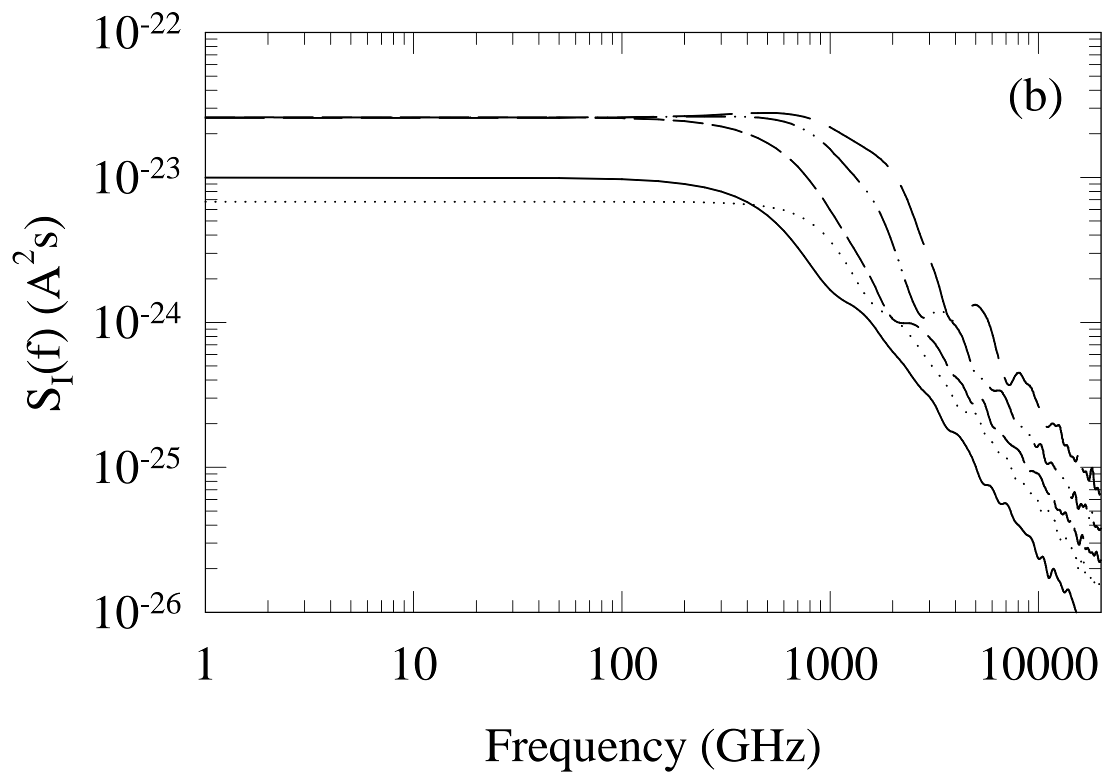

Figure 14

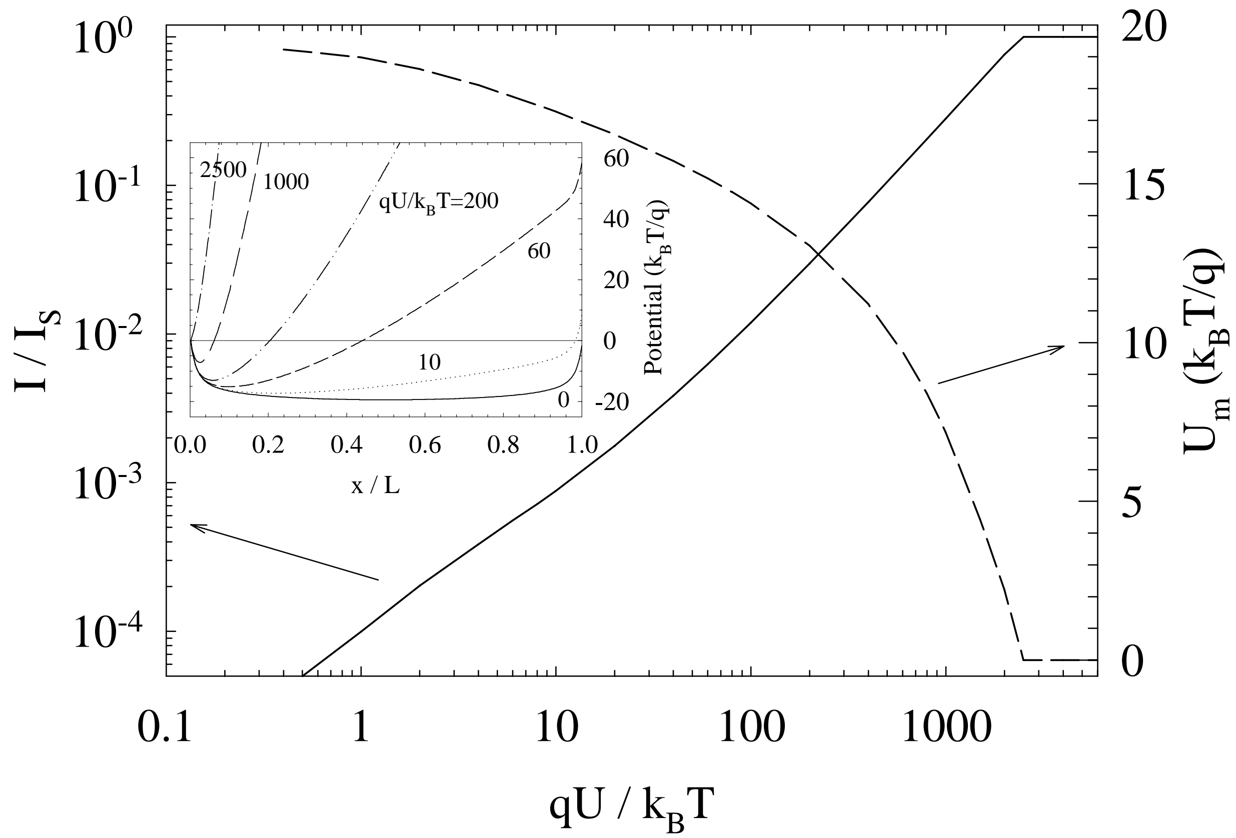

Figure 15

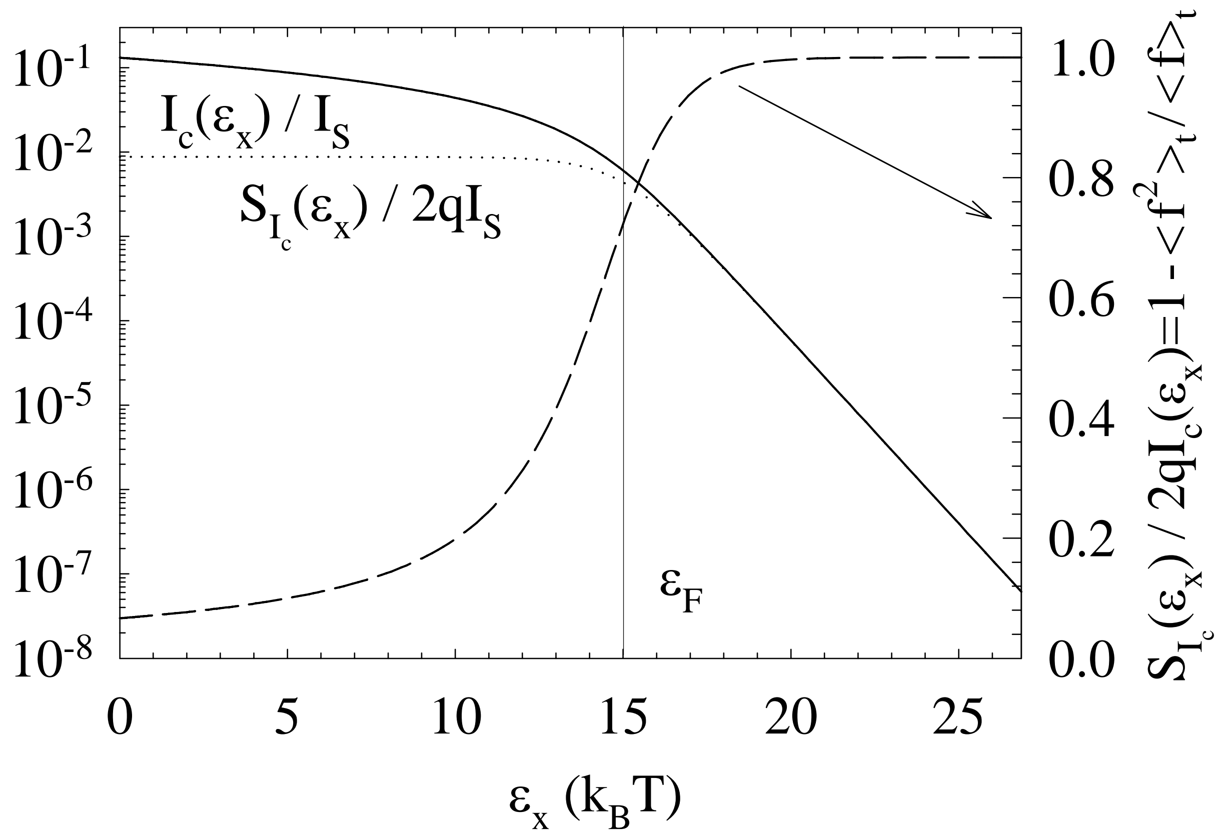

Figure 16

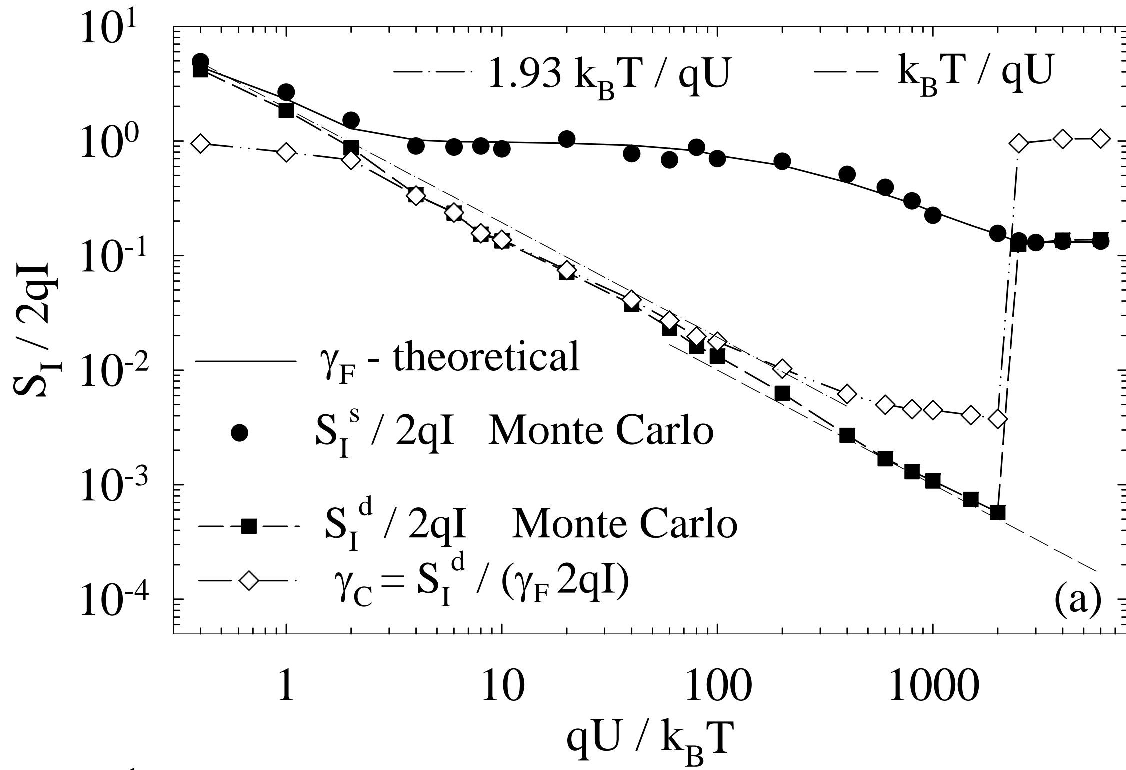

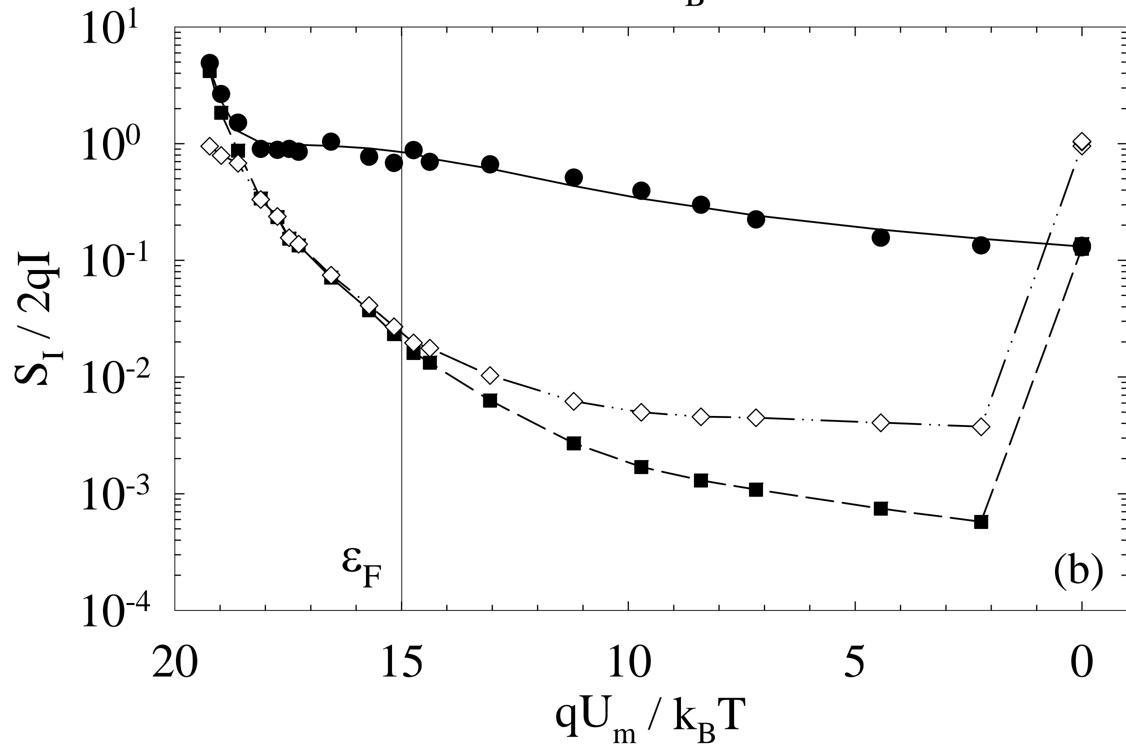

Figure 17

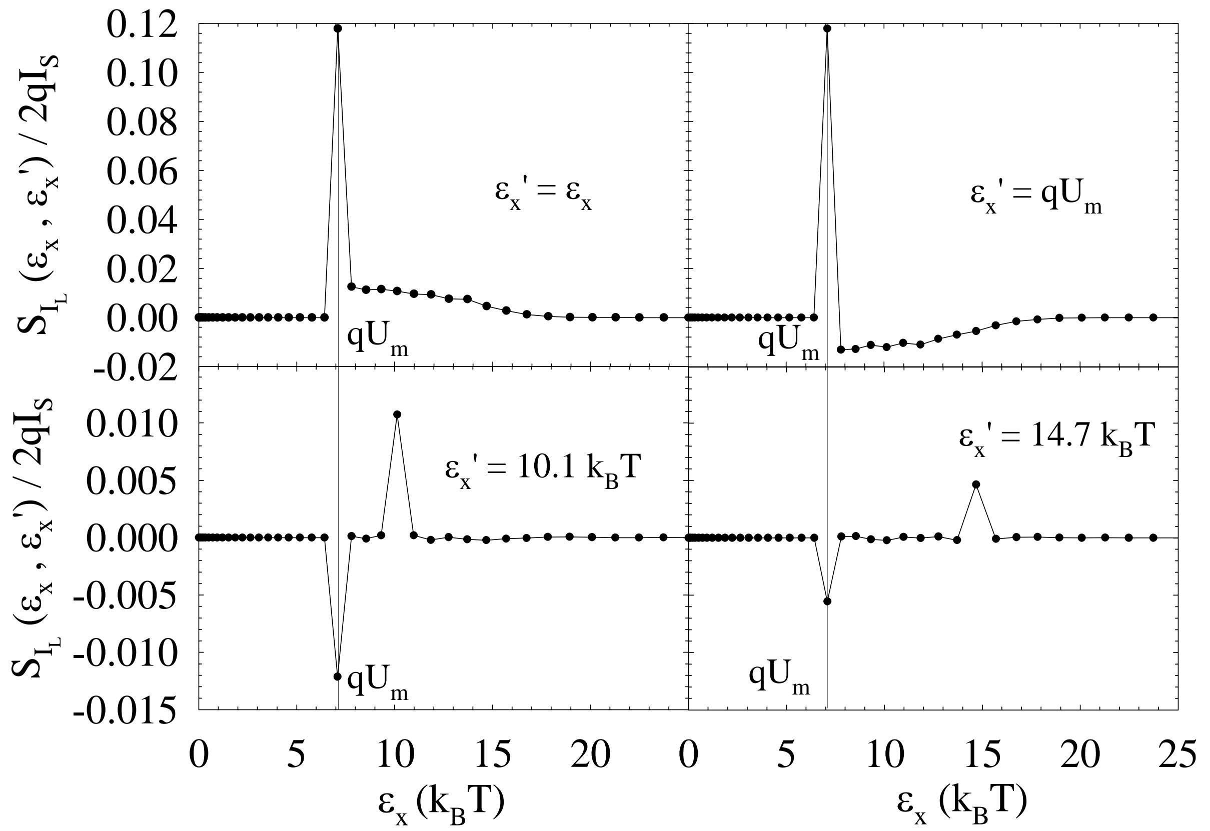

Figure 18

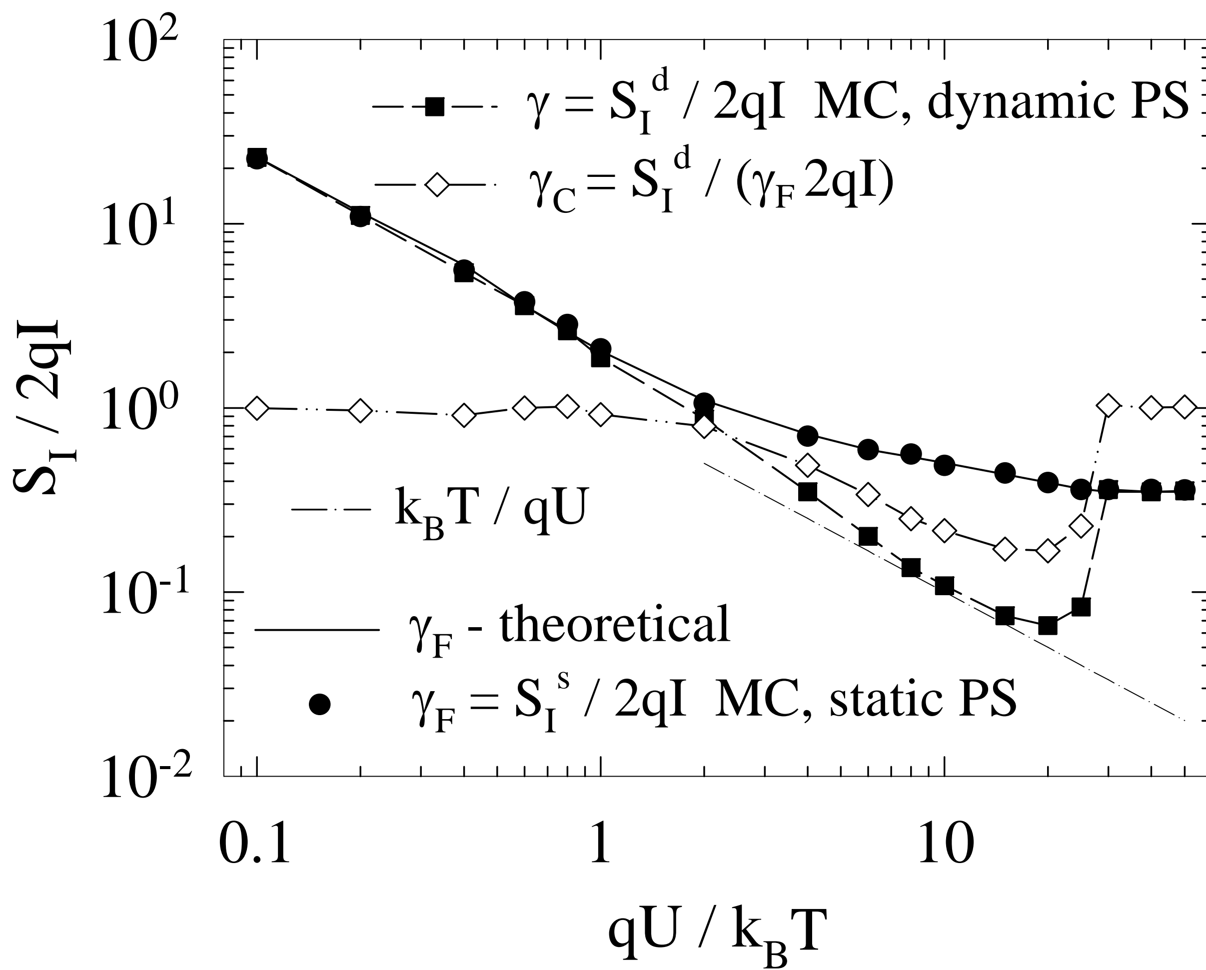

Figure 19

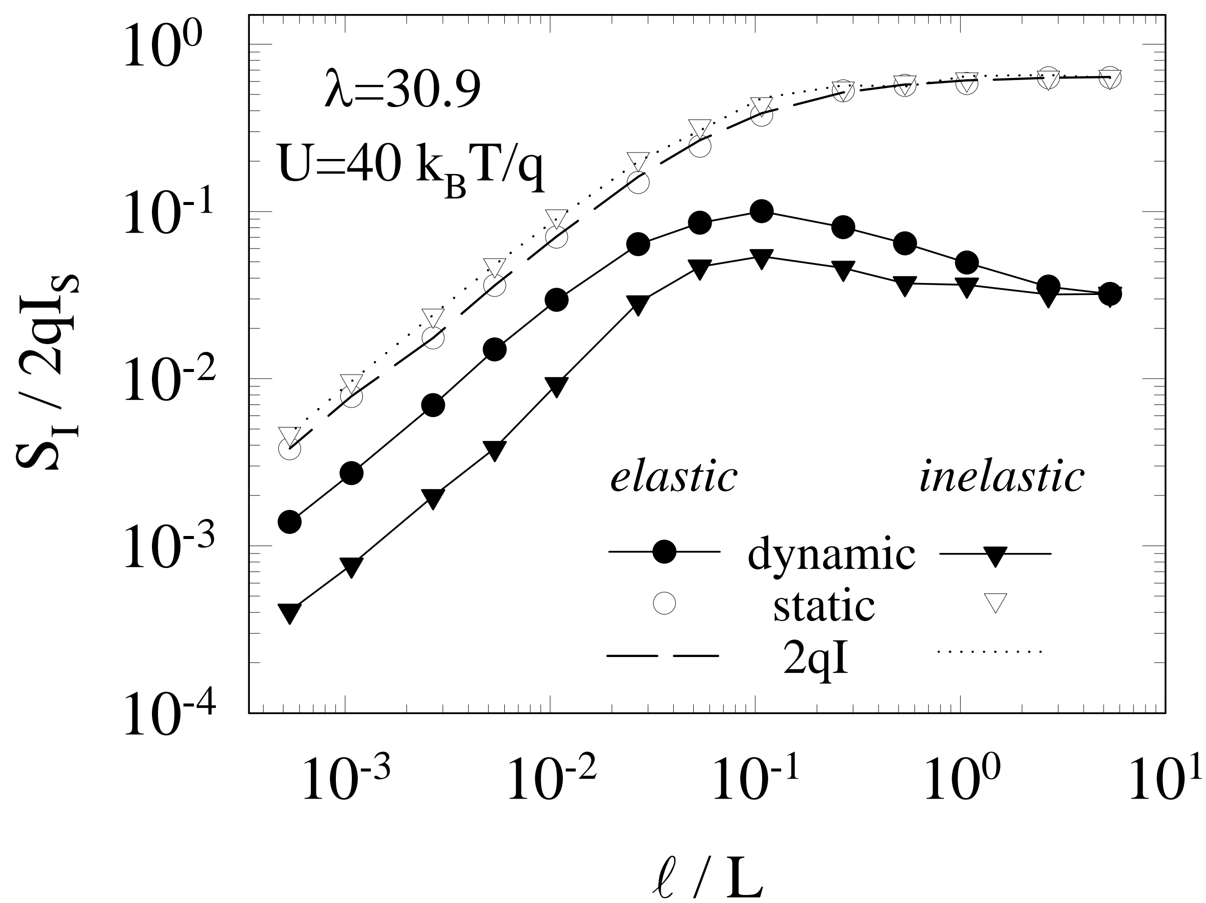

Figure 20

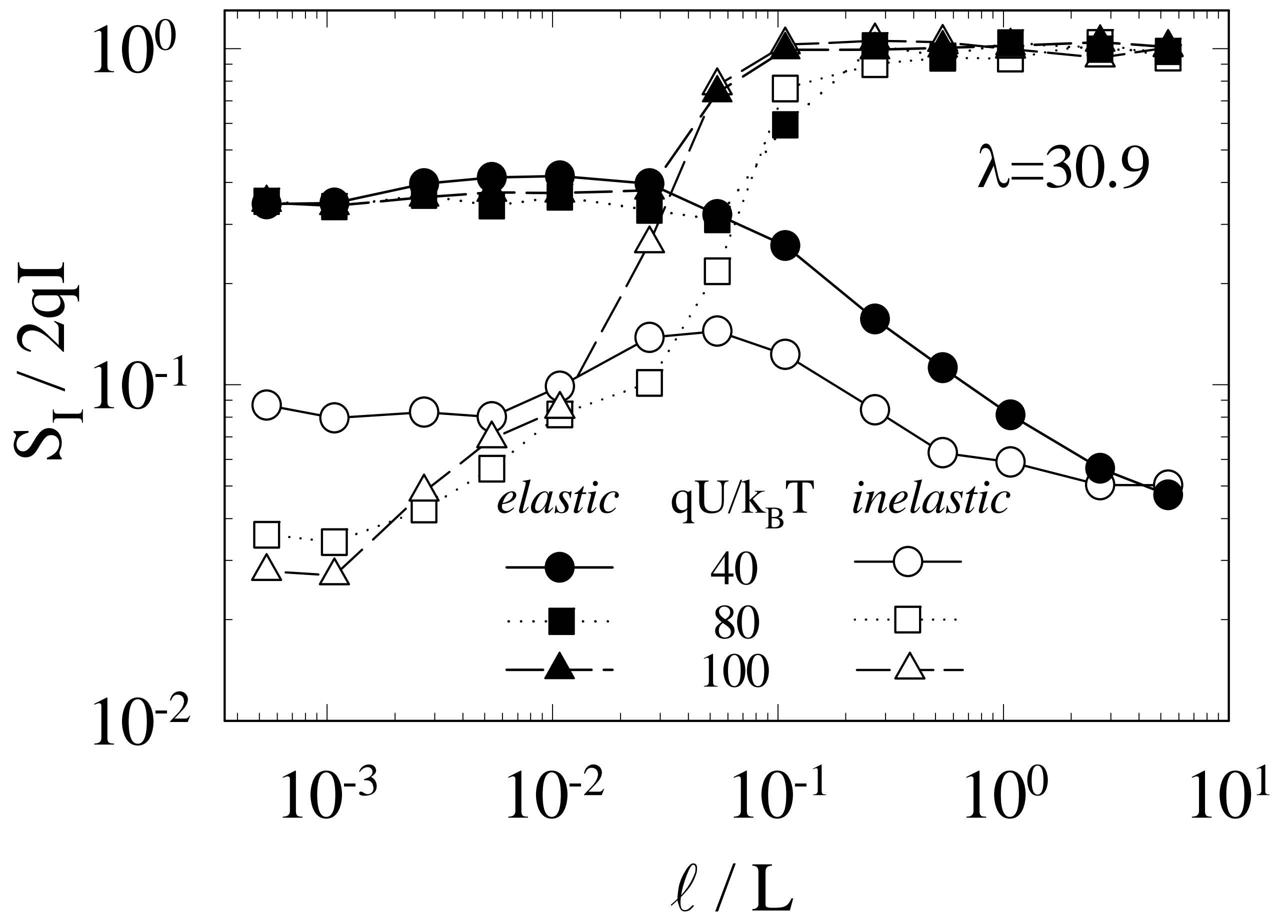

Figure 21

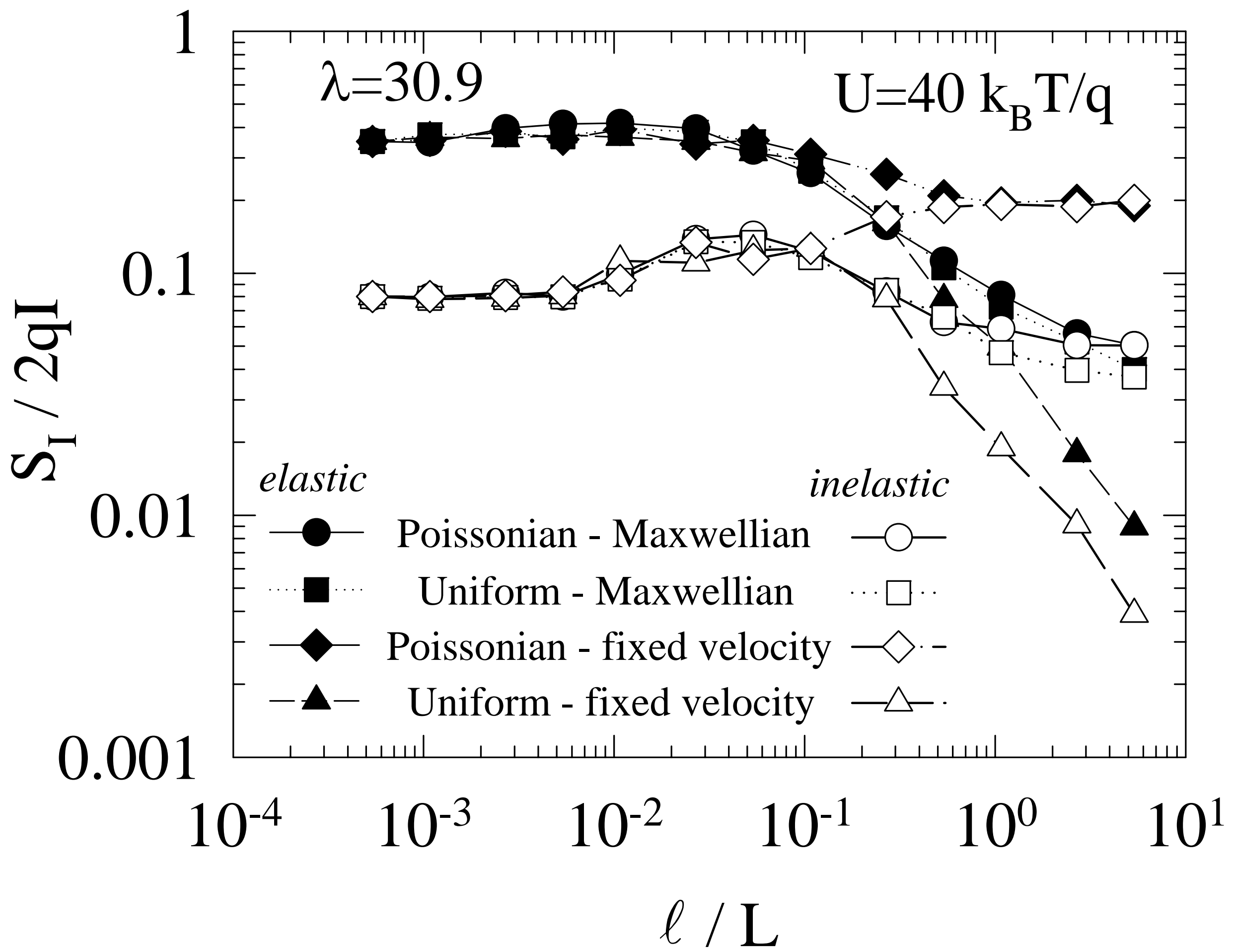

Figure 22

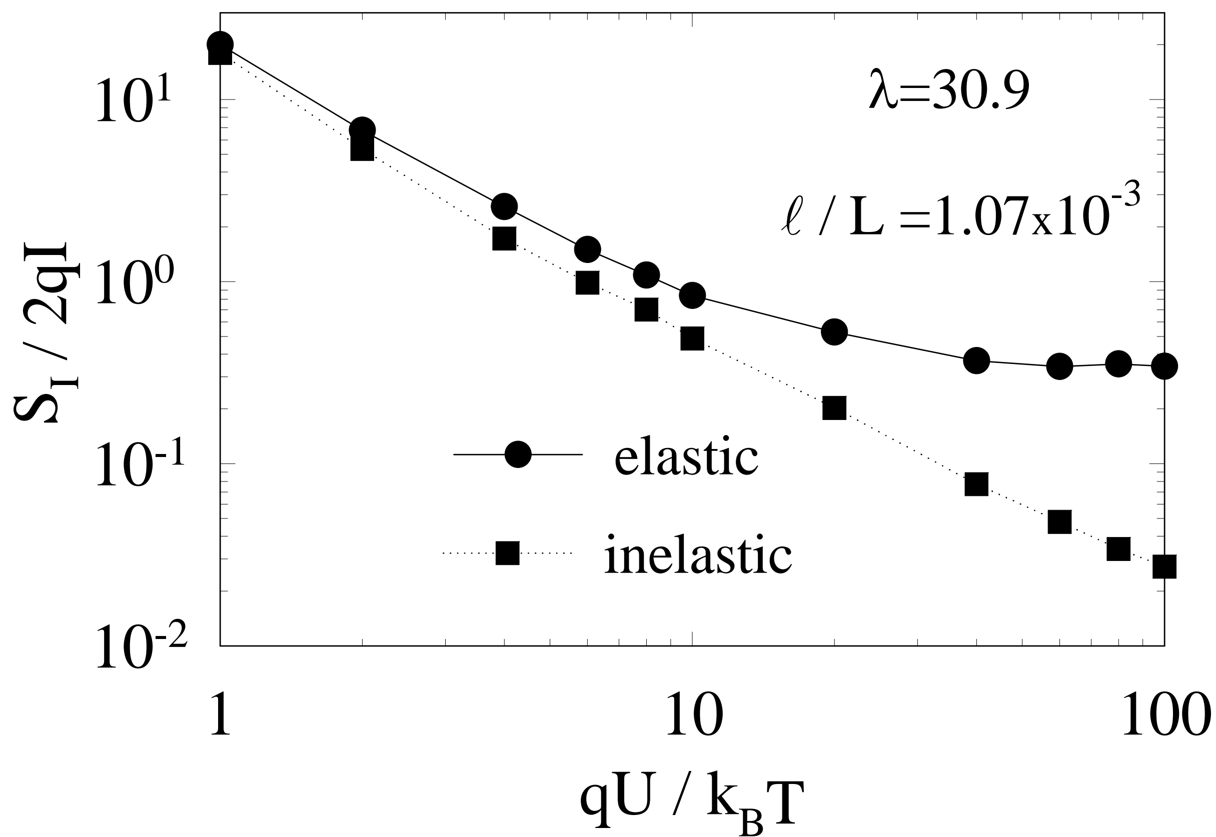

Figure 23

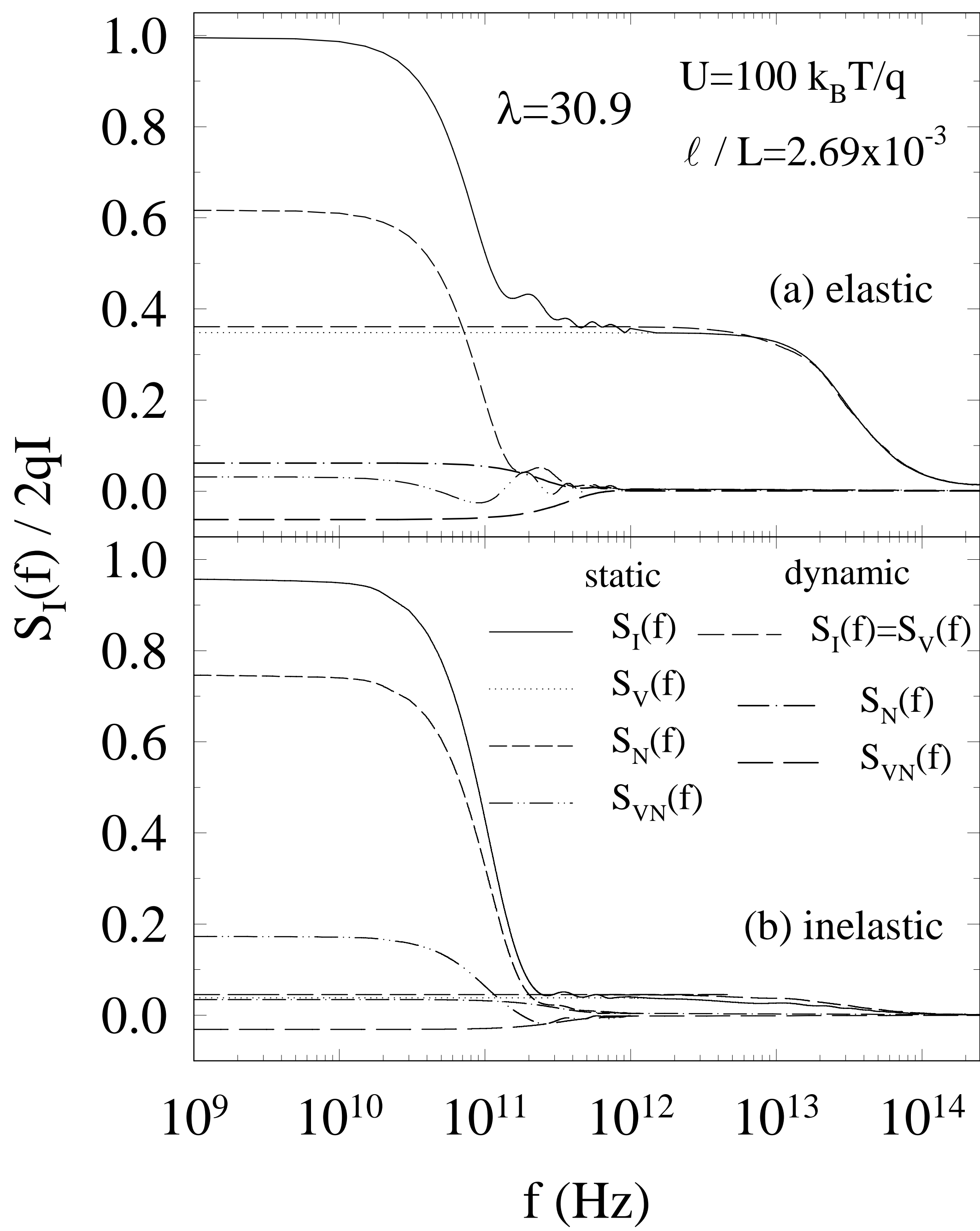

Figure 24

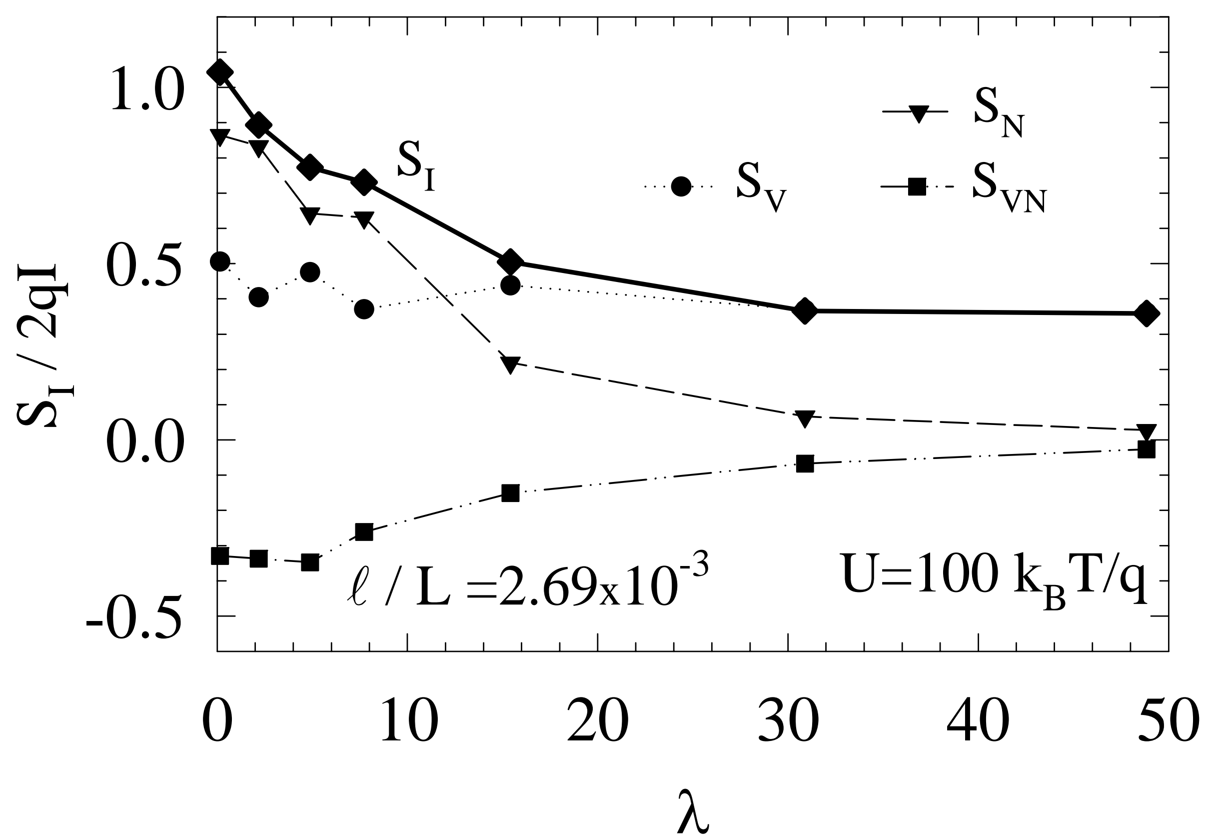

Figure 25

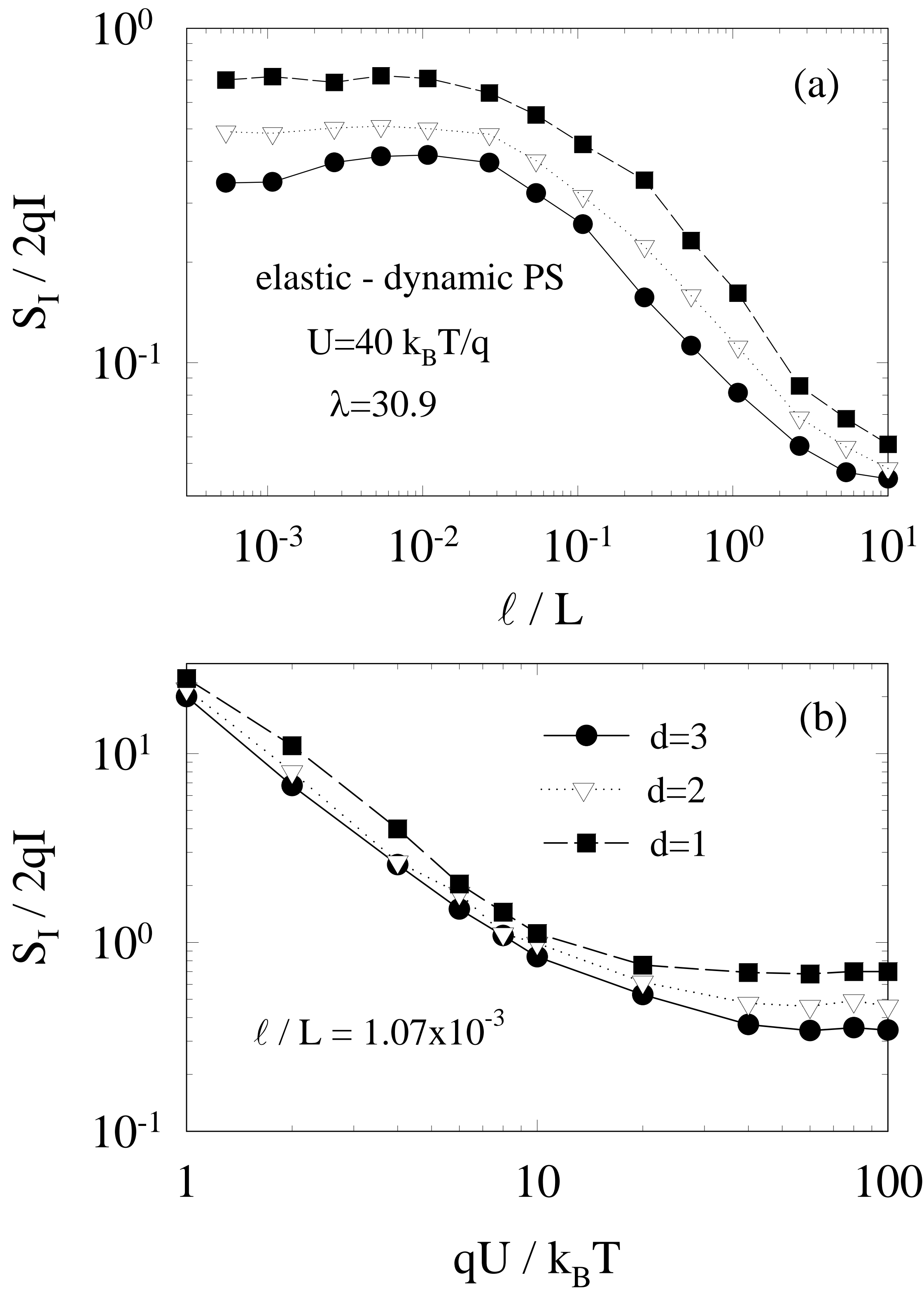

Figure 26

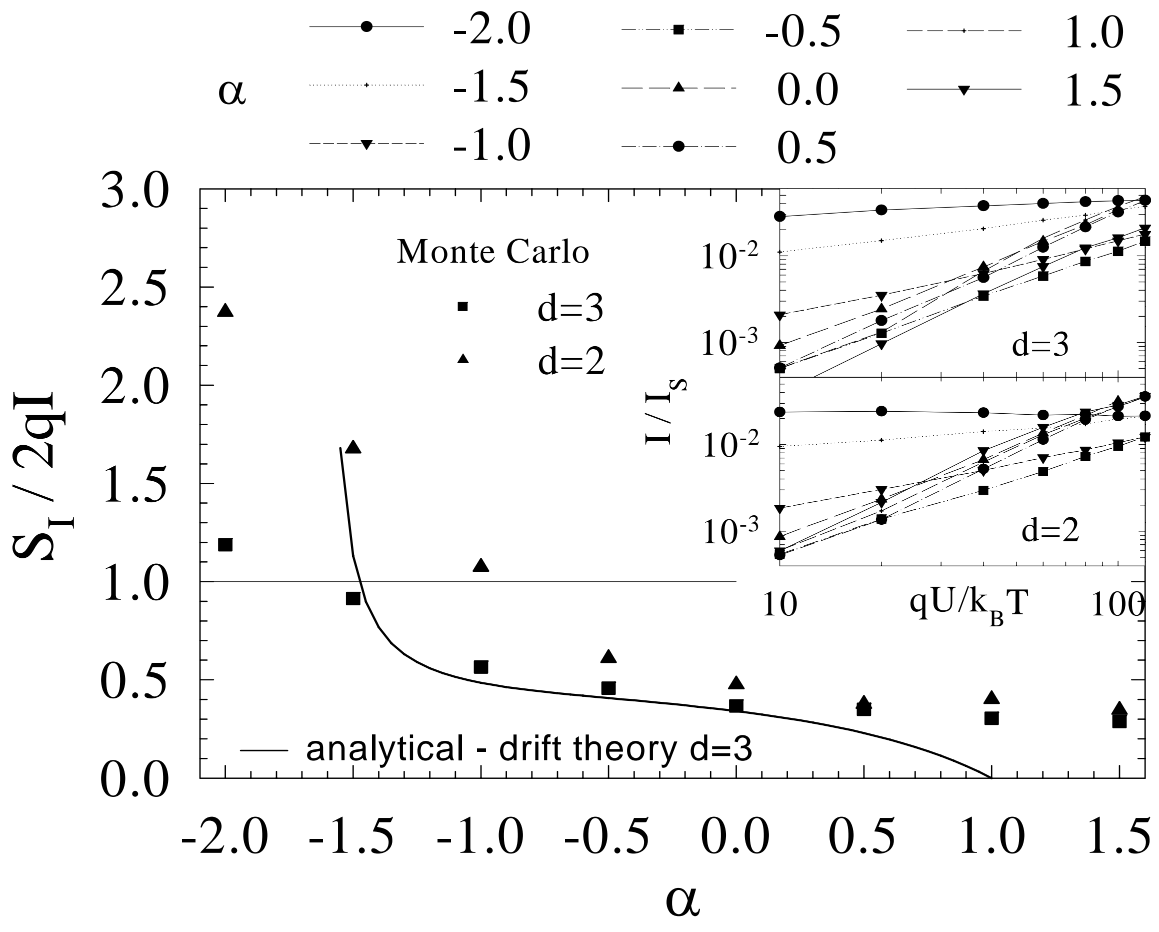

Figure 27

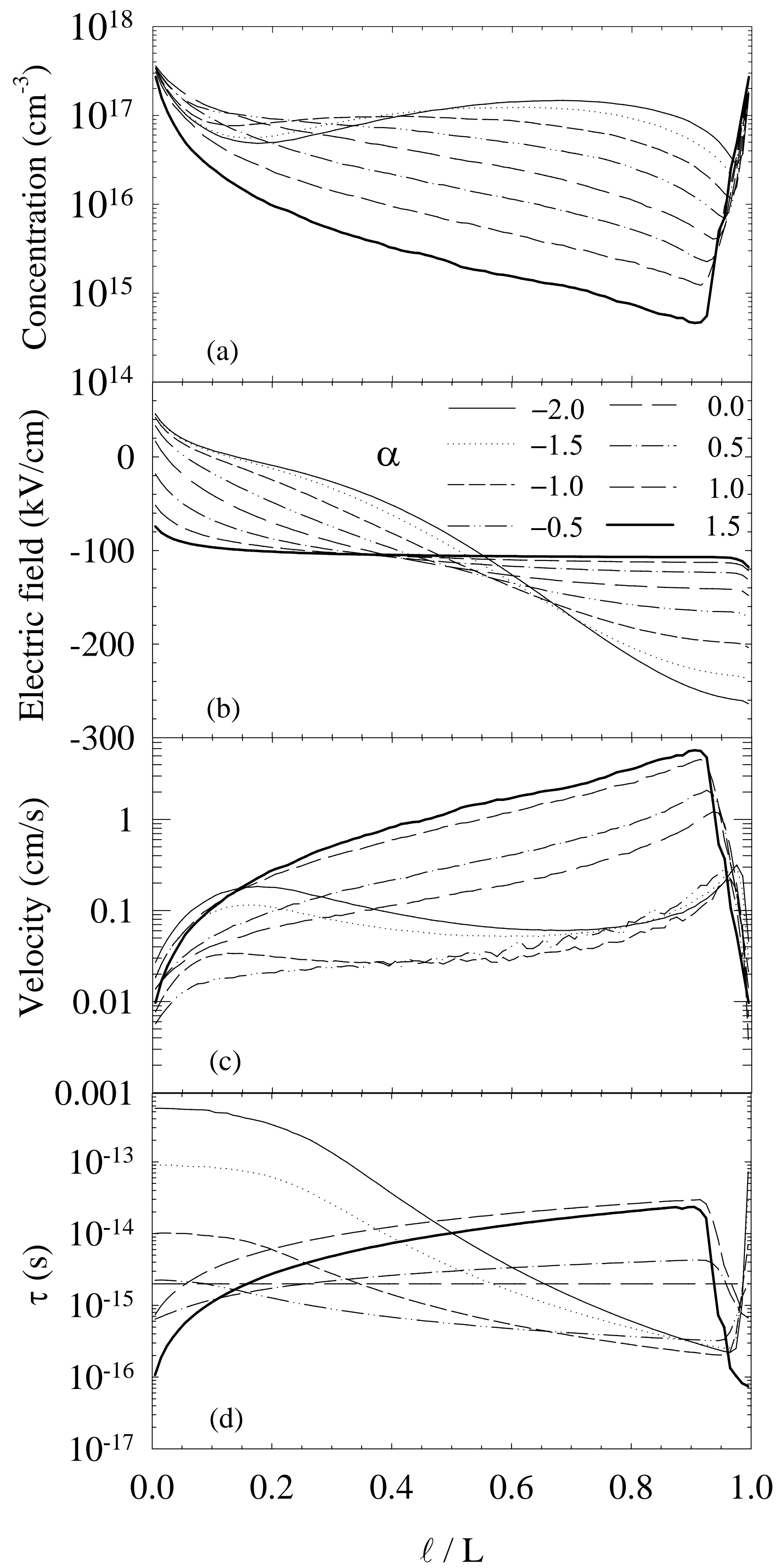

Figure 28

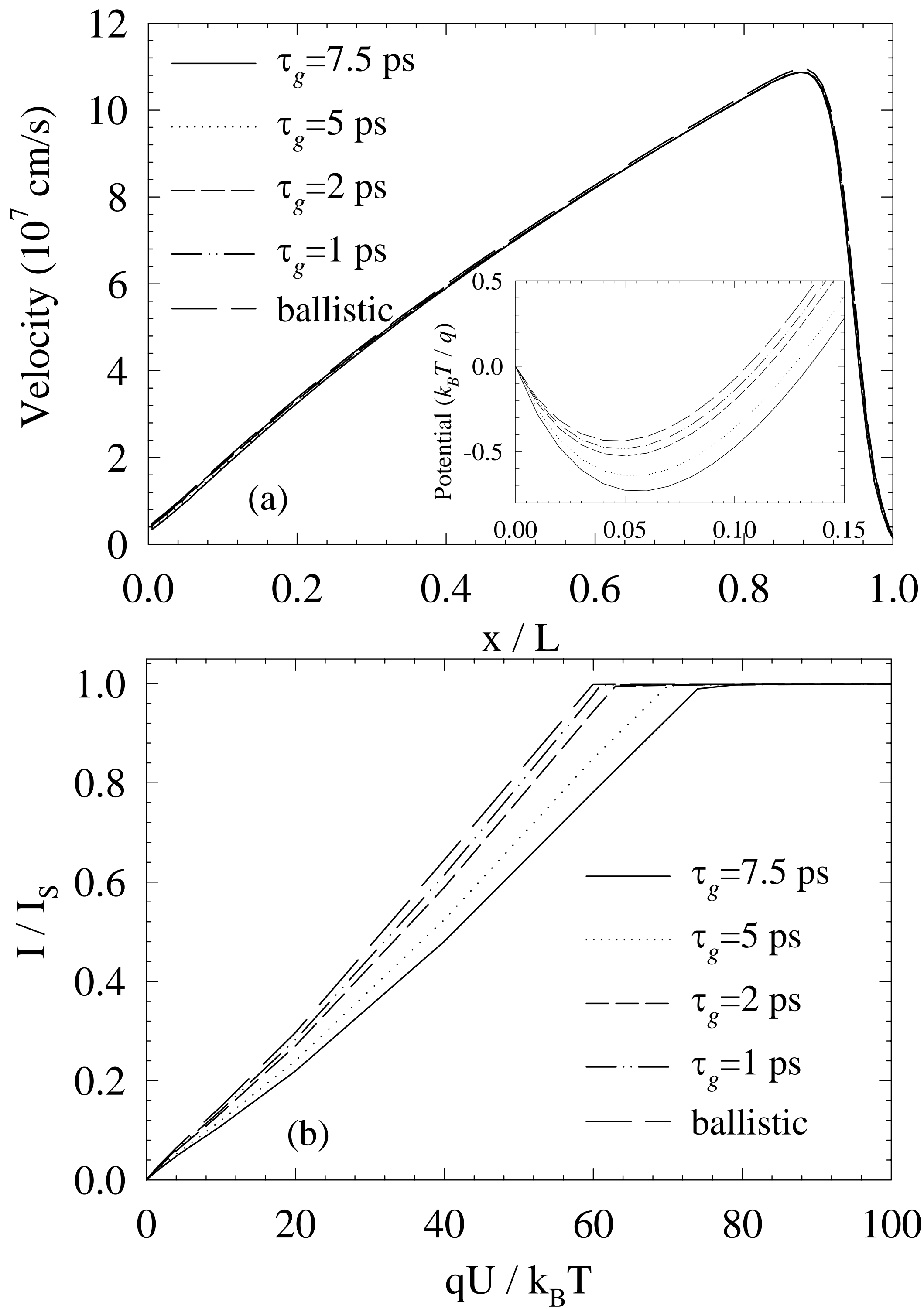

Figure 29

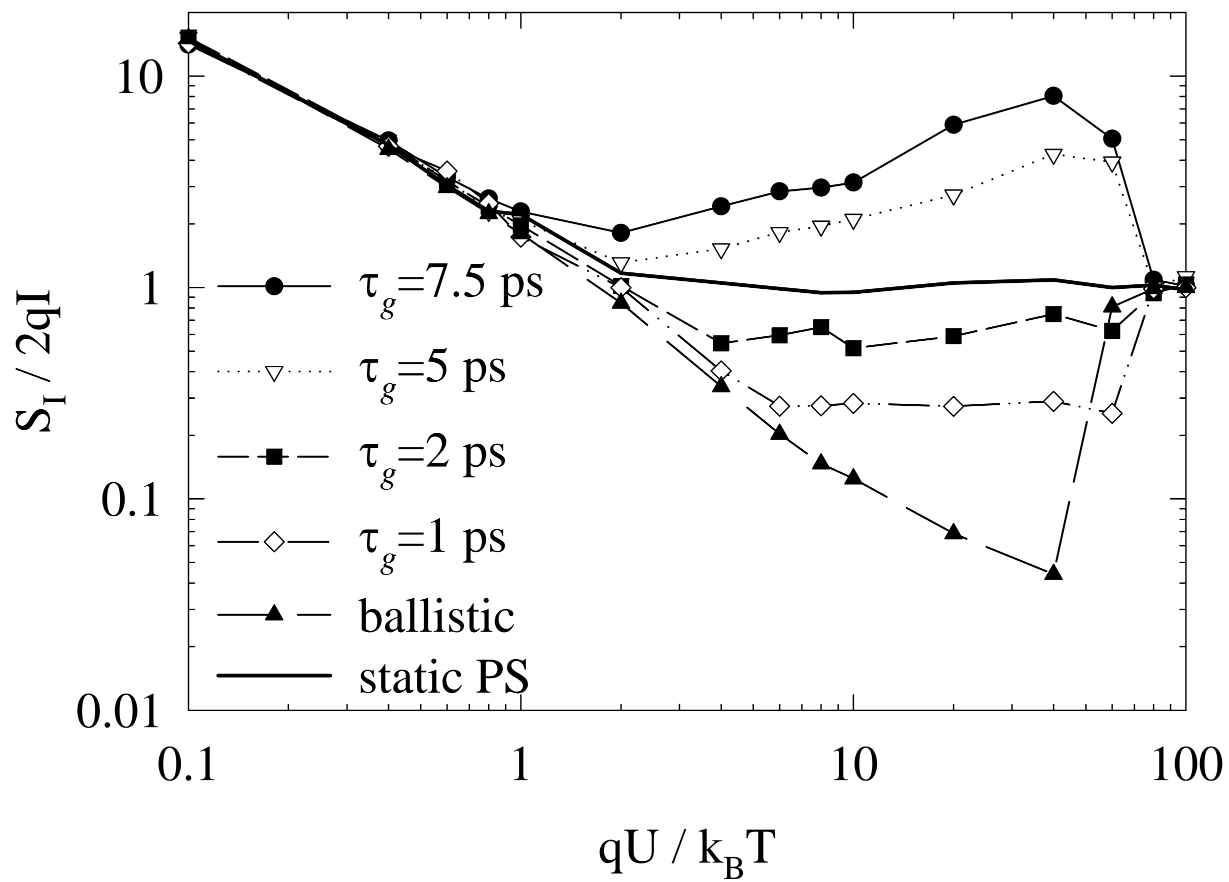

Figure 30

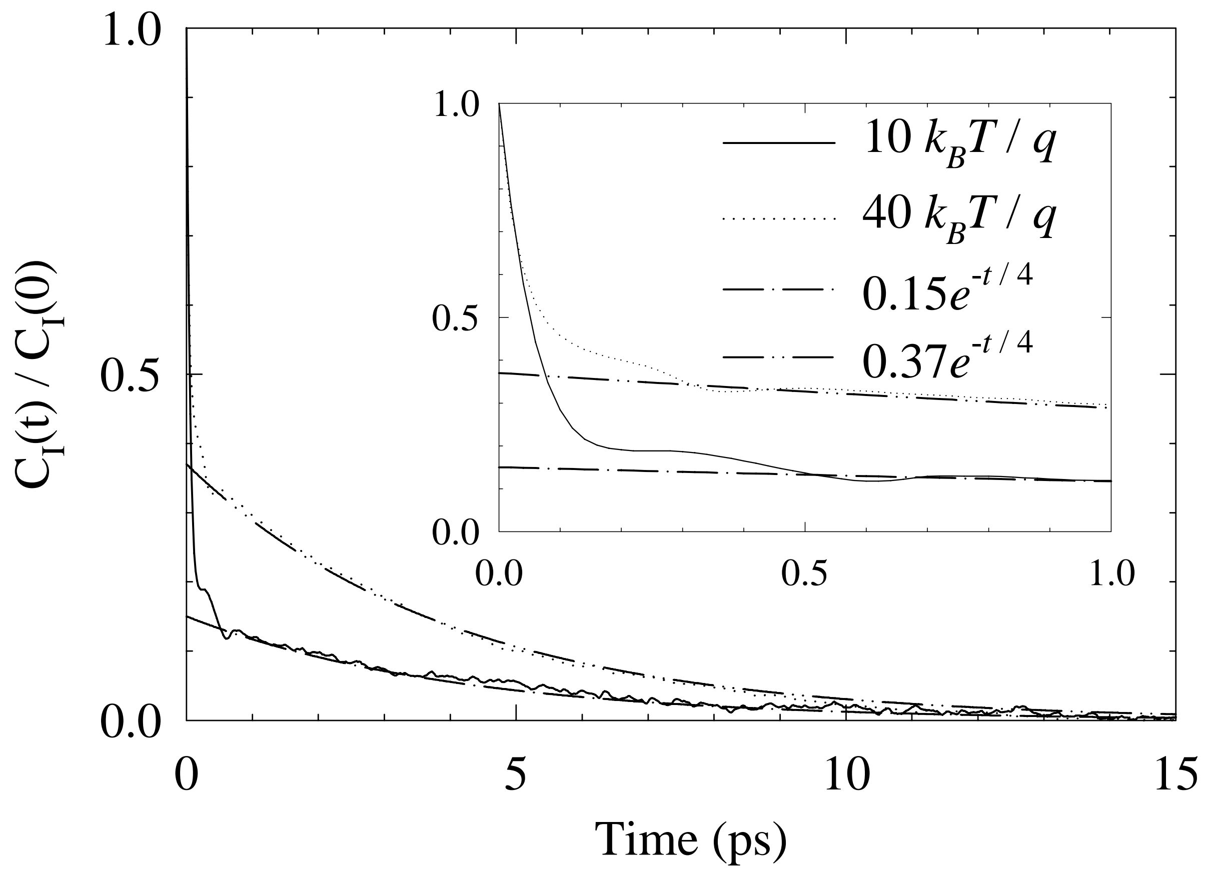

Figure 31

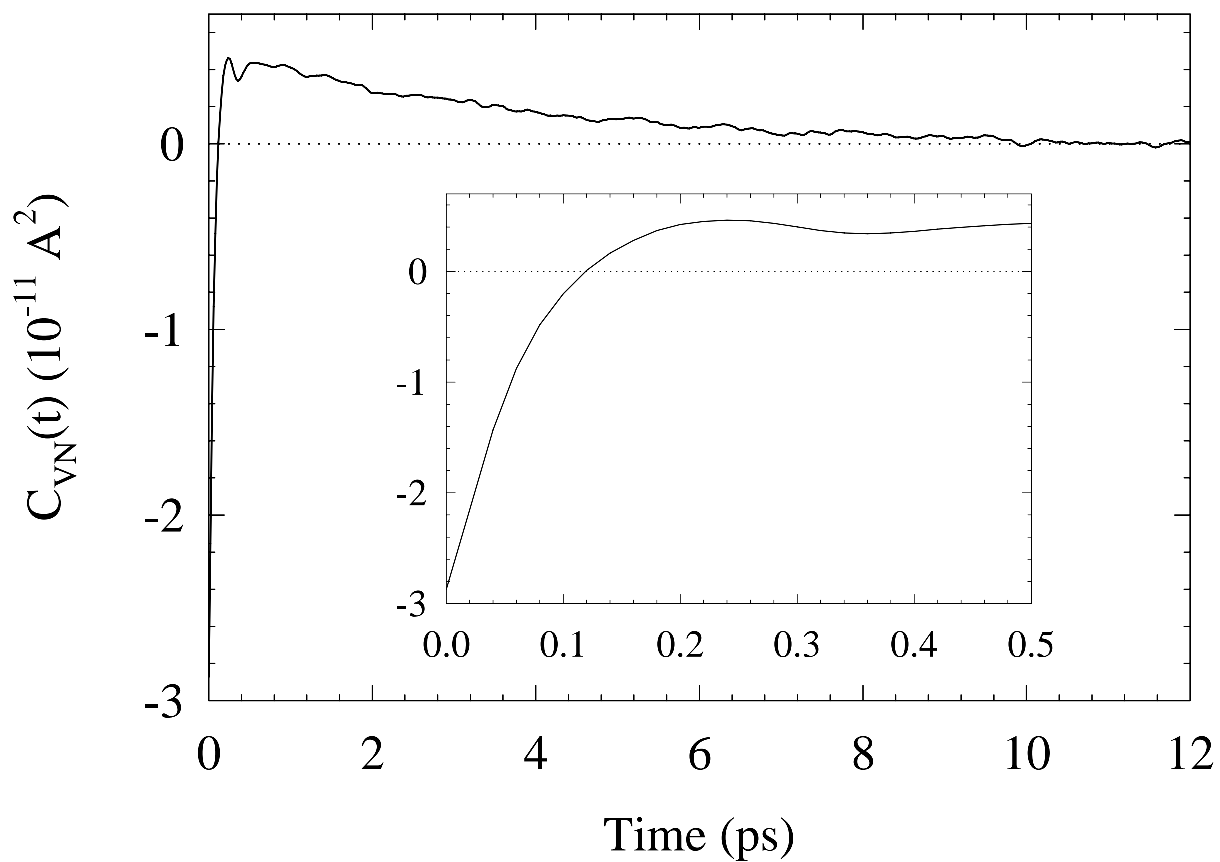

Figure 32

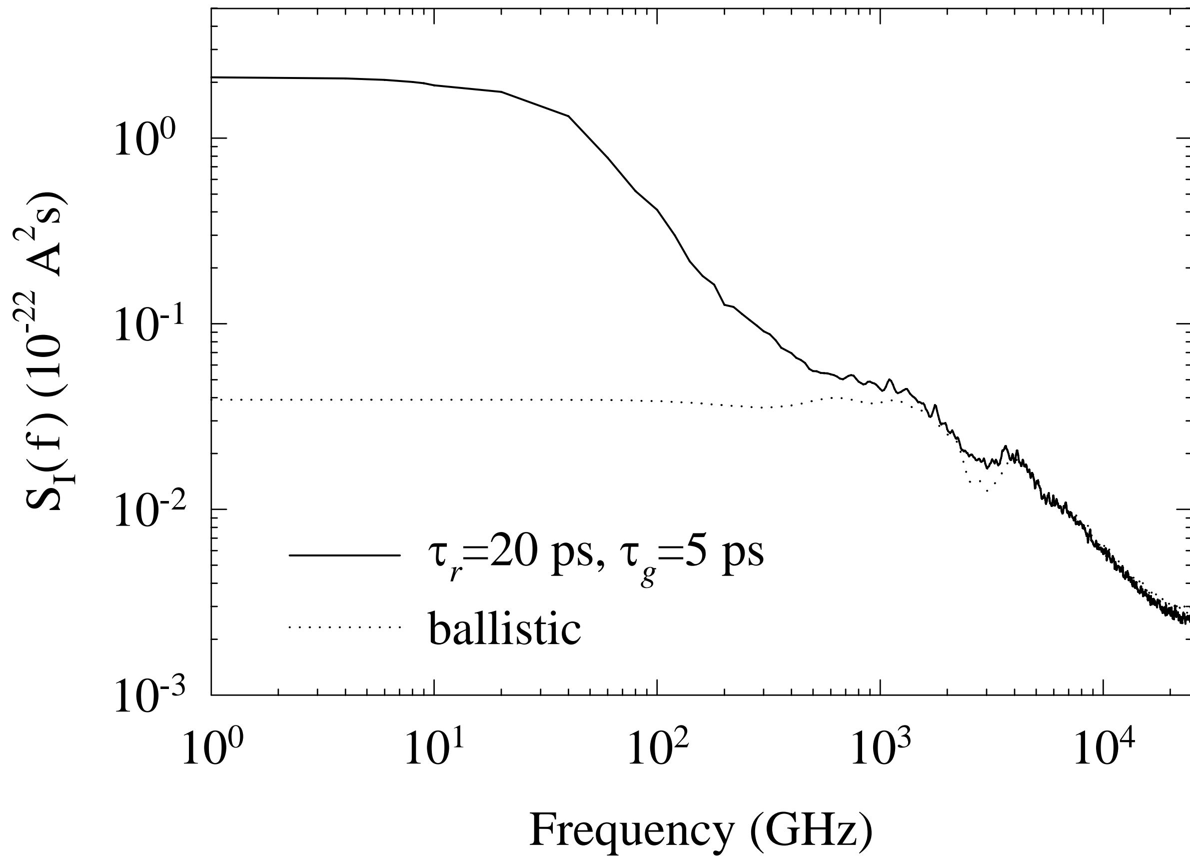

Figure 33

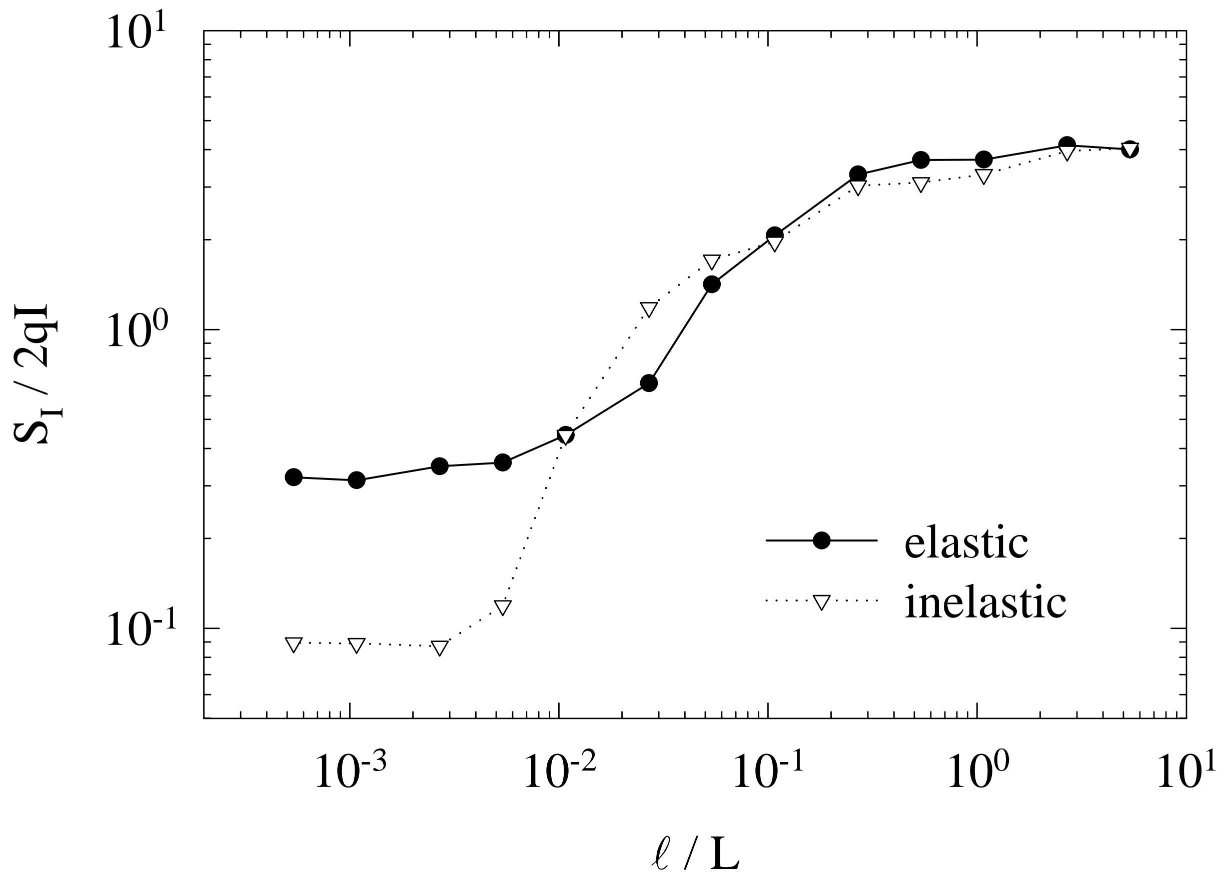

Figure 34